# Role of Defect Interactions with Embrittlement Species in Iron: a Multiscale Perspective

by

Ilaksh Adlakha

A Dissertation Presented in Partial Fulfillment
of the Requirements for the Degree
Doctor of Philosophy

Approved July 2015 by the
Graduate Supervisory Committee:

Kiran Solanki, Chair
Marc Mignolet
Nikhilesh Chawla
Hanqing Jiang
Yongming Liu

ARIZONA STATE UNIVERSITY

August 2015

# ABSTRACT

Hydrogen embrittlement (HE) is a phenomenon that affects both the physical and chemical properties of several intrinsically ductile metals. Consequently, understanding the mechanisms behind HE has been of particular interest in both experimental and modeling research. Discrepancies between experimental observations and modeling results have led to various proposals for HE mechanisms. Therefore, to gain insights into HE mechanisms in iron, this dissertation aims to investigate several key issues involving HE such as: a) the incipient crack tip events; b) the cohesive strength of grain boundaries (GBs); c) the dislocation-GB interactions and d) the dislocation mobility.

The crack tip, which presents a preferential trap site for hydrogen segregation, was examined using atomistic methods and the continuum based Rice-Thompson criterion as sufficient concentration of hydrogen can alter the crack tip deformation mechanism. Results suggest that there is a plausible co-existence of the adsorption induced dislocation emission and hydrogen enhanced decohesion mechanisms. In the case of GB-hydrogen interaction, we observed that the segregation of hydrogen along the interface leads to a reduction in cohesive strength resulting in intergranular failure. A methodology was further developed to quantify the role of the GB structure on this behavior.

GBs play a fundamental role in determining the strengthening mechanisms acting as an impediment to the dislocation motion; however, the presence of an unsurmountable barrier for a dislocation can generate slip localization that could further lead to intergranular crack initiation. It was found that the presence of hydrogen increases the strain energy stored within the GB which could lead to a transition in failure mode. Finally, in the case of body centered cubic metals, understanding the complex screw

dislocation motion is critical to the development of an accurate continuum description of the plastic behavior. Further, the presence of hydrogen has been shown to drastically alter the plastic deformation, but the precise role of hydrogen is still unclear. Thus, the role of hydrogen on the dislocation mobility was examined using density functional theory and atomistic simulations. Overall, this dissertation provides a novel atomic-scale understanding of the HE mechanism and development of multiscale tools for future endeavors.

*To my family for their continued support and encouragement throughout my life.*

# ACKNOWLEDGMENTS

I would like to express my sincere gratitude to the many people without whose support this dissertation would not have materialized. First, I would like to thank my advisor Prof. K.N. Solanki, for his guidance, encouragement and belief in me throughout this endeavor. Further, he allowed me the freedom to direct this research project according to my understanding, providing an opportunity to develop independent and innovative thinking. Next, I would like to express my gratitude to my committee members: Prof. M. Mignolet, Prof. N.K. Chawla, Prof. Y. Liu and Prof. H. Jiang for their support and helpful remarks that improved the quality of this research. I would like to extend special thanks to Dr. Mehul Bhatia, Sudhanshu S. Singh, Vipin Agarwal, Mansa Rajagopalan, Benyamin Gholami, Scott Turnage and Nitin Muthegowda for several engaging technical and non-technical conversations that enhanced my experience in graduate school.

Finally, I would like to acknowledge the continued support of Dr. W. Mullins and Dr. A.K. Vasudevan from the Office of Naval Research. This work was supported by the Office of Naval Research, contract No. N000141110793.

TABLE OF CONTENTS

Page

LIST OF TABLES ..... ix

LIST OF FIGURES ..... x

CHAPTER

1 MOTIVATION ..... 1

2 BACKGROUND AND RESEARCH OBJECTIVE ..... 4

2.1 Background ..... 4

2.2 Literature Review on Hydrogen Embrittlement ..... 5

2.3 Research Objectives ..... 12

3 EFFECT OF HYDROGEN ON THE INCIPIENT CRACK TIP EVENTS IN α-Fe ..... 17

3.1 Introduction ..... 17

3.2 Methodology ..... 19

3.2.1 Generalized Stacking Fault Energies (GSFE) ..... 19

3.2.2 Studying the Incipient Crack Tip Response with Mode I Fracture Specimens ..... 20

3.3 Results ..... 22

3.3.1 Theoretical Analysis of the Effect of Hydrogen on the Incipient Crack Tip Behavior ..... 22

3.3.2 Effect of Hydrogen on the Incipient Crack Tip Events in Iron ..... 24

CHAPTER Page

3.3.2.1 Orientation-I....24

3.3.2.2 Orientation-II....25

3.3.2.3 Orientation-III....27

3.4 Conclusions....29

4 THE ROLE OF GRAIN BOUNDARY STRUCTURE ON HYDROGEN SEGREGATION....31

4.1 Introduction....31

4.2 Methodology....35

4.3 Results....37

4.4 Conclusions....48

5 CRITICAL ASSESSMENT OF H EFFECTS ON SLIP TRANSMISSION ACROSS GRAIN BOUNDARIES IN α-FE....50

5.1 Overview....50

5.2 Introduction....51

5.3 Methodology....55

5.3.1 Equilibrium Grain Boundary Structures and Energies....56

5.3.2 Simulation Setup for the Grain Boundary-Dislocation Interaction in Fe....58

5.3.3 Introduction of Hydrogen around the Grain Boundary....59

CHAPTER Page

5.3.4 Quantifying the Energy Barrier for Slip Transmission.....60

5.4 Results .....60

5.4.1 Σ7 (123) STGB .....61

5.4.2 Σ13 (134) STGB .....64

5.4.3 Σ57 (178) STGB .....66

5.5 Discussion .....67

5.6 Conclusions .....72

6 THE EFFECT OF HYDROGEN ON DISLOCATION MOBILITY IN IRON...74

6.1 Introduction .....74

6.2 Methodology .....78

6.3 Results .....80

6.3.1 Loading by Applying Pure Shear Stress along the Burgers Vector Direction.....82

6.3.2 Loading by Combined Application of Shear Stress Perpendicular and Parallel to the Burgers Vector Direction .....83

6.4 Summary .....84

CHAPTER Page

7 ENERGETICS, STABILITY AND INTERACTION OF GRAIN BOUNDARY TRIPLE JUNCTIONS WITH POINT DEFECTS ..... 85

7.1 Introduction ..... 85

7.2 Methodology ..... 88

7.3 Results ..... 91

7.3.1 Vacancy ..... 96

7.3.2 Self-Interstitial Atom (SIA) ..... 98

7.3.3 Hydrogen ..... 99

7.4 Conclusions ..... 102

REFERENCES ..... 104

APPENDIX

A OVERVIEW OF ATOMISTIC SIMULATIONS ..... 134

LIST OF TABLES

Table Page

1: The Different Crystallographic Orientations Employed in the Mode-I Specimen ..... 22

2: Mean Statistics for Gaussian Distribution of One-Interstitial (H-Int) and Two-Interstitial Hydrogen (2H-Int) Segregation to α-Fe STGBs. ..... 44

3: A List of the Coefficient Variables (P1 And P2) Values with Varying Defect Configurations and GB Tilt Systems Extracted Using Equation 8. The R (Linear Coefficient Factor) Values Indicate a Very Strong Correlation Between the Distribution Parameter $\alpha$ and Atomic Volume Vvor. ..... 45

4: The Symmetric Tilt Gbs with the Corresponding p3 And p4 (Coefficient) Values for Both Hydrogen Defect Configuration were Extracted Using Equation 9. The R (Linear Coefficient Factor) Values Indicate a Very Strong Correlation Between The Distribution Parameter, β And Length Scale, l. ..... 46

5: Grain Boundary CSL Description, Misorientation Angle, GB Energy, the Predicted and Observed Slip Plane for the GBs Examined in This Work. ..... 57

6: Details of Grain Boundary Triple Junctions along with the CSL and the Misorientation ($\theta$) for Each GB Interface. ..... 89

LIST OF FIGURES

Figure Page

1: a) Fatigue Data under Various Environmental Conditions Elucidating the Role of Environment, and b) Landing Gear Before and after a Few Flight Missions (Courtesy of Dr. Vasudevan, ONR) ..... 2

2: a) The Brittle Crack Advance in the Presence of Hydride Formation Ahead of the Crack Tip α-Ti (Shih, Robertson, And Birnbaum 1988). b) The Presence of Hydrogen Decreases the Dislocation-Dislocation Interaction and Thereby Increasing the Dislocation Mobility (P. Ferreira, Robertson, And Birnbaum 1998). c) The Crack Tip with Slip Bands and Blunting in Fe-3% Si Under Vaccum and d) in the Presence of Hydrogen, the Crack Tip Remains Sharp (Vehoff And Rothe 1983). ..... 9

3: The Geometric Representation of a Fracture Specimen That Was Subjected to Mode-I Loading by Displacing Boundary Atoms Using the Molecular Statics Framework. . 21

4: a) The Effect of Hydrogen on the Generalized Stacking Fault Energy for Fe. b) The Effect of Hydrogen Coverage on the Unstable Stacking Fault Energy in Fe. c) The Resultant Change in Critical Stress Intensity Factor for Dislocation Nucleation Using the Rice-Thompson Criterion. ..... 24

5: a) The Incipient Cleavage Crack Advance along the (110) Plane for the $(010)[001]$ Orientation Is in Agreement with the Theoretical Predictions. b) The Presence of a Hydrogen Rich Environment Ahead of the Crack Tip Reduces the Critical Stress Intensity Factor Required for Cleavage. The Atoms Were Colored According to Atomic Volume Estimated by the Voronoi Tessellation. ..... 25

Figure Page

6: a) The Emission of an Edge Dislocation Ahead of the Crack Tip with an Orientation of $(111)[11\bar{2}]$. b) The Presence of H Shifts the Slip Plane Away from the H Rich Environment. The Atoms were Colored According to Common Neighbor Analysis (CNA) Such that BCC Atoms Are Blue and Defects White and Hydrogen Atoms Were Depicted with Red Color. ..... 26

7: The Effect of H Coverage on the Critical Stress Intensity Factor for a Dislocation Nucleation in $(111)[11\bar{2}]$. a) The Hydrogen Free Crack Tip Event Had a Nucleation of Edge Dislocation. b) The Incipient Events When H Atoms Were Placed along the Slip Plane Lead to a Decrease in the Critical Stress Intensity Factor Required for the Dislocation Nucleation. c) The Effect of a H Rich Region on the Dislocation Mobility. The Atoms Were Colored According to CNA, Where Blue Represents the BCC Lattice Atoms, White Represents the Defect Atoms and Red Represents the Hydrogen Atoms. ..... 27

8: The Effect of H Coverage on the Crack Tip Deformation for the $(010)[10\bar{1}]$ Crack Orientation. a-b) Show the Crack Tip Events for a Hydrogen Free Crack Tip. c-d) Shows Premature Crack Propagation, Due to the Presence of H Atoms Ahead of the Crack Tip. The Dashed Curve Outlines the Initial Crack Geometry. The Atoms Were Colored According to CNA, Blue Represents the BCC Lattice Atoms, White the Defect Atoms and Red the Hydrogen Atoms. ..... 29

Figure Page

9: (a) The Periodic Simulation Cell Setup with Two Symmetric GB Interfaces Spaced 12 nm Apart. The Minimum Periodic Lengths in the Orthogonal Directions Parallel to the GB Plane Were 3 and 7 Å. (b) The Body-Centered Cubic Unit Cell with the Hydrogen Configurations: Single Hydrogen and Two Hydrogen in an Interstitial Site. (c) <110> Symmetric Tilt Grain Boundary Energy as a Function of Misorientation Angle with the Low-Σ GBs Identified. ..... 39

10: The GB Structures are Highlighted with the Help of the Atomic Volume Estimated by Voronoi Tessellation ($V_{vor}$). Atomic Volume is Maximum (14.8 $Å^3$) at the GB and Decays to the Bulk Value (11.6 $Å^3$)..... 40

11: The Segregation Energy of an Interstitial Hydrogen Atom as a Function of Distance from the GB for <100>, <110> and <111> STGBs. The Segregation Energies were Divided into 1 Å Bins. The Red Lines are Medians, the Blue Box Ends are the $25^{th}$ and $75^{th}$ Percentiles, the Black Whisker Ends are Extreme Minimum and Maximum Values, and the Green Dotted Lines are Mean Segregation Energies. ..... 42

12: The Segregation Energies at $d/d_{\{hkl\}} = 1$ (One Atomic Layer Away from the GB Plane) for the Two Defect Configurations and Various <100>, <110>, <111> and <112> STGBs was Plotted on the Stereographic Triangle Using the Polar and Azimuthal Angles. The Color Bar Corresponds to the Maximum and Minimum Segregation Energy Thresholds for Both Hydrogen Defect Configurations. ..... 43

Figure Page

13: The Evolution of Hydrogen Segregated GB Energy ($E_{gb}^{\alpha}$) As a Function of Local Hydrogen Concentrations for the Σ53 (720), $\theta$ = 31.89°. As the Change in GB Energy $E_{gb}^{\alpha}$ Approaches Zero, There Is No Significant Energy to be Gained from Further Trapping Hydrogen Atoms at the Boundary. This Transition Demarcates the Trapping Limit of Hydrogen for this Interface..... 47

14: The <111> Symmetric Tilt Grain Boundary Structures in α-Fe Used in this Work. Atoms are Colored Based on the Atomic Volume Estimated by Voronoi Tessellation on a Scale of 11.64 $Å^3$ to 13.20 $Å^3$..... 57

15: a) A Schematic Representation of the Atomistic Model Employed to Study the Interaction Between a Screw Dislocation and the <111> STGB in α-Fe. b) Differential Displacement Map of the Compact Core in Fe and the Atomic Colors Emphasize the Different (111) Planes. ..... 59

16: a-d) The Interaction of a Screw Dislocation with the Σ7 (123) GB under the Applied Shear Strain ($\gamma_{yz}$) along the Burgers Vector Direction. The Inset b) Shows the Magnified GB Structure Colored According to the Atomic Volume Estimated by Voronoi Tessellation as Described Earlier. d) The Schematic Representation of the Slip Transmission Mechanism. e) The Influence of Hydrogen Atoms on the Dislocation-Grain Boundary Interaction. The Magnified View in e) Shows the Hydrogen Atom Positions Depicted by Black Circles. The Atoms Were Colored According to the Local Atomic Shear Strain Invariant ($\gamma_s$) on a Scale of 0 to 0.5. .... 63

Figure Page

17: a-b) The Interaction of a Screw Dislocation with the Σ13 (134) GB under the Applied Shear Strain ($\gamma_{yz}$) along the Burgers Vector Direction. The Inset a) Shows the Magnified GB Structure Colored According to the Atomic Volume Estimated by Voronoi Tessellation. c) The Change in Atomic Events for the Dislocation-Grain Boundary Interaction in the Presence of Hydrogen. The Atoms Were Colored According to the Local Atomic Shear Strain Invariant ($\gamma_s$) on a Scale of 0 to 0.5. d) The Schematic Representation of the Change in Slip Transmission Mechanism in the Presence of Hydrogen. ..... 65

18: a) The Interaction of a Screw Dislocation with the Σ57 (178) GB under the Applied Shear Strain ($\gamma_{yz}$) along the Burgers Vector Direction. b) The Atomic Events of Hydrogen on the Slip Transmission Mechanism. The Atoms Were Colored According to the Local Atomic Shear Strain Invariant ($\gamma_s$) on a Scale of 0 To 0.5. c) The Schematic Representation of Influence of Hydrogen on the Slip Transmission. ..... 67

19: The Effect of Hydrogen on the Slip Transmission Barrier Through <111> Symmetric Tilt Grain Boundaries. ..... 70

20: Schematic Representation of the Effect of Hydrogen on the Intergranular Fatigue Crack Initiation. The Top Half Shows the Hydrogen Free Interaction of Incident Dislocation Density of $\rho_0$ and the Emitted Dislocation Density is $\rho_e$. In Presence of Hydrogen, the Incident Dislocation Density $\rho_{0,H}$ Increases in Comparison to Hydrogen Free Because of the Shielding Effect Afforded by the Hydrogen Environment Surrounding a Dislocation. The Emitted Dislocation Density $\rho_{e,H}$ Is Lower than in the Hydrogen Free Case $\rho_{e,H} < \rho_e$. ..... 72

Figure Page

21: Differential Displacement Maps for the Anisotropic Linear Elasticity Solution for a) the Easy-Core, b) Hard-Core and c) Split-Core Configurations. The Atomic Positions Are Represented by Different Colors to Emphasize the Distinct {111} Planes. ..... 77

22: The Schematic Representation of the Simulation Cell. The Fixed Region (Gray) Atoms Are Held Fixed Through the Minimization and the Relaxed Region (Blue) Atoms Are Allowed to Relax During the Minimization Process. The Angle Between the MRSSP and the $(\bar{1}01)$ Plane Is Defined by $\chi$ (Measured in a Clockwise Sense). ..... 79

23: The Peierls Potentials for Various Interatomic Potentials for Fe Using Molecular Dynamics. The Energy Barrier for Dislocation Motion was Calculated by Moving an Isolated Dislocation by One Periodic Length Using the NEB Method. ..... 81

24: The Generalized Stacking Fault Energy Curve by Displacing along the <111> Direction Over {110}, {112} and {123} Planes. The Displacement Is Normalized by the Magnitude of the Burgers Vector $\left(\frac{a}{2}[111]\right)$. ..... 82

25: A Comparison Between the Schmid Behavior and the Observed Peierls Stress for $\tau = 0$ MPa, $\tau = 114$ MPa and $\tau = -114$ MPa (Equation 17b) for Various MRSSP Orientations. ..... 84

26: Schematic Showing Construction of a GB TJ Configuration. The GBs were Minimized Separately and a Wedge was Carved Out Along the {001}/{011} Plane Represented by Dashed Lines. ..... 88

Figure Page

27: The Minimized Atomic Configuration of: a) Σ3-Σ3-Σ9, b) Σ3-Σ9-Σ27, c) Σ3-Σ11-Σ33, d) Σ3-Σ19-Σ57, e) Σ3-Σ27-Σ81 and f) Σ3-Σ33-Σ99 TJs. Atoms were Colored According to the Local Variation in Hydrostatic Stress from -10 to 10 GPa. ..... 92

28: (a) The Net Change in Volume at the TJ. In General, a Clear Trend Can Be Observed that High CSL GB TJs Underwent Large Volume Change During Formation of the TJ. (b) the Resolved Line Tension Acting along the TJ. c) The Excess Energy Due to Formation of the TJ..... 95

29: The Atomic Variation in Vacancy Binding Energy Near a) Σ3-Σ3-Σ9 and b) Σ3-Σ33-Σ99 TJs. The Atoms Were Colored Based on the Vacancy Binding Energy at Each Site. c) The Mean Vacancy Binding Energy as a Function of Radial Distance from the TJ. A Total of 10 Concentric Bins Were Defined ($r_{i-1} \leq r \leq r_i$) up to 2 nm from the TJ. White Atoms Correspond to the Bulk Binding Energy (~ 0 eV) and Black Atoms Represent the Minimum Vacancy Binding Energy of 2.5 eV. ..... 97

30: The Mean Binding Energy for a Self-Interstitial Atom as a Function of Radial Distance from the TJ. A Total of 10 Concentric Bins Were Defined ($r_{i-1} \leq r \leq r_i$ ) up to 2 nm from the TJ..... 99

31: The Atomic Variation in Vacancy Binding Energy Near a) Σ3-Σ3-Σ9 and b) Σ3-Σ11-Σ33 TJs. The Atoms Were Colored Based on the Vacancy Binding Energy at Each Site. c) The Mean Vacancy Binding Energy as a Function of Radial Distance from the TJ. A Total of 10 Concentric Bins Were Defined (ri-1 ≤ r ≤ ri ) up to 2 nm from the TJ. White Atoms Correspond to the Bulk Binding Energy (~ 0 eV) and Black Atoms Represent the Minimum Vacancy Binding Energy of 0.75 eV. ..... 100

Figure Page

32: The Unique Behavior of the Σ3-Σ3-Σ9 TJ in Comparison to the Constituent GBs, in Terms of Variations in Hydrogen Concentration for a Range of Temperatures (Equation 25, $X_b^H = 0.28\%$). ..... 102

# CHAPTER 1

## 1 MOTIVATION

Steel is widely used in construction, marine, aerospace and nuclear applications because of the high strength to cost ratio. A wide variation in mechanical properties can be achieved by the addition of trace elements (carbon, manganese, niobium, vanadium, molybdenum, silicon, chromium and nickel) and controlling the thermal processing. However, unless the material is stable chemically in the operating environment the enhanced properties such as ductility, strength and toughness would degrade. The operational or processing exposure to hydrogen is a prime example of environment driven degradation. The continued exposure to a rich hydrogen environment in most metallic systems leads to embrittlement which could result in a premature failure of the structural components. Throughout modern history, there have been several large scale corrosion driven structural failures such as the gas pipeline burst in Louisiana (1965), the Silver bridge collapse in West Virginia (1967), and the swimming pool accident in Uster, Switzerland (1987) that have resulted in the loss of several lives and large monetary expenses. Therefore, HE in metals has been a topic of intense research dating back almost 150 years (Johnson 1874; Pfeil 1926; Vehoff and Rothe 1983; Shih, Robertson, and Birnbaum 1988; P. Ferreira, Robertson, and Birnbaum 1998; Birnbaum and Sofronis 1994; Lufrano, Sofronis, and Birnbaum 1998). Despite these efforts, there is a lack of agreement on the mechanism responsible for embrittlement (M. Louthan Jr et al. 1972; Gangloff, RP and Somerday 2012; Somerday and Sofronis 2013; S. Lynch 2012; S. P. Lynch 2013)

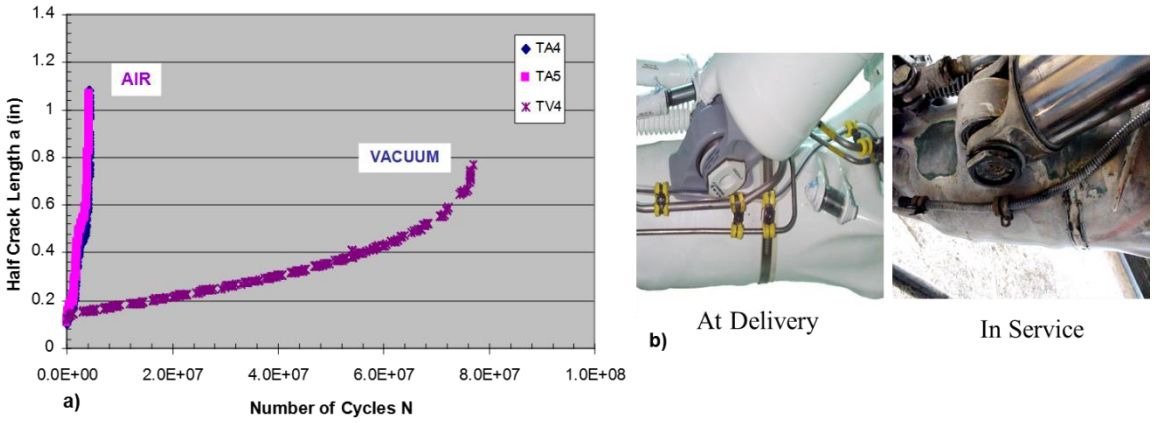


Figure 1: a) Fatigue data under various environmental conditions elucidating the role of environment, and b) landing gear before and after a few flight missions (Courtesy of Dr. Vasudevan, ONR)

The lack of understanding hinders the effective mitigation of embrittlement damage, especially in structural components for the naval applications and the oil industry. According to the recent LMI Cost of Corrosion Study (Herzberg, Ambrogio, and Barker 2006), the annual cost of corrosion for U.S. Navy Ships and Aviation in 2010 was a combined ~$5.75 billion. More than 80% of structural failures were due to combined environmental and mechanical loading. This translates into, on average, 20% down time due to unscheduled maintenance every year (Nickerson 2015). Consequently, harsh environmental conditions in combat zones and the aging of fleets are of paramount concern and require a comprehensive predictive framework with optimized corrosion resistance fatigue properties. In the case of the oil and gas industry, a large fraction of maintenance cost is spent either to prevent leaks or plug them. In fact, a recent report suggests that the cost of corrosion is about $3.7 billion annually (Kane 2006). That does not include intangible long-term costs, such as environmental impacts due to leaks and oil spills. Therefore, reducing the environmental risk of oil spills by extending the lifetime

performance of structural components is a big concern for the oil industry. The strength, ductility and toughness of these structural alloys are affected by the presence of point defects and impurities, such as hydrogen and sulphur. These defects result from diverse environmental conditions, such as dilute aqueous solution and sulfide exposure (Carneiro, Ratnapuli, and de Freitas Cunha Lins 2003; Gu, Luo, and Mao 1999; Woodtli and Kieselbach 2000; Parkins 2000). Therefore, in this work the HE phenomenon in α-Fe was studied in a consistent manner by synergistically using the knowledge accrued across various length scales to gain a better understanding.

# CHAPTER 2

# 2 BACKGROUND AND RESEARCH OBJECTIVE

## 2.1 Background

The safety and integrity of naval and oil industry infrastructure requires the effective mitigation of stress corrosion cracking and fatigue resistance that typically occurs in ferritic steel subjected to aggressive environments. The effects of mechanical loads coupled with harsh environment conditions results in local damage near highly stressed areas leading to the nucleation and growth of small surface cracks that interact, coalesce and eventually lead to a catastrophic failure if undetected. The effects of diverse environments on the strength, ductility and toughness of these structural alloys has been researched extensively (Carneiro, Ratnapuli, and de Freitas Cunha Lins 2003; Gu, Luo, and Mao 1999; Woodtli and Kieselbach 2000; Parkins 2000). One example would be loss by a factor of 2 to 6 in the fracture toughness/fatigue threshold of 4340 steel and 7075-T6 aluminum alloy in dilute sodium chloride (NaCl) solution.

The underlying mechanism lacks broader applicability across various metals. For instance, in titanium the formation of hydrides ahead of the crack tip was found to be responsible for failure (Birnbaum 1984). However, at higher stress intensity the crack was found to propagate by the process of enhanced localized plasticity (Shih, Robertson, and Birnbaum 1988). Thus, suggesting that the local stress state determines the operating mechanism. Furthermore, in the case of stainless steel and Fe there have been reports of enhanced dislocation mobility in the presence of hydrogen (P. Ferreira, Robertson, and Birnbaum 1998; S. Wang et al. 2014). On the other hand, hydrogen has been shown to

increase susceptibility to decohesion (Troiano 1960; R. A. Oriani 1972; Vehoff and Rothe 1983). These instances clearly highlight the ambiguity concerning the HE mechanism. Therefore, to gain insights into the HE mechanism, the following multi-scale issues need to be examined: a) the chemical process by which the oxide layer on the surface is penetrated by the hydrogen atoms to enter the microstructure; b) the influence of the interactions of the hydrogen atoms with the microstructural features (grain, grain boundary, crack, triple junctions, dislocations etc.) on the transport mechanism and c) the effect of hydrogen on the surface energies of the GBs. This dissertation will focus on understanding the interaction of hydrogen with defects (crack, dislocation and grain boundary) from the perspective of deformation behavior.

## 2.2 Literature Review on Hydrogen Embrittlement

In this section, a literature review of the proposed HE mechanisms affecting both the physical and chemical properties of many intrinsically ductile metals, including nickel (Vehoff and Rothe 1983; Lassila and Birnbaum 1986; Lassila and Birnbaum 1987; Lassila and Birnbaum 1988; Jun Song and Curtin 2011), aluminum (Scamans 1978; Pouillier et al. 2012), iron (Johnson 1874; Pfeil 1926; Vehoff and Rothe 1983; Andrew 1914; Bernstein 1970; Bhatia and Solanki 2013; Masatake Yamaguchi et al. 2011; Hwang and Bernstein 1983; S. Wang et al. 2013; S. Wang et al. 2014) and titanium (Shih, Robertson, and Birnbaum 1988; Nelson, Williams, and Stein 1972; Hack and Leverant 1982; Birnbaum 1984) will be discussed. In spite of the extensive research on the subject matter multiple hypotheses have been proposed to explain the underlying mechanism (Cotterill 1961; M. Louthan Jr et al. 1972; Ian M. Robertson et al. 2015). The proposed HE mechanisms include:

- Hydride formation

Magnesium, zirconium, titanium, niobium, tantalum and other transition, rare earth and alkaline rare earth metals form hydrides when the hydrogen concentration exceeds the solid solubility. The aggregation of hydrogen at regions of high dilatational stresses (typically at the crack tip) leads to the nucleation of a small size hydride and with increasing stresses, leads to the formation of other smaller hydrides that finally coalesce and lead to brittle fracture behavior (Birnbaum 1984; Shih, Robertson, and Birnbaum 1988) (Figure 2a). The advance of the crack tip further causes redistribution of hydrogen atoms around it, leading to hydride formation. This cyclic process of precipitation-fracture takes places until material failure.

- Hydrogen reaction embrittlement

  The absorbed hydrogen at elevated temperatures reacts with carbides, oxides and other solute elements present in the microstructure to form high pressure steam or methane. This leads to the formation of internal voids and cracks. Copper and steel alloys are mostly affected by the mechanism when exposed to hot hydrogen bearing gases. An example of the chemical reaction that takes places between a copper alloy and absorbed hydrogen:

$$Cu_2O + 2H = 2Cu + H_2O$$

  The hydrogen attack in steel poses a significant problem for petrochemical applications. In this case, the absorbed hydrogen reacts with carbon to form methane, further leading to gas pockets that act as sites for internal voids and crack (Parthasarathy, Lopez, and Shewmon 1985; During 1997).

- Hydrogen enhanced localized plasticity (HELP)

The enhanced dislocation activity in the presence of hydrogen was first inferred by Beachem et al. (Beachem 1972). These conclusions were drawn from the analysis of the ductile features on the fracture surface of the specimen. This was a significant shift from the conventional thinking on the subject matter. Nonetheless, there was a lack of direct microstructural observation of enhanced dislocation activity. To address this dearth in observations, Birnbaum et al. (Shih, Robertson, and Birnbaum 1988; Sofronis and Birnbaum 1995a; Birnbaum and Sofronis 1994; I. Robertson and Birnbaum 1986; P. Ferreira, Robertson, and Birnbaum 1998; S. Wang et al. 2014; Ian M. Robertson et al. 2015) using *in situ* transmission electron microscopy observed enhanced dislocation velocity in the presence of hydrogen. On the other hand, the of removal hydrogen gas caused the dislocation motion to retard. An illustration of the enhanced dislocation mobility in the presence of hydrogen is shown Figure 2b. The positions of the dislocations with and without hydrogen were superimposed such that they show a decrease in the separation distance between dislocations in the presence of hydrogen. The underlying mechanism was based on the idea that the segregation of hydrogen atoms around the dislocations distorts the stress field of the dislocation consequently decreasing the resistance to the dislocation motion posed by the microstructural obstacles (shielding effect) (Birnbaum and Sofronis 1994; Sofronis and Birnbaum 1995a). However, for this mechanism to have a permanent influence, it requires that the hydrogen atmosphere around the dislocation travel with it. This imposes a constraint on the temperature and strain rate window in which this mechanism can be observed.

- Hydrogen enhanced decohesion (HEDE)

In this model, hydrogen accumulates within the lattice leading to the decrease in the cohesive strength of parent atoms (Pfeil 1926; Troiano 1960; R. A. Oriani 1972). The hydrogen atoms segregate like other impurity atoms along the GBs and ahead of the crack tip where the tensile stress is maximum thereby decreasing the cohesive strength. It has been shown in several experimental works that accumulation of hydrogen ahead of the crack tip sharpens the crack tip (Vehoff and Rothe 1983) (Figure 2c-d). The presence of hydrogen at the GBs, has been examined using quantum (Masatake Yamaguchi et al. 2011) and atomistic (Solanki et al. 2012; Rajagopalan, Tschopp, and Solanki 2014) methods that report considerable loss in the cohesive strength of the interface. This mechanism is agreed to be the operating means of failure for materials that do not from hydrides.

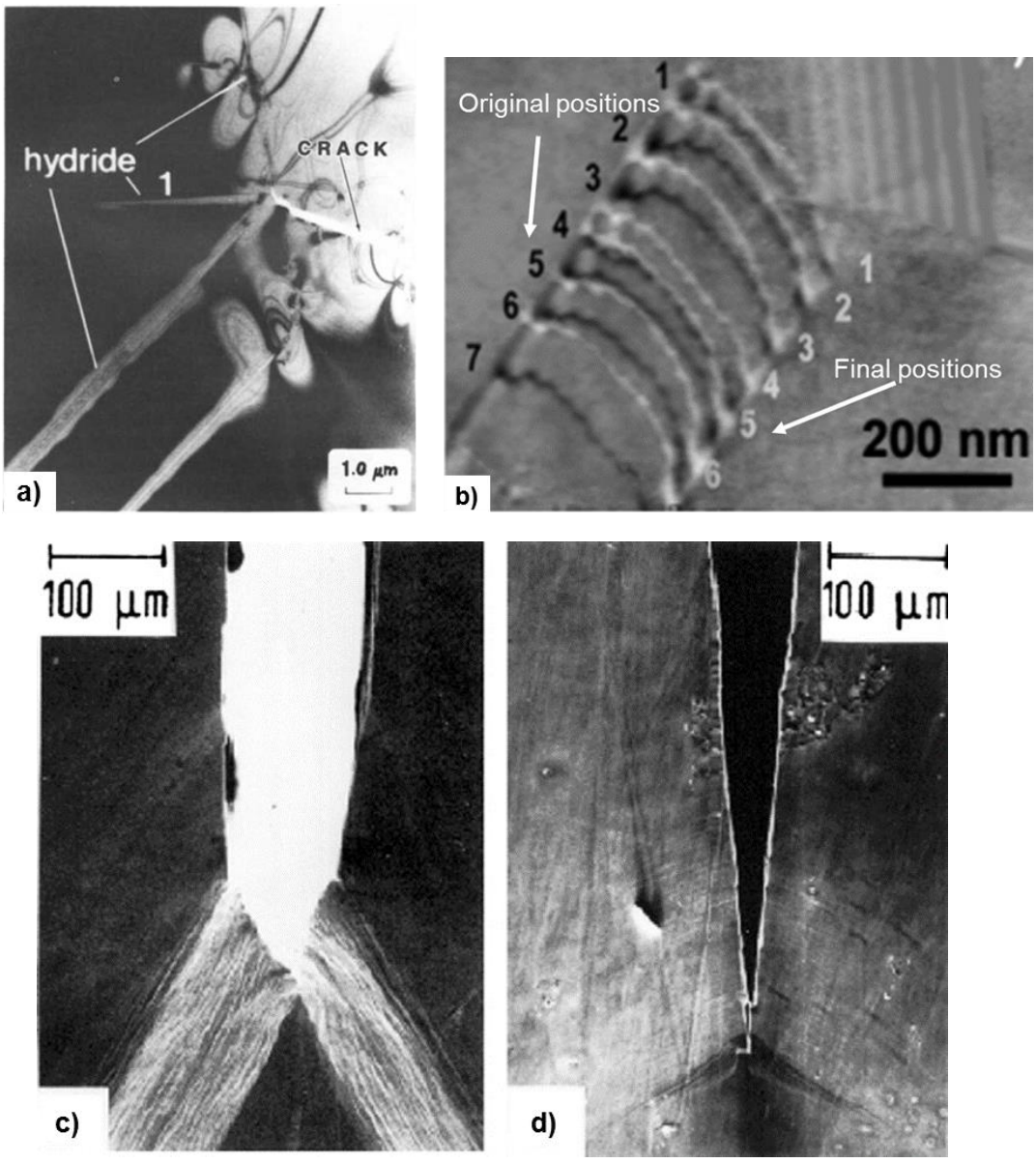


Figure 2: a) The brittle crack advance in the presence of hydride formation ahead of the crack tip α-Ti (Shih, Robertson, and Birnbaum 1988), b) the presence of hydrogen decreases the dislocation-dislocation interaction and thereby increasing the dislocation mobility (P. Ferreira, Robertson, and Birnbaum 1998), c) The crack tip with slip bands and blunting in Fe-3% Si under vaccum and d) In the presence of hydrogen, the crack tip remains sharp (Vehoff and Rothe 1983).

- Adsorption induced dislocation emission (AIDE)

The model proposes the notion that the hydrogen atoms absorbed by the crack surface decrease the dislocation nucleation barrier (S. P. Lynch 1988). Unlike, the HELP mechanism, the external hydrogen atoms play a critical role in the nucleation aspect. The adsorption of hydrogen on the crack tip weakens the interatomic bonds facilitating dislocation emission. The nucleation of dislocations leads to high stress build up within the plastic zone leading to void nucleation and coalescence ahead of the crack tip and coalescence.

The HE mechanisms discussed here do not encompass all the proposed mechanisms in literature. For instance, hydrogen induced ductile to brittle phase transition (Nelson 1994; Jun Song and Curtin 2011; Jun Song and Curtin 2012) or hydrogen triggered phase transformation (Rozenak and Eliezer 1987) along with several others have questionable descriptions of the HE phenomenon. Overall, it has been shown that hydrogen can cause a material to either harden or soften by interacting with dislocations or impurities (I.M. Robertson 2001; Kimura and Matsui 1987). Hydrogen can increase dislocation mobility (Sofronis, Liang, and Aravas 2001b; P. J. Ferreira, Robertson, and Birnbaum 1998) by shielding the elastic interactions between dislocations and other point defects (Sofronis and Birnbaum 1995b). Hydrogen can also induce shear localization and associated plastic instabilities that lead to premature material failure (Sofronis, Liang, and Aravas 2001c). Furthermore, hydrogen diffusion along the GBs and interfaces encourages intergranular failure due to the decohesion mechanism (Matsui, Kimura, and Moriya 1979; Masatake Yamaguchi 2011). Researchers also suggest that hydrogen promotes void nucleation based on experimental data for steels (Kwon and Asaro 1990; M. . Louthan Jr. et al.

1972; R A Oriani 1978; R.A. Oriani and Josephic 1979; T. D. Lee, Goldenberg, and Hirth 1979), nickel alloys (Tang and Thompson 1994; A. W. Thompson 1985) and aluminum alloys (You, Thompson, and Bernstein 1995; Bonakdar et al. 2012). Hydrogen can affect plastic flow by lowering the energy barrier for dislocation slip, thereby enhancing strain localization and also by reducing the dislocation spacing that can affect observed strain hardening (Davenport and Estrup 1990). However, some of these experimental studies have shown discrepant views such as the yield and flow stresses in a uniaxial tension support both increasing (Asano and Otsuka 1976; Ulmer and Altstetter 1991; Abraham and Altstetter 1995a; Watson, Meshii, and Shen 1988) and decreasing (Beachem 1972; Matsui, Kimura, and Moriya 1979; Eastman et al. 1982). Similarly some strain hardening experiments have been questioned for experimental setup error (Myers et al., others 1992; Abraham and Altstetter 1995a; Abraham and Altstetter 1995b). The interplay of the variables that influence embrittlement complicates the separation of which properties affect and do not affect HE such as slip versus cleavage. The difficulties with preparing and fully characterizing experimental samples have made the prospect of accurate simulations appealing. Thus, the various HE mechanism can be carefully examined by observing the influence of hydrogen on the crack tip response using atomistic simulations (Jun Song and Curtin 2012).

## 2.3 Research Objectives

Understanding the fundamental issues that are involved in HE is still a work in progress (S. P. Lynch 2013). In fact, the indeterminate understanding of the mechanistic origin of the HE hinders our ability to satisfactorily address this issue. HE affects several infrastructural applications, such as petroleum, nuclear and naval structures. Therefore, the objectives of this dissertation aim to address some of the critical questions of the HE phenomenon:

1. Understanding the influence of hydrogen on incipient crack tip events in α-Fe.

A major concern with HE is the transition of the service component's mechanical behavior from ductile to low-toughness, brittle. Hydrogen permeates the microstructure through rapid diffusion along the GB networks or by ingress through cracks and diffusing with the dislocations ahead of the crack tip. Thus, it becomes difficult to avoid the interactions between microstructural features and hydrogen atoms. The crack tip presents a preferential trap site for hydrogen and sufficient concentration of hydrogen can change the incipient crack tip behavior to cleavage. Experiments are not definitive enough to separate the dominant factors as it varies based on the interpretation. Hence, a numerical simulation of the problem provides an appealing alternative. For instance, atomic-scale simulations can offer critical understanding regarding the effect of hydrogen on crack tip events (Jun Song and Curtin 2011; Jun Song and Curtin 2012; Matsumoto et al. 2009; S. Taketomi, Matsumoto, and Miyazaki 2010). Thus, examining the competition between dislocation nucleation vs. cleavage under the influence of hydrogen at the atomic length scale can provide insights into the underlying mechanism (Chapter 3). In this section, two distinctly different HE mechanisms were observed depending on the crack orientation: a)

the critical stress intensity factor required for dislocation emission was found to decrease, thereby promoting plastic behavior during deformation (AIDE) and b) the presence of hydrogen around the crack tip reduced the cohesive energy along the cleavage plane, thereby promoting brittle failure (HEDE).

2. Quantifying the role of the GB structure on the hydrogen segregation.

The GBs are the weakest microstructural link during embrittlement, as segregation of hydrogen atoms at the interface reduces the cohesive strength. This behavior leads to sudden catastrophic failure at sub-critical loads due to intergranular fracture. Additionally, the variation in the underlying atomic structure of the GBs results in distinct material behavior. A great deal of research has been conducted on understanding and quantifying these effects across a wide range of scenarios (Kumar, King, and Schwartz 2000; Kumar, Schwartz, and King 2002; Sangid et al. 2011; Tschopp et al. 2012a; Kashinath, Misra, and Demkowicz 2013; N. R. Rhodes, Tschopp, and Solanki 2013; Adlakha et al. 2014; Rajagopalan et al. 2014; Bhatia, Groh, and Solanki 2014; Adlakha and Solanki 2015). The technological advances in 3D characterization capabilities offers experimental quantification of the variations in GB degrees of freedom associated with misorientation between grains and the GB plane (i.e., five-parameters GB character) (Taheri, Rollett, and Weiland 2004; Groeber et al. 2006; Taheri et al. 2010; Bulatov, Reed, and Kumar 2014). These insights coupled with the developments in thermo-mechanical processing techniques can be utilized in engineering the microstructure with desired interfaces (grain boundary engineering) (Watanabe 2011). This has been utilized in development of microstructures with tuned interfaces that have shown improved resistance to stress corrosion cracking (Cheung, Erb, and Palumbo

1994; Shimada et al. 2002; B. et al. 2013; Kobayashi et al. 2008; Kobayashi et al. 2011) and reduced susceptibility to HE (Watanabe and Tsurekawa 2004; Bechtle et al. 2009; Kobayashi et al. 2011). Firstly, this technique demands the systematic investigation of the role of the GB atomic structure on hydrogen segregation (Chapter 4). Here, the hydrogen segregation behavior was quantified across a large database of GBs. The energetic preference of hydrogen atoms to segregate close to each other along the GB was found. Lastly, a physically motivated model that related the intrinsic GB characteristics to the hydrogen segregation behavior was developed.

3. Assessing the effect of hydrogen on slip transmission across GBs in α-Fe.

The strength of a crystalline material is governed by the ability of the microstructure to pin the dislocation motion. In that sense, the GBs present a significant barrier to the dislocation motion through the microstructure. The initiation of a fatigue crack can take place solely due to mechanical loading, but it is highly unlikely. In an aggressive environment the susceptibility for fatigue crack initiation increases (Rice and Wang 1989; Bechtle et al. 2009; Novak et al. 2010; S. Wang et al. 2014). Thus, in order to design environmentally tolerant materials subjected to mechanical loads the influence of hydrogen on the dislocation-grain boundary (DGB) interaction needs to be examined (Chapter 5). This the first study that consistently examines the role of hydrogen on the DGB interactions at the atomic length scale. It was found that the presence of hydrogen increased the energy barrier for the slip transmission. Based on the findings the fatigue crack initiation was reexamined for the effect of hydrogen. The enhanced dislocation mobility due to the surrounding hydrogen atmosphere (HELP) provides an effective transport medium to deposit hydrogen atoms along the GB. On the other hand, the

increasing concentration of hydrogen leads to a reduction in the cohesive strength of the interface. Therefore, in the absence of a feasible mechanism for the trapped dislocation intergranular crack initiation becomes a viable option. These insights will aid in the development of multi-scale predictive capabilities and the optimization of the interfacial network for a polycrystalline material subjected to mechanical loads in an aggressive environment.

## 4. Quantifying the role of hydrogen on the dislocation mobility in α-Fe

A predictive model that can capture the physical aspects at the atomic scale of the plastic deformation is critical in order to design structural materials. In the case of body centered cubic (BCC) metals, this task has proven challenging due to the complexity associated with the non-Schmid nature of plastic flow (Rodney and Martin 2000; Itakura, Kaburaki, and Yamaguchi 2012; Proville, Rodney, and Marinica 2012; Ventelon and Willaime 2010; Hale, Zimmerman, and Weinberger 2014; Hale et al. 2015; Lim et al. 2015; Gröger, Bailey, and Vitek 2008; Duesbery and Vitek 1998; Christopher R. Weinberger, Tucker, and Foiles 2013; Christopher R. Weinberger et al. 2012). At room temperature, the plastic deformation takes place primarily by the glide of the $a/2\langle 111\rangle$ screw dislocations. Thus, in order to accurately model the role of hydrogen on dislocation motion, atomistic simulations are required to evaluate the change in the continuum description of the yield surface in the presence of hydrogen (Chapter 6). Here, we present preliminary results from the methodology developed to examine the effect of hydrogen on the non-Schmid behavior of the Peierl's stress.

5. Investigate the intrinsic properties and the hydrogen segregation behavior of grain boundary triple junctions.

Nanocrystalline materials (mean grain size, $d < 100$ nm) have enhanced mechanical properties compared to polycrystalline materials ($d > 1$ μm). The technological advances in material processing have made nanocrystalline materials a viable option (Valiev, Xia, and Langdon 2009). However, the stability of the nanocrystalline microstructure at elevated temperature has been a challenge. It has been long established that the structural stability, mechanical behavior and fracture of nanocrystalline materials are often driven by GBs (planar defects), triple junctions (line defects), and their underlying structures (Meyers, Mishra, and Benson 2006; Gleiter 2000). Hence, the intrinsic properties of the triple junction (TJ) that influence the material properties requires attention in the development of interface-dominant materials, especially in the case of nanocrystalline materials where TJs constitute a large volume fraction (Gleiter 2000). Further, the presence of hydrogen around the TJ can increase the susceptibility to crack nucleation as the TJs act as effective sinks for defect aggregation (Chapter 7). In this chapter we present a future research idea, the following key insights were accrued: a) a systematic methodology to study the effect of TJ on structural stability was developed; b) a strong energetic preference for self-interstitial atom around the TJ over a vacancy defect was observed and c) the defect segregation behavior across a wide range of temperature for a TJ were found to be distinctly different from the constituent GBs.

# CHAPTER 3

# 3 EFFECT OF HYDROGEN ON THE INCIPIENT CRACK TIP EVENTS IN α-Fe

## 3.1 Introduction

HE has been a consistent problem in the application of metals in harsh environmental settings for decades (Rogers 1968; Merrick 1989; Energy et al. 2004; P. R. Rhodes, Skogsberg, and Tuttle 2007). In the past, various mechanisms in the literature including hydrogen-enhanced decohesion (HEDE) (Troiano 1960; R. A. Oriani 1972; R. A. Oriani and Josephic 1974; Gerberich, Marsh, Hoehn, Venkataraman, Huang, et al. 1993; Gerberich, Marsh, Hoehn, Venkataraman, and Huang 1993), hydrogen-enhanced local plasticity (Birnbaum and Sofronis 1994; Abraham and Altstetter 1995a; Sofronis, Liang, and Aravas 2001a), adsorption-induced Hydrogen dislocation emission (S. P. Lynch 1988; Y. Liang and Sofronis 2003) and cleavage (Gahr, Grossbeck, and Birnbaum 1977; Shih, Robertson, and Birnbaum 1988; Oda and Noguchi 2005) all of which have been developed to explain the HE phenomenon in Fe. However, these proposed theories are often contradictory resulting in a lack of agreement on the underlying mechanism. For instance, whether HE occurs due to dislocation starvation, a significant increase in dislocation density due to an increase in dislocation mobility or reduction in surface/cohesive energies is still not understood.

Atomistic (Matsumoto et al. 2009; S. Taketomi, Matsumoto, and Miyazaki 2010; Jun Song and Curtin 2011; Jun Song and Curtin 2012; Solanki et al. 2012; Rajagopalan et al. 2014; Bhatia, Groh, and Solanki 2014) and quantum mechanics-based (Masatake Yamaguchi 2011; Zhao and Lu 2011a; Itakura, Kaburaki, and Yamaguchi 2012)

simulations have been increasingly utilized in investigations of the fundamental HE mechanism. These studies include hydrogen-dislocation core interactions (Zhao and Lu 2011a; Bhatia, Groh, and Solanki 2014), GB segregation (Solanki et al. 2012; Solanki et al. 2013; Rajagopalan, Tschopp, and Solanki 2014) and the effect of hydrogen on crack tip events (Matsumoto et al. 2009; S. Taketomi, Matsumoto, and Miyazaki 2010; Jun Song and Curtin 2012).

In this work, we examine the influence of hydrogen on the incipient crack tip events in α-Fe. The objective was to gain atomistic insights into stress-corrosion mechanisms for HE in iron. A multi-scale approach was employed by utilizing the density functional theory (DFT) and atomistic simulations. The effect of hydrogen on generalized stacking fault energy was quantified with the help of density functional theory. Further, these findings were employed in evaluating the Rice-Thompson criterion to predict the critical stress intensity factor required for dislocation nucleation ahead of a crack tip. The predicted behavior was compared against the observed incipient crack tip events using atomistic simulations for different single crystal orientations in Fe subjected to Mode-I loading conditions. It was found that the increasing coverage of hydrogen on the shear plane decreases the generalized stacking fault energy, thereby decreasing the critical stress intensity factor for dislocation emission. On the other hand, the presence of hydrogen reduces the cohesive strength of the material (Jiang and Carter 2004). Further, it was found that the presence of hydrogen decreased the critical stress intensity required for cleavage and dislocation nucleation in different crack orientations.

Therefore, implying the co-existence of both characteristics of HE depending on the crack orientation: a) the critical stress intensity factor for dislocation nucleation ahead of the crack tip decreases in the presence of hydrogen and b) The presence of hydrogen ahead of crack tip promotes brittle behavior by weakening the interatomic bonds along the cleavage plane.

## 3.2 Methodology

### 3.2.1 *Generalized Stacking Fault Energies (GSFE)*

Here, DFT calculations to characterize GSFE curves were performed using the Vienna Ab-initio Simulation Package (VASP) plane wave electronic structure code (Kresse and Hafner 1993; Kresse and Furthmüller 1996a; Kresse and Furthmüller 1996b). The generalized stacking fault energy serves as a measure of energy required to nucleate a dislocation in a ductile material. The projector augmented wave (PAW) (Blöchl 1994; Kresse and Joubert 1999) potentials were used to represent the nuclei and core electrons up to the 3p shell with $3d^7$ and $4s^1$ as valence electrons for Fe. Exchange and correlation was treated with generalized gradient approximation (GGA) using the PBE formulation (Perdew, Burke, and Ernzerhof 1997) with an energy cutoff of 380 eV and the Monkhorst Pack k-point of 14x18x1. To compute energy differences along the slip directions, periodic boundary conditions were maintained along the X <112> and Y <111> directions; whereas, a vacuum of 15 Angstrom was introduced along the third direction (Z <110> direction). An incremental shear displacement of 0.01% was applied on the top of the unit cell along the Y direction. Each displacement increment was followed by a

nonlinear conjugate gradient energy minimization process with energy criteria of 0.1 meV on each atom.

3.2.2 *Studying the Incipient Crack Tip Response with Mode I Fracture Specimens*

A parallel molecular dynamics code (large-scale atomic/molecular massively parallel simulator, LAMMPS (Plimpton 1995)) with a semi-empirical embedded atom method (EAM) (M. S. Daw and Baskes 1984) potential was used to study the role of H on plastic events and the subsequent crack dynamic behavior in $(111)\ [11\bar{2}]$ (Orientation-I) and $(010)\ [10\bar{1}]$ (Orientation-II) crack orientations (refer Table 1 for details). For an overview of atomistic simulations refer to Appendix A. In this work, we employed the EAM potential of Ramasubramaniam et al. (Ashwin Ramasubramaniam, Itakura, and Carter 2009a) to describe the Fe-H system, which is based on the Fe EAM potential of Hepburn and Ackland (Hepburn and Ackland 2008). The Fe-H potential was parameterized using an extensive database of energies and configurations from DFT calculations of the dissolution and diffusion of hydrogen in bulk α-Fe, the binding of hydrogen to free surfaces, vacancies and dislocations as well as other cross interactions between hydrogen and Fe. Moreover, the binding and the formation energies corresponding to multiple hydrogen-segregations to bulk α-Fe are consistent with the values predicted using ab initio calculations and experimentation (Hayward and Deo 2011a). This potential has been used to study hydrogen-dislocation core interactions (Shinya Taketomi, Matsumoto, and Miyazaki 2008; Zhao and Lu 2011b), GB segregation (Matsui, Kimura, and Moriya 1979; Masatake Yamaguchi 2011; Solanki et al. 2012; Rajagopalan, Tschopp, and Solanki 2014) and subsequent decohesion (Solanki et al. 2013) as well as the effect of hydrogen on generalized stacking fault energies (Shinya

Taketomi, Matsumoto, and Miyazaki 2010) and surface energies (Ashwin Ramasubramaniam, Itakura, and Carter 2009b; Jiang and Carter 2003), and it has shown good agreement with DFT results. Therefore, in this work the aforementioned potential was deemed appropriate for studying the role of hydrogen on crack tip deformation.

Molecular statics (0 K) fracture simulations were performed using the displacement field corresponding to a semi-infinite crack being subject to stress intensity factor ($K_I$) at infinity (Figure 3). These simulations were used to quantify the critical stress intensity factor for the first plastic/cleavage event from the crack tip and to corroborate with the Rice-Thompson predictions. The cylindrical specimens were loaded along the X ($u$), Y ($v$) and Z ($w$) directions using the following conditions:

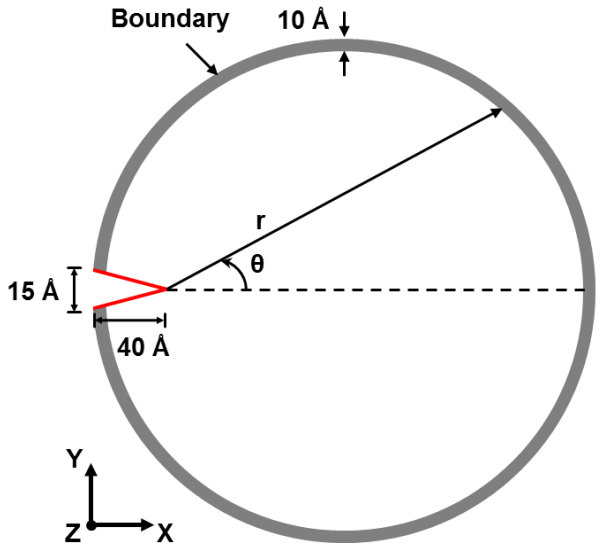


Figure 3: The geometric representation of a fracture specimen that was subjected to Mode-I loading by displacing boundary atoms using the molecular statics framework.

$$u(r,\theta) = K_I \frac{1+\vartheta}{E}\sqrt{\frac{r}{2\pi}}cos\frac{\theta}{2}(2-4\vartheta+2sin^2\theta)$$
$$v(r,\theta) = K_I \frac{1+\vartheta}{E}\sqrt{\frac{r}{2\pi}}sin\frac{\theta}{2}(4-4\vartheta+2cos^2\theta)$$
$$w(r,\theta) = 0 \qquad (1)$$

where $K_I$ is the stress intensity factor for a Mode-I loading, $\vartheta$ is the Poisson's ratio ($\vartheta = 0.3$), E is the Young's modulus (E = 230 GPa), and $r$ and $\theta$ are the polar coordinates defined from the crack tip as shown in Figure 3. These displacement boundary conditions were applied to atoms within 1 nm of the cylindrical surface as shown in Figure 3. The displacement fields were varied by incrementally changing the stress intensity factor ($\Delta K = 1.5 \times 10^{-3}$ MPa$\sqrt{m}$) (Ringdalen Vatne et al. 2013; Ko et al. 2013). The boundary along the Z direction was modeled with a periodic boundary condition while the X and Y boundaries were modeled as free surfaces. The minimum dimension for the entire specimen at equilibrium was approximately 20 nm in radius and was 4 nm thick along the Z direction (~300,000 atoms). Atoms were deleted to create an atomistically sharp crack of 4 nm length. Each displacement increment was followed by a nonlinear conjugate gradient energy minimization process.

Table 1: The different crystallographic orientations employed in the Mode-I specimen

| | **X** | **Y** | **Z** |
|---|---|---|---|
| Orientation-I | $[100]$ | $[010]$ | $[001]$ |
| Orientation-II | $[\bar{1}10]$ | $[111]$ | $[11\bar{2}]$ |
| Orientation-III | $[\bar{1}0\bar{1}]$ | $[010]$ | $[10\bar{1}]$ |

3.3 Results

3.3.1 *Theoretical Analysis of the Effect of Hydrogen on the Incipient Crack Tip Behavior*

The effect of hydrogen on the generalized stacking fault energy (GSFE) curve of Fe was plotted as a function of shearing distance along the Burgers vector direction $\left(\frac{a}{2}\langle 111\rangle\right)$ (Figure 4a). The presence of segregated hydrogen atoms in the vicinity of the shear plane

significantly decreases the stacking fault energy barrier (Figure 4a). Further, the Rice-Thompson (RT) criterion (Rice 1992) was employed to predict the critical stress intensity factor for a dislocation nucleation ahead of the crack tip. The RT criterion is dependent on the angle between normal to the crack tip *and* the slip direction ($\phi$) and *f* defines the geometry factor dependent on the angle between the slip plane and crack plane.

$$K_{disl} \geq f\sqrt{\frac{2\mu\gamma_{us}}{1-\vartheta}[1+(1-\vartheta)tan\phi]} \qquad (2)$$

where $\mu$ is the shear modulus. To quantify the effect of hydrogen on critical stress intensity factor, we used the calculated unstable stacking fault energy ($\gamma_{us}$) from Figure 4b. The effect of hydrogen on critical stress intensity factor was quantified with the help of the change in unstable stacking fault energy in the presence of hydrogen (Figure 4b). It was found that increasing hydrogen concentrations decrease the critical stress intensity factor required for dislocation nucleation ahead of the crack tip (Figure 4c). This creates opportunities for localized plasticity, which is consistent with the available experimental data. Therefore, the theoretical analysis appears to be consistent with the mechanisms suggested in the HELP model (Birnbaum and Sofronis 1994) and AIDE model (S. P. Lynch 1988). However, examining the effect of hydrogen on the crack tip deformation in a continuum framework several assumptions are made. For instance, the competition between the crack tip events is evaluated for an athermal scenario (T = 0 K). Further, the analysis ignores the anistropic effect in estimating the dislocation emission. Lastly, there is no accountability for dislocations processes not directly related to the crack tip

deformation. Therefore, the RT criterion can only serve as an indicative tool for studying the effect of hydrogen on incipient crack tip events.

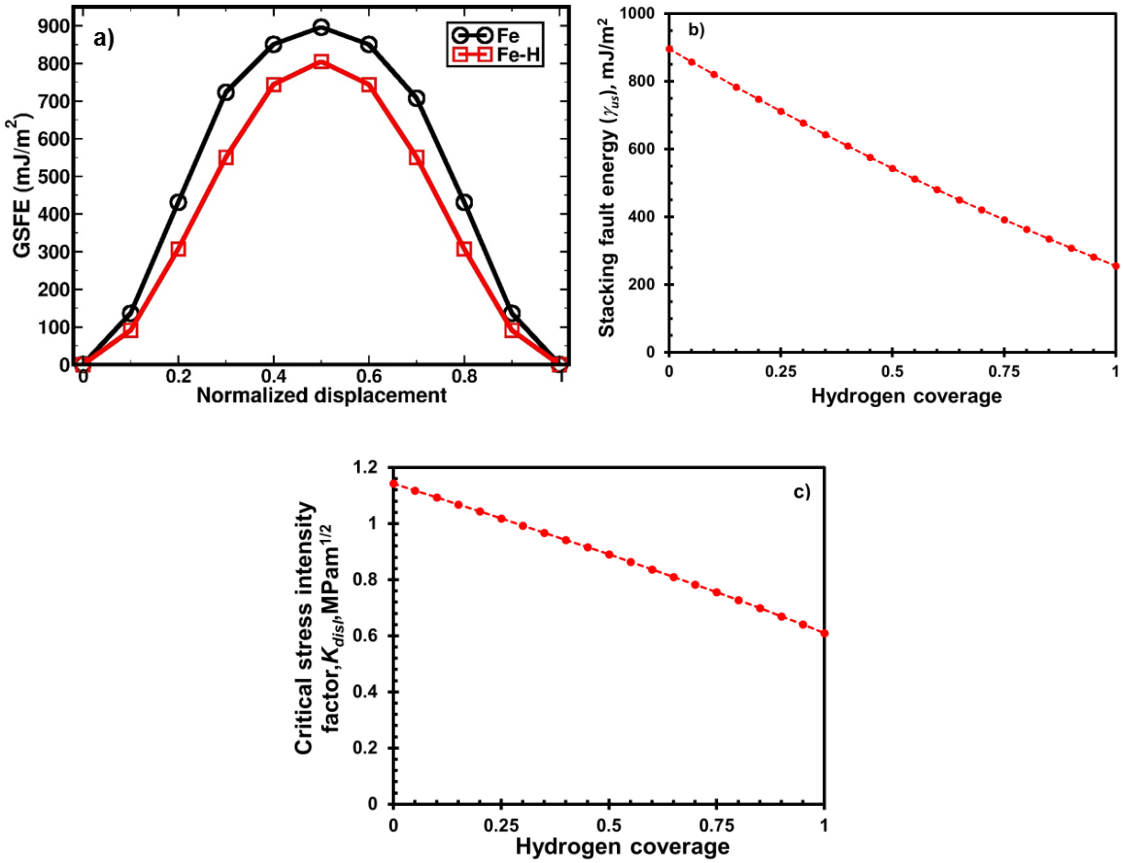


Figure 4: a) The effect of hydrogen on the generalized stacking fault energy for Fe. b) The effect of hydrogen coverage on the unstable stacking fault energy in Fe. c) The resultant change in critical stress intensity factor for dislocation nucleation using the Rice-Thompson criterion.

3.3.2 *Effect of Hydrogen on the Incipient Crack Tip Events in Iron*

3.3.2.1 *Orientation-I*

The influence of hydrogen on the incipient events for the (010)[001] crack orientation was examined here. In the absence of hydrogen at the crack tip, the crack growth takes place along the (110) plane at a critical stress intensity factor of 0.59

MPa$\sqrt{m}$ (Figure 5a). This is consistent with surface energy variations in iron, the (110) plane has the lowest surface energy.

An initial concentration ($c_0$) of $4 \times 10^{-4}$ of hydrogen was introduced ahead of the crack tip. The presence of hydrogen reduces the critical stress intensity factor (0.48 MPa$\sqrt{m}$) required for initiation of cleavage behavior along the (110) plane (Figure 5b).

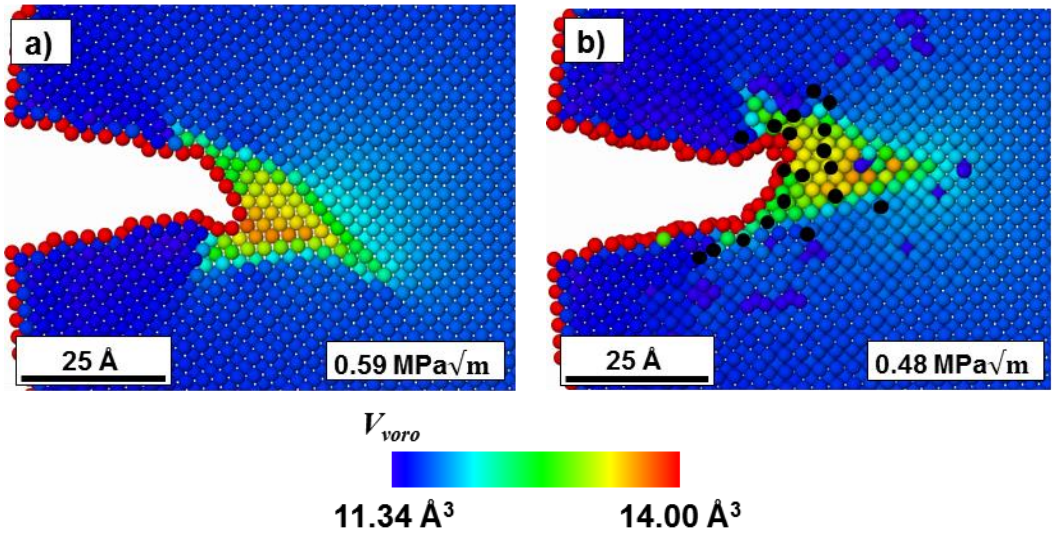


Figure 5: a) The incipient cleavage crack advance along the (110) plane for the $(010)[001]$ orientation is in agreement with the theoretical predictions. b) The presence of a hydrogen rich environment ahead of the crack tip reduces the critical stress intensity factor required for cleavage. The atoms were colored according to atomic volume estimated by the Voronoi tessellation.

3.3.2.2 *Orientation-II*

Here, we investigate the interplay between various embrittlement mechanisms observed in hydrogen rich environments by examining the incipient crack tip event for the $(111)[11\bar{2}]$ crack orientation. The presence of hydrogen on the slip plane where dislocation nucleation took place for pure Fe causes the dislocation nucleation to occur on another plane (Figure 6) similar results have been seen for the dislocation emission in a Ni-H system (J. Song, Soare, and Curtin 2010).

Thus, it was found that the presence of hydrogen ahead of the crack tip decreases the critical stress intensity factor required for dislocation nucleation. However, the dislocation propagation was preferred along an alternate slip plane that was free of hydrogen (see Figure 6b).

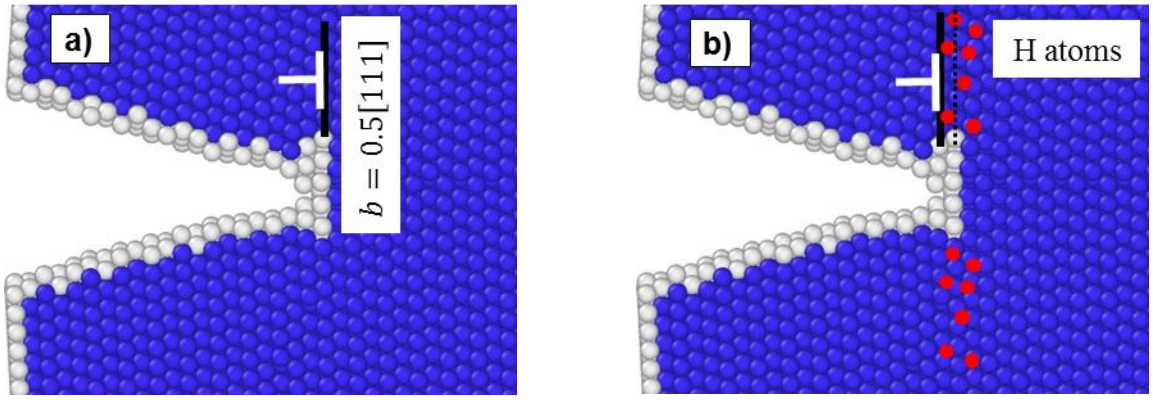


Figure 6: a) The emission of an edge dislocation ahead of the crack tip with an orientation of $(111)[11\bar{2}]$. b) The presence of H shifts the slip plane away from the H rich environment. The atoms were colored according to common neighbor analysis (CNA) such that BCC atoms are blue and defects white and hydrogen atoms were depicted with red color.

An edge dislocation was nucleated with a Burgers vector of $\frac{a}{2}[111]$ at $K_I$ = 1.35 MPa.m$^{1/2}$ (Figure 7a). In the presence of hydrogen ahead of the crack tip, the nucleation of the dislocation took place at $K_I$ = 1.2 MPa.m$^{1/2}$ (Figure 7b). The critical stress intensity factor for the dislocation emission decreases in the presence of hydrogen, promoting an increase in plastic behavior during deformation (S. P. Lynch 1984). However, the edge dislocation gets pinned in a hydrogen atmosphere until $K_I$ reaches 1.4 MPa.m$^{1/2}$ (Figure 7c). This is in agreement with previous findings in literature (P. Ferreira, Robertson, and Birnbaum 1998; P. J. Ferreira, Robertson, and Birnbaum 1999; Tapasa, Osetsky, and Bacon 2007; I. Robertson and Birnbaum 1986; Bhatia, Groh, and Solanki 2014) that solute rich environments present an obstacle to dislocation motion. However, the hardening provided by a hydrogen atmosphere is relatively small compared to carbon,

and is only observable at the small time scales accessed by atomistic simulations. Hydrogen has a high diffusivity at room temperature in iron to move along with the glissile dislocations and provides a shielding effect on the interactions between dislocations. Thus, creating conditions for enhanced mobility at room temperature (S. Wang et al. 2014; P. J. Ferreira, Robertson, and Birnbaum 1999; P. Ferreira, Robertson, and Birnbaum 1998; I. Robertson and Birnbaum 1986).

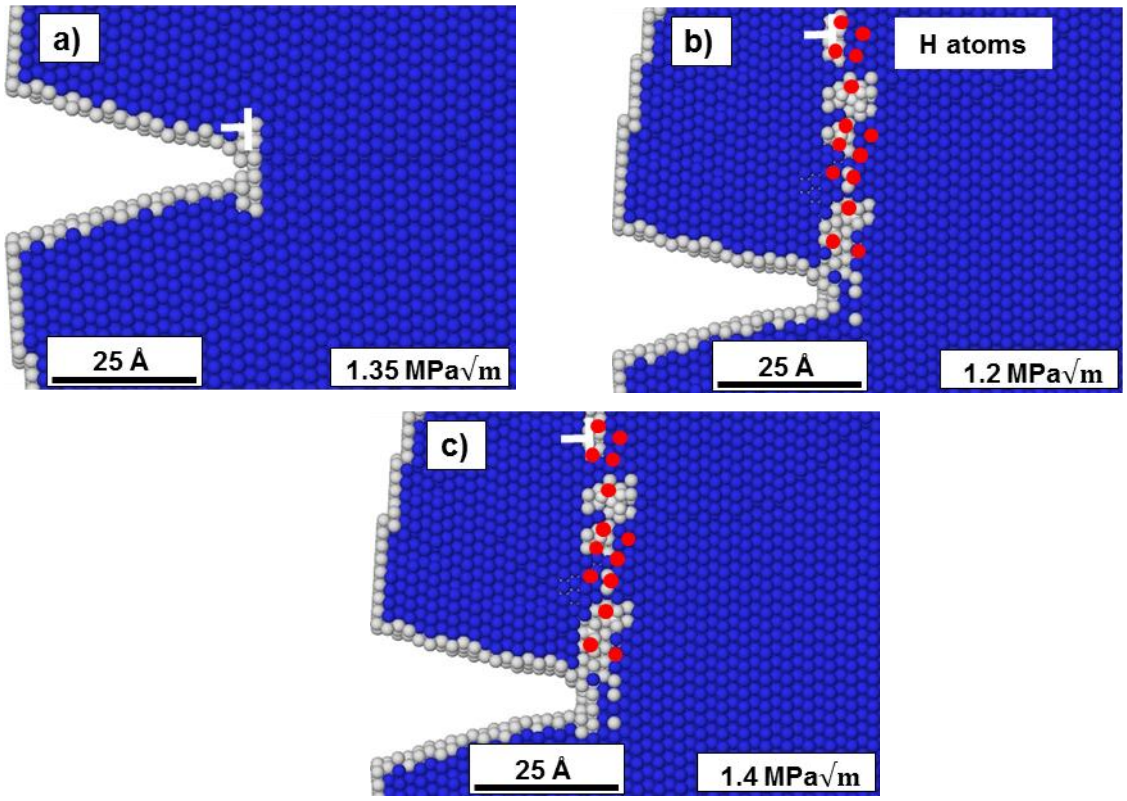


Figure 7: The effect of H coverage on the critical stress intensity factor for a dislocation nucleation in $(111)[11\bar{2}]$. a) The hydrogen free crack tip event had a nucleation of edge dislocation. b) The incipient events when H atoms were placed along the slip plane lead to a decrease in the critical stress intensity factor required for the dislocation nucleation. c) The effect of a H rich region on the dislocation mobility. The atoms were colored according to CNA, where blue represents the BCC lattice atoms, white represents the defect atoms and red represents the hydrogen atoms.

3.3.2.3 *Orientation-III*

The crack plane was oriented along the $(010)$ plane and the crack front along the $[10\bar{1}]$ direction. This orientation is known to exhibit crack propagation along the (010)

cleavage plane under the Mode I fracture. The effect of H ahead of the crack tip on brittle fracture behavior was studied by random addition of H atoms along the cleavage plane ahead of the crack tip. The critical stress intensity factor for the crack growth decreased from 0.85 MPa.m$^{1/2}$ to 0.73 MPa.m$^{1/2}$ in the presence of hydrogen (Figure 7). These findings clearly show that hydrogen reduces the material resistance during brittle fracture (HEDE).

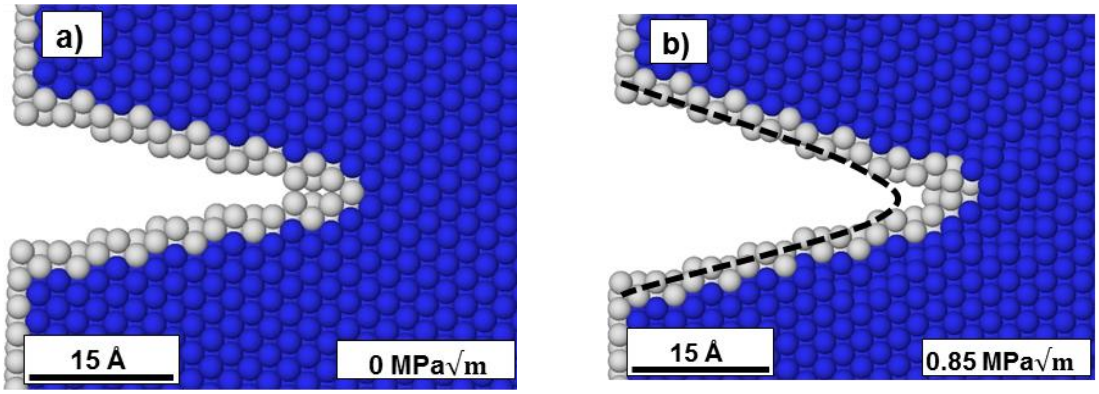

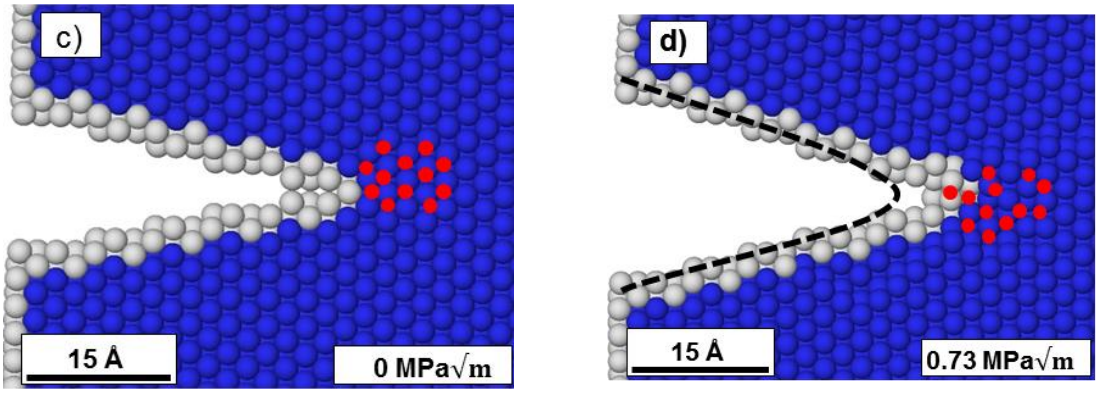


Figure 8: The effect of H coverage on the crack tip deformation for the $(010)[10\bar{1}]$ crack orientation. a-b) show the crack tip events for a hydrogen free crack tip. c-d) shows premature crack propagation, due to the presence of H atoms ahead of the crack tip. The dashed curve outlines the initial crack geometry. The atoms were colored according to CNA, blue represents the BCC lattice atoms, white the defect atoms and red the hydrogen atoms.

3.4 Conclusions

The following conclusions can be drawn based on studying the influence of hydrogen on the incipient crack tip events in α-Fe:

1. The presence of hydrogen has a dual role on the dislocation motion in α-Fe as it aids in the nucleation of dislocation from the crack tip. Simultaneously, the hydrogen rich atmosphere offers an initial microscopic resistance to the dislocation motion. The hydrogen atoms have an energetic preference to segregate around the dislocation core (Bhatia, Groh, and Solanki 2014). However, the resistance is only observable at the small time scales examined by atomistic simulations as at room temperature hydrogen readily diffuses along with mobile dislocations.
2. The presence of hydrogen atoms ahead of the crack tip were found to reduce the work done for initiating a cleavage fracture.

3. In this study, we have successfully demonstrated the co-existence of both characteristics of HE: a) the hydrogen enhanced plasticity where the critical stress intensity factor for dislocation nucleation ahead of the crack tip decreases and a shielding effect is created by the segregation of hydrogen atoms around the dislocation, thereby reducing dislocation-dislocation interaction (Bhatia and Solanki 2013) and enhancing the mobility of dislocations (HELP); b) The presence of hydrogen reduces the work of decohesion by reducing the strength of interatomic bonds on the cleavage plane.

# CHAPTER 4

# 4 THE ROLE OF GRAIN BOUNDARY STRUCTURE ON HYDROGEN SEGREGATION

## 4.1 Introduction

Grain boundaries act as preferential sites for impurity segregation (Sadananda and Vasudevan 2011; S. Lynch 2012; Barnoush and Vehoff 2010; Solanki et al. 2012; Birnbaum and Sofronis 1994). Aggregation of sufficient concentration at the interface can lead to a sudden intergranular failure (Rice and Wang 1989). This is a serious problem for structural components in aggressive environments such as α-Fe based alloys that fail catastrophically in the presence of dilute NaCl solutions. The degrading effects of HE were first observed almost 140 years back (Johnson 1874). Since, a great deal of research on understanding the HE mechanism has been carried out (Pfeil 1926; Vehoff and Rothe 1983; Shih, Robertson, and Birnbaum 1988; P. Ferreira, Robertson, and Birnbaum 1998; Birnbaum and Sofronis 1994; Lufrano, Sofronis, and Birnbaum 1998). Due to the high diffusivity, the hydrogen atoms permeate the microstructure rapidly along the GB networks, dislocations and voids etc leading to mechanical degradation. However, it is the intergranular embrittlement that leads to a sudden catastrophic failure. The susceptibility to intergranular fracture increases in the presence of adequate hydrogen concentration at the interface (Banerji, McMahon, and Feng 1978; McMahon Jr and Vitek 1979; Masatake Yamaguchi et al. 2011; McMahon 2001; Solanki et al. 2012; Rajagopalan, Tschopp, and Solanki 2014). The GB engineering approach tailors the microstructure with certain interfaces to mitigate intergranular fracture. Significant

progress has been made to develop embrittlement-resistant material systems through this approach (Palumbo, Doyle, et al. 1991; Palumbo, King, et al. 1991; Watanabe 1994; Aust, Erb, and Palumbo 1994; Watanabe and Tsurekawa 1999; Bechtle et al. 2009; Kobayashi et al. 2011). The fundamental step is the identification of the type of the relation that exists between the underlying GB structure and the segregation energy landscape in a quantitative manner. The solute segregation behavior is known to be greatly influenced the local atomic structure. This in turn affects the intergranular fracture behavior (Hondros et al. 1996; Lejček and Hofmann 1995; Lejček, Hofmann, and Paidar 2003). For instance, "special" low energy GBs such as twin GBs exhibit limited segregation potency and are, thus highly resistant to embrittlement (Masatake Yamaguchi et al. 2011; Masatake Yamaguchi 2011; Solanki et al. 2012; N. R. Rhodes, Tschopp, and Solanki 2013; Rajagopalan, Tschopp, and Solanki 2014; Tschopp et al. 2014). The GB character often encompasses the macroscopic degrees of freedom. In other words, it describes the five degrees of freedom associated with the misorientation between the crystallographic orientations of the two adjoining grains. Three degrees of freedom are used to define the misorientation between the two grains and two degrees of freedom are associated with the GB plane. The microscopic degrees of freedom cover the local structure arrangement that are dependent on the translations between adjoining grains which is important as well as the localized dislocation structure of the boundary.

In the past few decades, a lot of research has been conducted on developing techniques to describe the grain boundary's degrees of freedom (Burgers 1940; Bragg and Nye 1947; Read and Shockley 1950; Bishop and Chalmers 1968; Hirth and Balluffi 1973; Hirth 1974; Grimmer, Bollmann, and Warrington 1974; Pond, Smith, and Vitek

1979; A. P. Sutton and Vitek 1980) and their influence on physical properties. These models have utilized dislocation arrays, disclinations and coincident site lattice (CSL) to describe microscopic and macroscopic degrees of freedom of GBs. Based on identifying the favored GB for the corresponding GB systems, these methodologies (A. Sutton and Vitek 1983; Rittner and Seidman 1996; Bristowe and Crocker 1978; Pond 1979; Pond, Smith, and Vitek 1979; Ingle and Crocker 1980; Vitek, Smith, and Pond 1980; A. Sutton 1982; A. Sutton 1989) described the structural elements comprising symmetric tilt, asymmetric tilt, twist and twin GBs. They determined that the favored GBs are entirely composed of unique structural units that cannot be decomposed into other GB structures. Experimentally, GB structure has been observed using field ion microscopy and high resolution transmission electron microscopy (Brandon 1966; Pond 1977; Balluffi 1977; Bristowe and Crocker 1978; Merkle and Wolf 1992).

Experimental studies are often limited in examining solute segregation near GBs because of the complicated atomic structure. On the other hand, atomistic and first principle calculations can be effectively utilized to explore the complicated interactions between the GB structure and solute atoms (Masatake Yamaguchi, Shiga, and Kaburaki 2004; M. Yamaguchi, Nishiyama, and Kaburaki 2007; Masatake Yamaguchi 2011; Solanki et al. 2012; Rajagopalan, Tschopp, and Solanki 2014; Tschopp et al. 2012b). For instance, Yamaguchi et al. (Masatake Yamaguchi 2011) used density functional theory to examine the segregation of boron and carbon to iron GBs and found that these trace elements can be beneficial by strengthening GB cohesion. These results indicate that the segregation behavior of these elements plays an important role in GB embrittlement or strengthening (Cr) behavior. Further, the presence of sulphur and hydrogen was found to

drastically decrease the cohesive strength. These results highlight the importance of the solute elements on the embrittlement/strengthening mechanism at the GB. Additionally, the underlying GB structure can greatly influence the segregation behavior. The segregation behavior of solutes/vacancies around microstructural features such as grain boundaries, dislocation core and TJs have been examined to understand the role of the underlying atomic structure (Solanki et al. 2012; N. R. Rhodes, Tschopp, and Solanki 2013; Rajagopalan, Tschopp, and Solanki 2014; Bhatia and Solanki 2013; Adlakha and Solanki 2015). These studies provide a generalized framework for exploring how GB character over a large number of boundaries can affect the solute segregation behavior.

Molecular statics simulations were employed to investigate the influence of the underlying atomic structure on the hydrogen segregation behavior and the consequent embrittlement for the Fe-H system. A database consisting of <100>, <110>, <111> and <112> symmetric tilt GBs in α-Fe were generated at 0 K with the help of LAMMPS (Plimpton 1995). In this work, two hydrogen defect configurations were examined: a) a single hydrogen atom at an interstitial and b) two hydrogen atoms at an interstitial. The following research shows that both the GB structure and the hydrogen defect configuration play a significant role in hydrogen segregation and the subsequent embrittlement of α-Fe. However, an increased energetic preference due to the hydrogen-hydrogen interaction was found for the case of two hydrogen atoms at an interstitial site. Finally, a physically motivated model capturing the probabilistic segregation behavior was developed for various hydrogen defect configurations thereby enabling the identification of GB interfaces for mitigating the HE by using the intrinsic properties of the interface.

## 4.2 Methodology

Molecular statics simulations using the semi-empirical embedded atom method (EAM) (Murray S. Daw and Baskes 1983; M. S. Daw and Baskes 1984) potentials were used to describe the Fe-H system (Ashwin Ramasubramaniam, Itakura, and Carter 2009a). The reader is encouraged to refer to Appendix A for an overview to atomistic simulation methods. This potential was parameterized using an extensive database of energies and configurations from DFT calculations of dissolution and diffusion of H in bulk α-Fe, the binding of H to free surfaces, vacancies and dislocations as well as other cross interactions between H and Fe atoms. The formation and binding energies of multiple H atoms within a monovacancy in bulk α-Fe using this potential were found to be in good agreement with DFT predictions and experiments (Hayward and Deo 2011a).

The equilibrium 0 K GB structure and energy was calculated using a bicrystal computational cell with three-dimensional (3D) periodic boundary conditions consisting of two grains. The minimum distance between the two periodic boundaries in each computational cell was 12 nm (see Figure 9a). As with past work (Tschopp, Spearot, and McDowell 2008; Tschopp et al. 2012b; Solanki et al. 2012), an atom deletion criterion along with multiple initial configurations with various in-plane rigid body translations were utilized to accurately obtain an optimal minimum energy GB structure via the nonlinear conjugate gradient energy minimization process.

A large database consisting of <100>, <110>, <111> and <112> symmetric tilt grain boundaries (STGBs) in α-Fe were generated at 0 K. Next, the segregation behavior of various defect configurations was computed for the database of GBs. This was carried out by examining the atomic sites within a distance of 15 Å of the GB plane as possible

defect sites. In this study, we focus on interstitial instead of the substitutional configurations, as the previous study established the energetic preference for hydrogen to occupy an interstitial site rather than the substitutional site in α-Fe (Solanki et al. 2012). For the interstitial hydrogen, the hydrogen atom was placed 0.5 Å away from the Fe atom in a direction parallel to the GB plane. For the two hydrogen interstitial configuration, the hydrogen atoms were placed 0.5 Å away from the Fe atom along two orthogonal directions parallel to the GB plane (Figure 9b). In this manner, each hydrogen defect configuration is associated with a GB atomic site in the minimum energy structure. In the remainder of the analysis, the spatial locations of the initial defect sites are used for subsequent analyses involving distances, such as for GB distances.

For each atomic site (α) for a particular GB these hydrogen defect configurations were placed and the simulation cell was relaxed using the nonlinear conjugate gradient energy minimization process. The potential energy of the computational cell was calculated and the process was repeated for each atomic site across various GBs. The segregation energy of the interstitial hydrogen defect configuration for an atomic site α was calculated as follows:

$$E_{seg}^{\alpha} = (E_{GB}^{\alpha} - E_{GB}) - (E_{bulk}^{H} - E_{bulk}) \quad (3)$$

where, $E_{GB}^{\alpha}$ and $E_{GB}$ are the potential energies of the GB structure with and without the hydrogen defect configuration. $E_{bulk}^{H}$ and $E_{bulk}$ are the potential energies of a single crystal bulk Fe simulation cell with and without the hydrogen defect configuration.

The embrittlement of α-Fe GBs in the presence of hydrogen was quantified by assessing the cohesive energy of the GB interface $(2\gamma_{int})$, which is the energy difference between the fractured surface $(2\gamma)$ and the GB $\left(E_{gb}^{\alpha}\right)$ at atomic site α [47]. In this case, for example, the GB energy $(E_{gb}^{\alpha})$ with hydrogen at atomic site α was calculated as

$$E_{gb}^{\alpha} = E_{GB} + E_{seg}^{\alpha} \tag{4}$$

where, $E_{GB}$ is the GB energy without hydrogen. The energy required to create surface along the GB plane in bulk with hydrogen $(2\gamma)$ at atomic site α was calculated as

$$2\gamma = 2\gamma_s + E_s^{\alpha} \tag{5}$$

where $2\gamma_s$ is the surface energy without hydrogen and $E_s^{\alpha}$ is the segregation energy of hydrogen on the free surfaces $2(\gamma - \gamma_s)$. Hence, the cohesive energy $(2\gamma_{int})$ of the GB in the presence of H is given by

$$2\gamma_{int} = 2\gamma - E_{gb}^{\alpha} = 2\gamma_s + E_s^{\alpha} - \left(E_{gb} + E_{seg}^{\alpha}\right) \tag{6}$$

Grain boundary embrittlement occurs when the presence of hydrogen reduces the cohesive energy of the interface $(2\gamma_{int})$ in comparison to the hydrogen free interface. The increasing segregation of hydrogen to the interface can cause a significant drop in cohesive strength, resulting in an intergranular failure.

## 4.3 Results

A range of GB structures that represent the variation in the GB character distribution in a polycrystalline sample were used to investigate the hydrogen segregation behavior. As an example, the GB energy as a function of the misorientation angle for the <110> STGB system is shown in Figure 9c; this is comparable to what has been previously

reported in the literature (A. Sutton and Vitek 1983; Solanki et al. 2012; Tschopp et al. 2012b; Tschopp et al. 2011; Rajagopalan, Tschopp, and Solanki 2014). The low-order CSL <110> STGBs (i.e., Σ3, Σ11 and Σ9 boundaries) are highlighted in Figure 9c. The two deep cusps are the Σ 3 (112) twin boundary (262 $mJ/m^2$) and the Σ 11 (332) (1039 $mJ/m^2$) (Figure 9c).

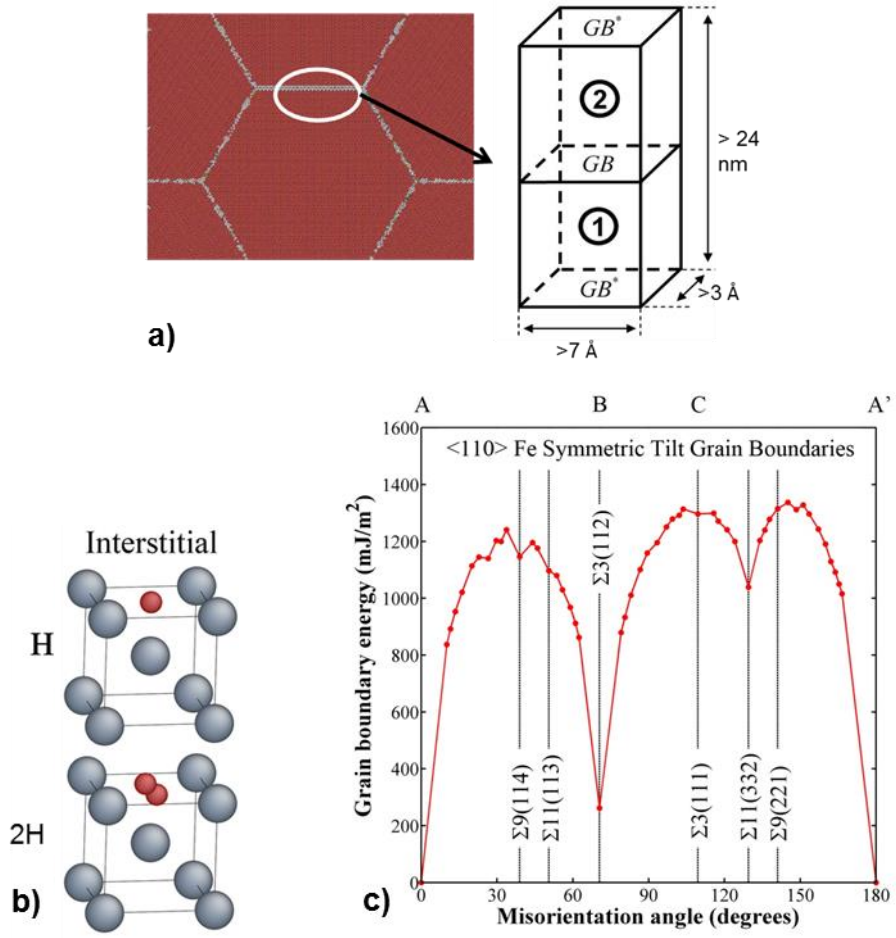


Figure 9: (a) The periodic simulation cell setup with two symmetric GB interfaces spaced 12 nm apart. The *minimum* periodic lengths in the orthogonal directions parallel to the GB plane were 3 and 7 Å. (b) The body-centered cubic unit cell with the hydrogen configurations: single hydrogen and two hydrogen in an interstitial site. (c) <110> symmetric tilt grain boundary energy as a function of misorientation angle with the low-Σ GBs identified.

The atomic structure for a few selected GBs is shown in Figure 10 with the help of atomic volume variation at the interface. The Σ5 GBs can be described as a "favored" GB as described by Sutton and Vitek (A. Sutton and Vitek 1983; A. Sutton 1989). According to the structural unit method, for each tilt axis there are a set of GB structures (favored GBs) that can aid in the structural decomposition of high angle GBs (A. Sutton 1989).

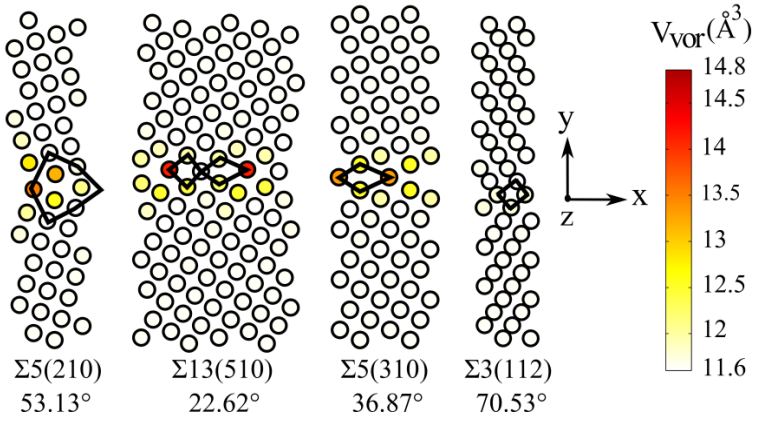


Figure 10: The GB structures are highlighted with the help of the atomic volume estimated by Voronoi tessellation ($V_{vor}$). Atomic volume is maximum (14.8 $Å^3$) at the GB and decays to the bulk value (11.6 $Å^3$).

The segregation energy as a function of the normalized interplanar distance ($d/d_{hkl}$, where d is the distance of the atomic site from the GB plane and $d_{hkl}$ is the interplanar distance of {*hkl*} plane in the bulk crystal) for the <111>, <110> and <100> tilt GBs was plotted in Figure 11. Due to the symmetric nature of the examined GBs, the magnitude of the normalized interplanar distance was used for the analysis. In an attempt to analyze the segregation behavior for all the GBs the site to site variation was divided into 1 Å bins. In Figure 11, the mean segregation energy (green dots) was found generally to be least for the atomic sites located one atomic layer away ($d/d_{hkl}$) from the GB, and the mean segregation energy converged to the bulk value further away from the interface. The red line in Figure 11 represents the median of the data while the top and bottom edges of the blue boxes represent the $25^{th}$ and $75^{th}$ percentiles. The dashed extremities of the box represent the range of energies for each bin, and the ends of the box denote the maximum and minimum values of the segregation energies for each bin. Positive segregation energies shown in Figure 10 suggest that it is not always energetically favorable for

interstitial H to segregate to the GB (i.e., some sites would in fact increase the total system energy). The mean behavior (with deviation) and the extreme value statistics shown in Figure 11 are critical for bridging the gap from the nanoscale to higher length scales. For example, a phase field model of impurity segregation would require both the energetics (i.e., computed herein) and kinetics to model the evolution of an inhomogeneous distribution of impurities in a polycrystalline solid solution.

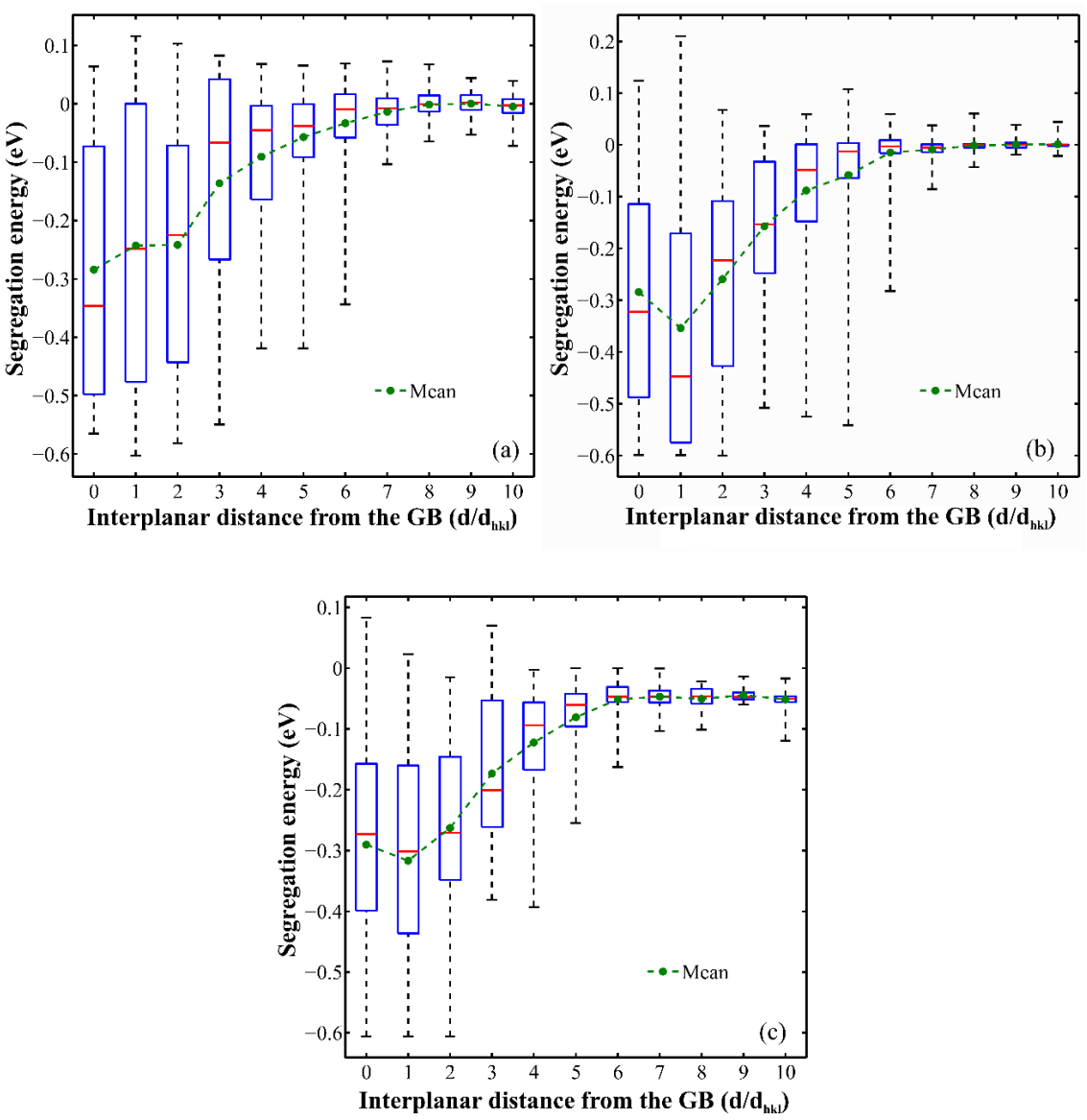


Figure 11: The segregation energy of an interstitial hydrogen atom as a function of distance from the GB for <100>, <110> and <111> STGBs. The segregation energies were divided into 1 Å bins. The red lines are medians, the blue box ends are the 25$^{th}$ and 75$^{th}$ percentiles, the black whisker ends are extreme minimum and maximum values, and the green dotted lines are mean segregation energies.

The energy required for the second hydrogen atom to occupy a position next to the first hydrogen atom was found to be non-additive in nature, due to the strong hydrogen-hydrogen interaction. The defect configurations exhibit a strong affinity for segregation

along the atomic plane adjacent to the GB plane ($d/d_{hkl}$ = 1). Therefore, the segregation energies at $d/d_{hkl}$ = 1 for all the GBs were mapped onto a stereographic triangle as a filled contour for both the defect configurations (Figure 12). This methodology helps in identification of GBs that can act as an effective sink or exhibit a very low energetic drive for hydrogen segregation. The single hydrogen segregation energy to a Σ3 (111), $\theta$ = 109.47° GB reported here was found to be in good agreement with the previously reported values in literature (He et al. 2013; Solanki et al. 2012; Masatake Yamaguchi 2011; Rajagopalan, Tschopp, and Solanki 2014). Since segregation has a direct influence on the GB cohesive energy (by reducing the interface energy), it is critical to identify interfaces that exhibit a low energetic drive for hydrogen.

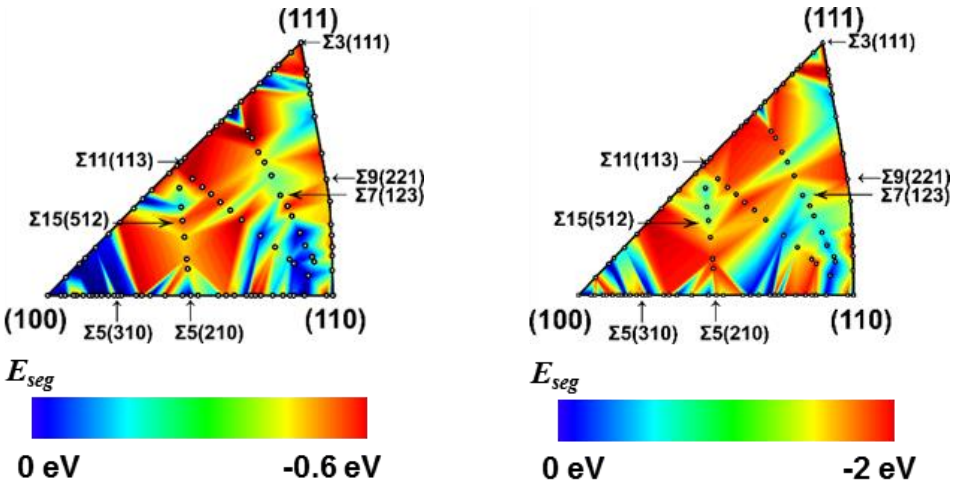


Figure 12: The segregation energies at $d/d_{\{hkl\}}$ = 1 (one atomic layer away from the GB plane) for the two defect configurations and various <100>, <110>, <111> and <112> STGBs was plotted on the stereographic triangle using the polar and azimuthal angles. The color bar corresponds to the maximum and minimum segregation energy thresholds for both hydrogen defect configurations.

To quantify and validate the correlation between the thermodynamic properties of the GB on the segregation behavior, an analytical model was formulated. The simplified model captures the intrinsic GB properties influencing the segregation behavior and

decay with the help of a Gaussian formulation with two parameters ($\alpha$ and $\beta$). The segregation energy as a function of distance from the GB plane is given by:

$$E_{seg} = \alpha exp\left(-\left(\frac{d/d_{hkl}}{\beta}\right)^2\right) \text{eV} \quad (7)$$

where, $\alpha$ represents the innate segregation propensity and $\beta$ is related to the segregation length scale for each defect configuration. For each interface in a particular tilt system, $\alpha$ and $\beta$ were extracted using Equation 7 for both the defect configurations (refer to Table 2 for mean values). The segregation propensity $(\alpha)$ and length scale $(\beta)$ increase with the addition of hydrogen interstitially to the defect configuration (Table 2).

Table 2: Mean statistics for Gaussian distribution of one-interstitial (H-int) and two-interstitial hydrogen (2H-int) segregation to α-Fe STGBs.

| **GB system** | **H-int** | | | | **2H-int** | | | |
|---|---|---|---|---|---|---|---|---|
| | $\alpha$ **(eV)** | $\beta$ | **R** | $\mathbf{R^2}$ | $\alpha$ **(eV)** | $\beta$ | **R** | $\mathbf{R^2}$ |
| <100> | -0.46 | -1.64 | 0.89 | 0.8 | -1.59 | -3.51 | 0.91 | 0.82 |
| <110> | -0.71 | -3.86 | 0.91 | 0.83 | -1.61 | -3.99 | 0.92 | 0.84 |
| <111> | -0.44 | -2.75 | 0.91 | 0.82 | -1.26 | -3.98 | 0.91 | 0.82 |
| <112> | -0.53 | -2.91 | 0.96 | 0.92 | -1.61 | -3.35 | 0.94 | 0.88 |

The site to site atomic volume variation plays a major role in dictating the segregation behavior, and our findings indicate the existence of a strong correlation between the atomic volume and the segregation energy (Table 2). In other words the GBs with a high atomic volume exhibit a higher segregation propensity for hydrogen defect configurations than the interfaces with a lower atomic volume. The linear correlation factor (R) and coefficient of determination ($R^2$) were found to determine the relationship between interfaces structural properties and segregation behavior. In general, R indicates the strength and nature of the linear correlation between two variables whereas $R^2$ represents the percentage of data points that are closest to the line of best fit.

The equation describing the linear relation between the segregation propensity $(\alpha)$ and the maximum atomic volume at the interface $(V_{vor})$ is given by

$$\alpha = \mathrm{p1} * V_{vor} + \mathrm{p2} \quad (8)$$

where, p1 and p2 are the coefficient variables relating the segregation propensity of the defect configuration with the site to site atomic volume variation around the interface (Table 3). Since, the segregation propensity $(\alpha)$ varies linearly with atomic volume $(V_{vor})$, GBs with enhanced segregation tendency can be effectively identified using GB metrics such as atomic volume .

Table 3: A list of the coefficient variables (p1 and p2) values with varying defect configurations and GB tilt systems extracted using Equation 8. The R (linear coefficient factor) values indicate a very strong correlation between the distribution parameter $(\alpha)$ and atomic volume $(V_{vor})$.

| **GB system** | **H-int** | | | | **2H-int** | | | |
|---|---|---|---|---|---|---|---|---|
| | **p1 (eV/Å$^3$)** | **p2 (eV)** | **R** | **R$^2$** | **p1 (eV/Å$^3$)** | **p2 (eV)** | **R** | **R$^2$** |
| <100> | -0.15 | 1.66 | -0.87 | 0.76 | -0.78 | 9.37 | -0.8 | 0.64 |
| <110> | -0.16 | 1.66 | -0.86 | 0.75 | -0.32 | 2.52 | -0.57 | 0.33 |
| <111> | -0.29 | 3.3 | -0.73 | 0.54 | -0.96 | 10.89 | -0.9 | 0.80 |
| <112> | -0.49 | 6.06 | -0.82 | 0.67 | -0.83 | 4.89 | -0.81 | 0.65 |

Additionally, a strong positive correlation was identified between the magnitude of $\beta$ and segregation length scale (Table 4). The segregation length scale accurately describes the GB strain decay and was calculated from the segregation data based on the three standard deviation $(3\sigma)$ criterion. In the case of a hydrogen atom at an interstitial site, the segregation length scale corresponding to the <100> and <111> was found to be lower in comparison to the <110> and <112> tilt GBs. The equation describing the

relation between the segregation length scale parameter ($\beta$) and the GB strain length scale ($l$) is given by

$$|\beta| = p3*l + p4 \quad (9)$$

where, p3 and p4 are the coefficient variables. The values of p3 and p4 for each tilt system and defect configuration are indicated in Table 4. The magnitude of $\beta$ varies linearly with segregation length scale thereby indicating a correlation between segregation energy and the inherent GB strain energy length scale.

Table 4: The symmetric tilt GBs with the corresponding p3 and p4 (coefficient) values for both hydrogen defect configuration were extracted using Equation 9. The R (linear coefficient factor) values indicate a very strong correlation between the distribution parameter, β and length scale, l.

| GB system | H-int | | | | 2H-int | | | |
|---|---|---|---|---|---|---|---|---|
| | **p3** | **p4** | **R** | **$R^2$** | **p3** | **p4** | **R** | **$R^2$** |
| <100> | 0.26 | 0.74 | 0.84 | 0.7 | 0.3 | 0.01 | 0.77 | 0.6 |
| <110> | 1.3 | -8.88 | 0.84 | 0.7 | 0.32 | -0.01 | 0.77 | 0.6 |
| <111> | 0.56 | -1.74 | 0.84 | 0.7 | 0.23 | 1.6 | 0.77 | 0.6 |
| <112> | 0.96 | -7.48 | 0.84 | 0.7 | 0.31 | -0.16 | 0.84 | 0.7 |

The aforementioned analysis shows that hydrogen defect configurations strongly segregate to the GB, which eventually leads to embrittlement. To elucidate the influence of hydrogen on the GB energy (Equation 4) and the cohesive energy (Equation 6), cleavage failure occurs when $2\gamma_{int} = 2\gamma$ (since $E_{gb}^{\alpha} \cong 0$). A decrease in the GB energy $\left(E_{gb}^{\alpha}\right)$ was observed with increasing local hydrogen concentration as shown in Figure 13. As $E_{gb}^{\alpha}$ approaches zero, there is no more energy to be gained by hydrogen trapping. This limit indicates the trapping concentration of hydrogen for this particular interface. To illustrate this the local hydrogen trapping limit for the Σ53 (720), $\theta$ = 31.89° interface

was found to be 4.4% (0.072 hydrogen atoms/nm$^2$), which resulted in decohesion ($2\gamma_{int} = 2\gamma$) of the interface leading to a brittle failure (Figure 13). Moreover, it was found that the underlying GB structure has a strong influence on the trapping limit for hydrogen. In the case of the Σ17 (410), $\theta$ = 28.07° GB, the local hydrogen trapping limit was found to be ~7% (0.096 hydrogen atoms/nm$^2$), as compared to 4.4% (0.072 hydrogen atoms/nm$^2$) for the Σ53 (720) interface.

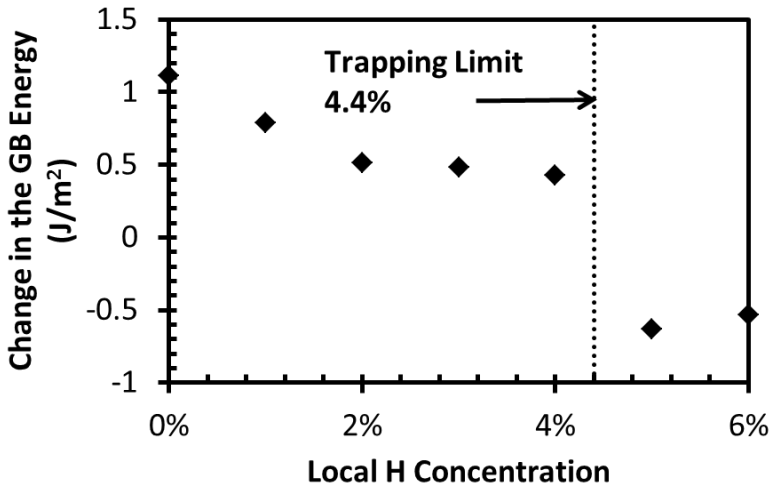


Figure 13: The evolution of hydrogen segregated GB energy ($E_{gb}^{\alpha}$) as a function of local hydrogen concentrations for the Σ53 (720), $\theta$ = 31.89°. As the change in GB energy $\left(E_{gb}^{\alpha}\right)$ approaches zero, there is no significant energy to be gained from further trapping hydrogen atoms at the boundary. This transition demarcates the trapping limit of hydrogen for this interface.

These findings quantify the crucial role played by the GB character in determining the hydrogen segregation behavior around the interface. Hence, the analysis employed in this work can aid in the identification of GBs with limited segregation propensity using intrinsic GB characteristics such as the misorientation, GB energy and site to site atomic volume around the interface.

## 4.4 Conclusions

In this work, we investigated the variation in single and two hydrogen interstitial segregation behavior for a large database of α-Fe symmetric tilt GBs. The following conclusions can be drawn from this work:

1. In general, the GB tilt axes (e.g. <100>, <110> and <111> tilt directions) had a lesser effect than the type of hydrogen defect configuration (see Figure 11 and 12). For instance, the segregation energy of <111> tilt GBs for a hydrogen atom at an interstitial site along the GB plane was ~99 % of the <100> tilt interfaces (Figure 11). On the other hand, the segregation energy of the <100> tilt GBs with hydrogen at an interstitial site was found to be about ~23% of the segregation energy of two hydrogen atoms at an interstitial site (Figure 12). Thus, the increased energetic preference due to the hydrogen-hydrogen interaction was found to be ~54% of the segregation energy of two hydrogen atoms at an interstitial site, creating a large driving force for two hydrogen atoms to reside alongside each other at the GB. An important implication of this is that this can cause a cross-over from a ductile regime to a brittle regime (S. Lynch 2012; Vehoff and Rothe 1983).
2. Grain boundaries with limited segregation potency for hydrogen such as Σ3 (112), $\theta$ = 70.53° (coherent twin boundary), Σ85 (0,7,11), $\theta$ = 64.94° and Σ291 (1, 11,13), $\theta$ = 11.65° were identified.
3. A physically-motivated model that accurately predicts the relationship between intrinsic GB properties on the hydrogen segregation behavior was formulated based on the results from the study.

4. The increasing concentration of hydrogen along the GB was found to decrease the interface energy. The trapping limit for the Σ53 (720) GB was found to be 4.4% and this H concentration caused decohesion of the interface. A strong correlation between the GB character and the trapping limit was observed.

In summary, this work provides atomistic perspective into examining the probabilistic nature of hydrogen segregation and consequent embrittlement of GBs. The identification of interfaces that are less susceptible to HE can form the basis for engineering polycrystalline microstructures resistant to intergranular failure during HE.

# CHAPTER 5

# 5 CRITICAL ASSESSMENT OF H EFFECTS ON SLIP TRANSMISSION ACROSS GRAIN BOUNDARIES IN α-FE

## 5.1 Overview

Grain boundaries present an effective barrier to dislocation motion, thereby strengthening the material. The understanding of the interactions between the GBs and dislocations is crucial in engineering microstructures with enhanced properties. The presence of a corrosive environment drastically deteriorates the service life of the material. HE has been a topic of intense research as it affects several structural metals by bringing about sudden ductile to brittle transition. During fatigue loading the presence of an adequate concentration of hydrogen at sites of dislocation pile-ups can cause intergranular failure. Therefore, there is a strong need to quantify the role of hydrogen on the energy barrier of the individual GBs. In this work, we employed molecular dynamics to study the interactions between screw dislocations and several <111> tilt GBs in Fe. It was found that the outcome of the dislocation-grain boundary (DGB) interaction depends strongly on the underlying GB structure. A strong correlation between the GB energy and the energy barrier for slip transmission was found. The presence of hydrogen causes the energy barrier for slip transmission to increase consistently by distorting the underlying GB structure. Based on the findings, the fatigue crack initiation under the influence of hydrogen was examined and it was found that plasticity acts as an effective transport for depositing hydrogen at the GB. The continuous segregation of hydrogen at the interface increases the susceptibility for intergranular failure.

## 5.2 Introduction

The mechanical properties of crystalline materials are strongly governed by the presence of obstacles (point defects, solute atoms, dislocation network, grain boundaries and precipitates) to the dislocation motion. The GBs play a fundamental role in determining the strengthening achieved as they present an effective barrier to the dislocation glide (Hall 1951; Petch 1954). Additionally, in most crystalline materials, the impedance of dislocation can generate the slip localization could eventually lead to a crack initiate in GBs (Essmann, Gösele, and Mughrabi 1981; Tanaka and Mura 1981; Differt, Esmann, and Mughrabi 1986; Zimmermann 2012), stress corrosion cracking (Yamashita et al. 1991; Was, Thaveeprungsriporn, and Crawford 1998), radiation damage evolution (Was * and Busby 2005; Was, Farkas, and Robertson 2012; Jiao and Was 2008; McMurtrey et al. 2011) and environmental corrosion (Bechtle et al. 2009; Novak et al. 2010; Palin-Luc et al. 2010; Crawford and Was 2013; Zhevnenko, Vaganov, and Gershman 2011). These issues have motivated a great deal of experimental (Soer and De Hosson 2005; Bieler et al. 2005; Brandl et al. 2007; Britton, Randman, and Wilkinson 2009; Polcarova et al. 1998; L. Wang et al. 2009; Gemperle, Gemperlová, and Zárubová 2004) and modelling (Saraev and Schmauder 2003; Jin et al. 2006; Cheng, Mrovec, and Gumbsch 2008; Bachurin, Weygand, and Gumbsch 2010; Sangid et al. 2011; Yuasa et al. 2014; Dewald and Curtin 2007a) efforts to gain insights to optimize the microstructure. In the case of intergranular failure, the nucleation and propagation of crack can take place solely due to the stress state, but this is a rare response. The presence of a corrosive environment further increases the tendency for intergranular failure. HE has been a major problem for structural materials, as the strength, ductility and toughness is greatly

reduced (Carneiro, Ratnapuli, and de Freitas Cunha Lins 2003; Gu, Luo, and Mao 1999; Woodtli and Kieselbach 2000; Parkins 2000). For instance, static and cyclic mechanical loads under harsh environmental service conditions result in local damage near highly stressed areas leading to the nucleation and growth of small surface cracks that interact, coalesce and eventually result in catastrophic failure if undetected. Hydrogen has a strong bias to segregate around internal cracks, dislocations, grain boundaries and TJs (Murray S. Daw and Baskes 1983; Masatake Yamaguchi et al. 2011; Bhatia, Groh, and Solanki 2014; Rajagopalan, Tschopp, and Solanki 2014). The segregation of adequate hydrogen along the GB leads to a reduction in the cohesive strength of the GB interface (Murray S. Daw and Baskes 1983; Masatake Yamaguchi et al. 2011), increasing the tendency for intergranular fracture (Rice and Wang 1989; Bechtle et al. 2009; Novak et al. 2010; S. Wang et al. 2014). The presence of segregated hydrogen along the GB can hinder the plastic flow across the grains, thereby promoting crack nucleation at the DGB site (S. Wang et al. 2014). There is a lack of systematic studies exploring the role of aggressive environments (such as hydrogen, liquid gallium and bismuth) on DGB interactions (Kacher et al. 2014).

On the other hand, several predictive models for the DGB interaction (Livingston and Chalmers 1957; T. C. Lee, Robertson, and Birnbaum 1989; Clark et al. 1992; Shen, Wagoner, and Clark 1986; Shen, Wagoner, and Clark 1988) have been developed based on the geometry of the slip systems and the stress state. Broadly, there are four possible outcomes of the DGB interactions: a) a direct transmission; b) a direct transmission with a residual dislocation along the GB; c) an indirect transmission with a residual dislocation occurring because the incoming and outgoing slip planes do not intersect and d) no

transmission because the dislocation is absorbed at the GB. The aforementioned scenarios can be summarized in terms of the Burgers vector of the incident ($b_i$), transmitted ($b_t$) and residual dislocations ($b_r$).

$$\overrightarrow{b_i} \rightarrow \overrightarrow{b_t} + \overrightarrow{b_r} \tag{10}$$

In order to predict the outcome of the DGB interaction several models have been proposed. The first of these models was proposed by Livingston and Chalmers (Livingston and Chalmers 1957) this is based on the geometry between the slip systems in the incident and transmitted grains. Shen et al. (Shen, Wagoner, and Clark 1986; Shen, Wagoner, and Clark 1988; Clark et al. 1992) addressed some of the shortcomings of the previous model by adding the criterion of maximum resolved shear stress to the geometry condition. Lastly, based on in-situ TEM experiments Lee et al. (T. C. Lee, Robertson, and Birnbaum 1989) proposed an additional criteria to the model by Shen et al. (Shen, Wagoner, and Clark 1986; Shen, Wagoner, and Clark 1988; Clark et al. 1992) that ensures the outcome based on the minimum residual dislocations along the GB, also known as the Lee-Robertson-Birnbaum (LRB) criterion. The geometric condition can be expressed in terms of the relative orientations of the slip planes relative to the GB plane in the following manner.

$$M = l_{in}.l_{out} \tag{11}$$

where, $l$ is the unit normal at the intersection of the incoming and outgoing slip plane with the GB plane. Unfortunately, the atomic level details of the interaction of individual GBs with dislocations still remain unclear. This has motivated several atomistic studies in FCC

(Dewald and Curtin 2007a; Sangid et al. 2011), BCC (Saraev and Schmauder 2003; Cheng, Mrovec, and Gumbsch 2008) and HCP (Yuasa et al. 2014) metals to validate these proposed models and to glean atomic-scale details regarding the complex DGB interactions. In previous atomistic (Dewald and Curtin 2007b; Dewald and Curtin 2007a) studies, the slip transmission was observed to violate the LRB criterion of the transmitted plane having the highest Schmid factor for all the slip planes. Based on these findings, it was suggested that the GB structure around the DGB interaction play a key role in determining the slip plane for the transmitted dislocation and there were several shortcomings of the LRB criterion. Furthermore, Sangid et al. (Sangid et al. 2011) quantified the energy barrier at the atomic scale for the GBs to permit slip transmission. The energy barrier presented by the GB for slip transmission was found to be closely related to the static GB energy. Therefore, a fundamental understanding of the effect of hydrogen on the motion of dislocations across the GBs and the intrinsic energy barrier for slip transmission is critical.

In this work, for the first time, we perform a systematic investigate the role of hydrogen on the slip transfer mechanism in α-Fe using molecular dynamics (10 K). In particular, we study the effect of hydrogen on the interactions between the screw dislocation and eight <111> symmetric tilt grain boundaries (STGBs). Further, the observed outcome for the slip transfer were compared with the predictions of the LRB criteria. Note that at low temperatures, the yield behavior of α-Fe is strongly governed by the glissile $a/2 < 111 >$ screw dislocation. It was found that the outcome of the DGB interaction depends strongly on the underlying GB dislocation network. The energy barrier for slip transmission across the GB was quantified by measuring the strain energy

flux across the DGB interaction site. A strong correlation was found between the GB energy and the energy barrier for slip transmission for both scenarios (hydrogen free and hydrogen rich environments). In other words, GBs with lower interfacial energy demonstrated a higher barrier for slip transmission. These findings are in agreement with previous experimental and modeling efforts. The introduction of hydrogen along the GB causes the energy barrier for slip transmission to increase consistently for all the GBs examined. Based on these findings, the fatigue crack initiation was examined and it was found that the higher energy barrier for slip transmission increases the dislocation pileup. However, the presence of hydrogen along the GB lowers the cohesive strength for the interface promoting intergranular crack nucleation. This provides an alternate relief mechanism for the trapped dislocations in the absence of feasible slip transmission.

## 5.3 Methodology

Molecular dynamics (MD) (large-scale atomic/molecular massively parallel simulator, LAMMPS (Plimpton 1995)) was utilized to study the effect of hydrogen on the interaction of the screw dislocation with several <111> symmetric tilt GBs (STGBs) (Figure 1) in α-Fe at 10 K (for details regarding atomistic simulations refer Appendix A). The semi-empirical embedded atom method description for modelling the Fe-H system (Ashwin Ramasubramaniam, Itakura, and Carter 2009a). The EAM potential is based on the Fe EAM potential (Hepburn and Ackland 2008). The Fe-H potential was parameterized using an extensive database of energies and configurations from density functional theory (DFT) calculations of the dissolution and diffusion of hydrogen in bulk α-Fe, the binding of hydrogen to free surfaces, vacancies and dislocations as well as other cross interactions between hydrogen and Fe. Moreover, the formation energies

corresponding to multiple hydrogen-segregations to bulk α-Fe are consistent with the values predicted using ab initio calculations and experimentation (Hayward and Deo 2011b). The interatomic potential was able to accurately capture the threefold non-degenerate screw dislocation core in agreement with DFT findings (Ventelon and Willaime 2010; Itakura, Kaburaki, and Yamaguchi 2012), and the binding behavior of hydrogen around the dislocation core was found to be in agreement (Ashwin Ramasubramaniam, Itakura, and Carter 2009a). The interatomic potential has been widely utilized to study the effect of hydrogen on dislocation mobility (S. Wang, Hashimoto, and Ohnuki 2013; Bhatia, Groh, and Solanki 2014), crack tip deformation (J. Song and Curtin 2014), GBs (Rajagopalan, Tschopp, and Solanki 2014; Liu et al. 2011; Solanki et al. 2012) and surface energies (Ashwin Ramasubramaniam, Itakura, and Carter 2009b; Jiang and Carter 2003) in Fe.

### 5.3.1 *Equilibrium Grain Boundary Structures and Energies*

The <111> STGBs selected for this work represent both the local minimum energy interfaces (Tschopp et al. 2012b) and a large range of possible misorientation angles (refer Figure 14 and Table 5). +The GB structure and minimum energy were calculated using a bicrystalline simulation cell with three-dimensional (3D) periodic boundary conditions consisting of two grains at 0 K as described by Rittner and Seidman (Rittner and Seidman 1996). The periodic boundaries (Y direction) were maintained with a separation distance of 12 nm between the boundaries. Several 0 K minimum energy GB structures were obtained through successive rigid body translations followed by an atom

deletion technique and energy minimization using a non-linear conjugate gradient method (Rittner and Seidman 1996; Tschopp, Tucker, and McDowell 2007).

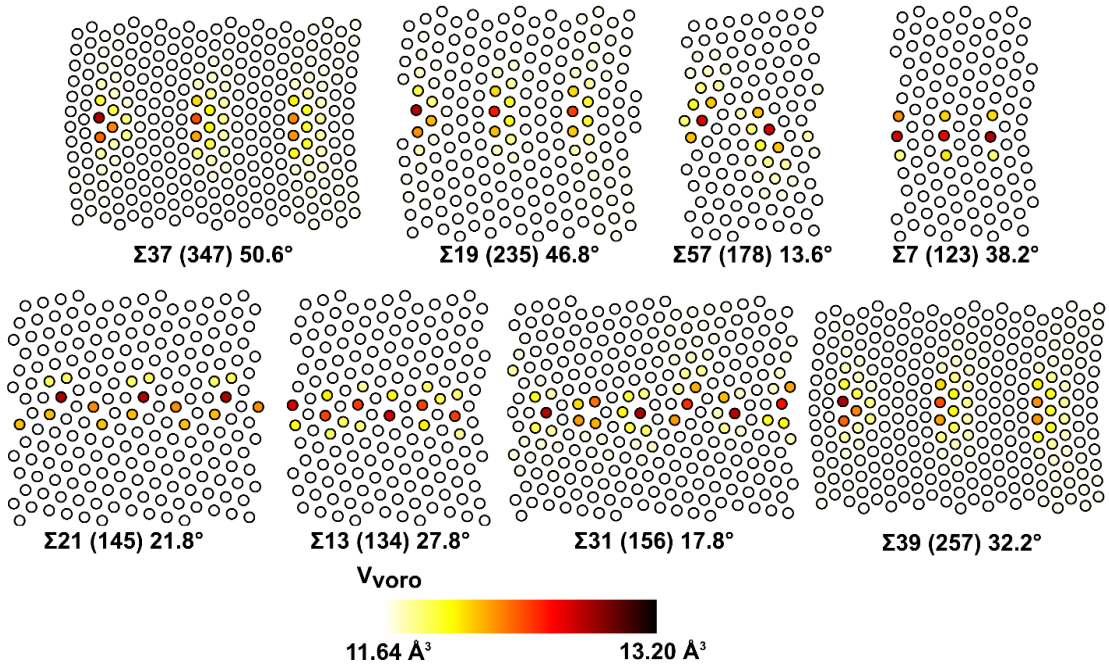


Figure 14: The <111> symmetric tilt grain boundary structures in α-Fe used in this work. Atoms are colored based on the atomic volume estimated by Voronoi tessellation on a scale of 11.64 $Å^3$ to 13.20 $Å^3$.

Table 5: Grain boundary CSL description, misorientation angle, GB energy, the predicted and observed slip plane for the GBs examined in this work.

| **CSL designation ($\Sigma$)** | **Misorientation angle, ($\theta$)** | **GB energy, ($mJ/m^2$)** | **Predicted outgoing slip plane** | **Observed outgoing slip plane** |
|---|---|---|---|---|
| *Σ37 (347)* | 50.6 | 760 | $(1\bar{1}0)$ | $(1\bar{1}0)$ |
| *Σ19 (235)* | 46.8 | 887 | $(1\bar{1}0)$ | $(1\bar{1}0)$ |
| *Σ57 (178)* | 13.6 | 1030 | $(10\bar{1})$ | $(10\bar{1})$ |
| *Σ7 (123)* | 38.2 | 1056 | $(1\bar{1}0)$ | $(1\bar{1}0)$ |

| | | | | |
|---|---|---|---|---|
| *Σ21 (145)* | 21.8 | 1114 | $(10\bar{1})$ | $(1\bar{1}0)$ |
| *Σ13 (134)* | 27.8 | 1117 | $(10\bar{1})$ | $(1\bar{1}0)$ |
| *Σ31 (156)* | 17.8 | 1127 | $(10\bar{1})$ | $(1\bar{1}0)$ |
| *Σ39 (257)* | 32.2 | 1137 | $(1\bar{1}0)$ | $(1\bar{1}0)$ |

5.3.2 *Simulation Setup for the Grain Boundary-Dislocation Interaction in Fe*

The orientation of the incident grain along the X $[\bar{1}\bar{1}2]$, Y $[1\bar{1}0]$ and Z [111] direction were fixed for all the DGB cases investigated (Figure 15a). The orientation of the transmitted grain was determined by the GB misorientation angle (Table 5). The simulation cell dimensions were approximately 400 Å × 400 Å × 40 Å. The screw dislocation was introduced by applying the Stroh's anisotropic displacement field (Hirth and Gehlen 1969) at a distance of ~50 Å away from the GB (Figure 15a). The initial displacement field is depicted with the help of the differential displacement map in Figure 15b. This was found to be consistent with previous studies (Clouet, Ventelon, and Willaime 2009; Itakura, Kaburaki, and Yamaguchi 2012). Subsequently, the free boundary conditions were prescribed along the X and Y directions and periodic boundary conditions along the Z direction (Burger's vector direction). The atomistic model was equilibrated at a temperature of 10 K using a canonical ensemble (NVT) for 5 ns. Subsequently, the pressure along the periodic direction (Z) was minimized using the isothermal-isobaric ensemble (NPT) for 15 ns. The top and bottom region (~10 Å) along the Y axis were fixed (Figure 15a) and an incremental displacement was applied to these atoms to obtain a constant shear strain rate ($\dot{\gamma_{yz}}$) of $10^8$ $s^{-1}$.

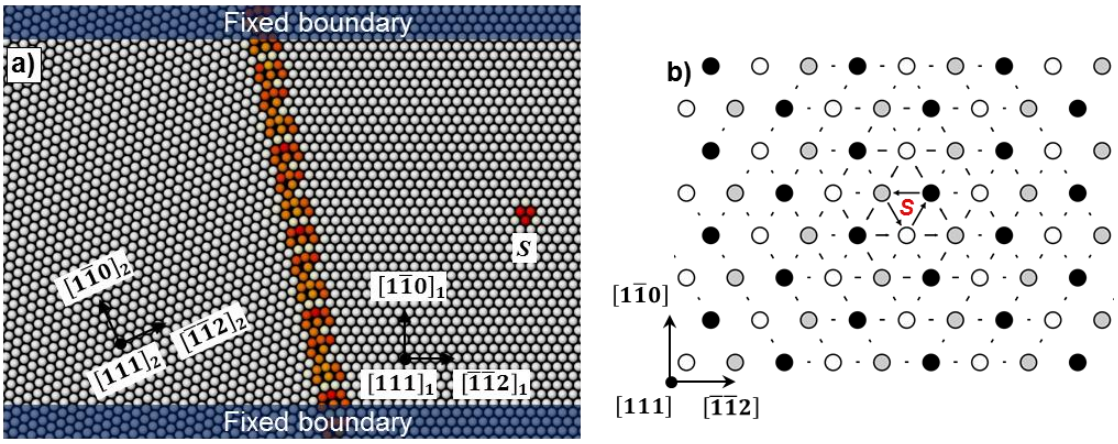


Figure 15: a) A schematic representation of the atomistic model employed to study the interaction between a screw dislocation and the <111> STGB in α-Fe. b) Differential displacement map of the compact core in Fe and the atomic colors emphasize the different (111) planes.

5.3.3 *Introduction of Hydrogen around the Grain Boundary*

The influence of hydrogen on the DGB interaction was examined by introducing hydrogen atoms around the GB. The hydrogen occupancy at a tetrahedral site, $\theta_i$ is dependent on the hydrogen binding energy ($E_b^i$) (Richard A. Oriani 1970) and the temperature ($T$) and can be expressed in the following manner:

$$\frac{\theta_i}{1-\theta_i} = \frac{\theta_{bulk}}{1-\theta_{bulk}} exp^{\left(\frac{E_b^i}{k_B T}\right)} \tag{12}$$

where, $\theta_{bulk}$ is the atomic fraction of hydrogen for the whole system and $k_B$ is the Boltzmann constant. In this work the hydrogen atomic fraction of $3\times10^{-4}$ was chosen. The binding energy indicates the preference of hydrogen atoms to remain at a particular site instead of a bulk lattice with positive values favoring binding and negative values opposing the same. A detailed survey on the site to site variation in the binding energy of hydrogen across several GBs can be found here (N. R. Rhodes, Tschopp, and Solanki 2013; Rajagopalan, Tschopp, and Solanki 2014). Hydrogen atoms were initially placed

along the GB based on the occupation probability for the GBs (Equation 12). Furthermore, the Monte-Carlo method was employed at 10 K to obtain a realistic hydrogen distribution around the GB at finite temperature.

5.3.4 *Quantifying the Energy Barrier for Slip Transmission*

The energy barrier for slip transmission across the GB was quantified by defining a control volume at the site of the DGB interaction (Sangid et al. 2011). The defected atoms (centrosymmetry parameter (Kelchner, Plimpton, and Hamilton 1998) > 0.5) within the control volume were used to estimate the energy barrier for slip transmission. The evolution of the net change in energy of the defected atoms during the loading process was quantified by comparing instantaneous energy ($E_t^i$) with reference/initial atomic energy ($E_r$). The net energy was normalized with the atomic volume occupied by the defect atoms in the reference configuration ($V$):

$$E_{barrier} = \frac{\sum_i^n E_t^i - E_r}{V} \tag{13}$$

5.4 Results

In this section, we discuss in detail the role of hydrogen on the atomic dislocation-grain boundary interactions for a selected few grain boundaries, such as Σ7 (123), Σ13 (134) and Σ57 (178). As discussed earlier, overall eight grain boundaries were used in this work which represents both the local minimum energy interfaces (Tschopp et al. 2012b) and a large range of possible misorientation angles. In this case, based on the Equation 10 the slip transmission across the <111> symmetric tilt grain boundaries does not leaves behind residual dislocation at the interface. Additionally, the isotropic elastic

displacement fields for the dislocation and the grain boundaries do not interfere with each other. Therefore, the grain boundary should not offer any resistance to dislocation glide. However, due to the anisotropic nature of both the defects at the atomic level the dislocation may require thermal activation or critical stress to transmit across the interface. Therefore, we selected three boundaries to understand the precise role of the atomic details during slip transmission using various metrics, such as the atomic shear strain invariant, common neighbor analysis and centrosymmetry parameter. As these interfaces show a very distinct behavior in the presence of hydrogen environment. For instance, in all three grain boundaries with addition of hydrogen, it was found that the underlying structure of the grain boundary was distorted, and thereby increases the energy barrier for slip transmission. Furthermore, the Σ13 (134) STGB shows change in the transmission mechanism, i.e., from a direct to indirect transmission, while the Σ7 (123) STGB shows no noticeable change in the transmission mechanism (i.e., indirect transmission with or without aggressive environments).

5.4.1 *Σ7 (123) STGB*

The influence of hydrogen on the atomic events in the DGB interaction for the Σ7 (123) GB was examined; the predicted outcome by the LRB criterion was transmission along the $(1\bar{1}0)_2$ plane (Table 5). As the applied shear strain increases, the screw dislocation overcomes the Peierls stress and begins gliding towards the GB by transforming into an extended core that is formed from the split core and appears to travel in a zig-zag manner by alternating on {110} planes (Figure 16a). At an applied shear strain ($\gamma_{yz}$) of 3%, the screw dislocation was absorbed into the GB (Figure 16b). The DGB interaction was observed to take place at a site of high atomic volume along the GB

as shown in the Figure 16b inset. The inset in Figure 16b shows the magnified view of the atomic Voronoi volume variation due to the formation of the GB (Figure 14). The absorption of the dislocation at this site affords a relatively easier absorption and rearrangement of the GB dislocation network. Subsequently, the dislocation is transmitted across the GB at an applied shear strain ($\gamma_{yz}$) of 5.7% (Figure 16c). The dislocation was transmitted across the GB in an indirect manner. In other words the GB sites for the dislocation absorption and transmission were separated from each other by 6 Å along the GB (Figure 16c). The dislocation transmits on the $(1\bar{1}0)_2$ which was found to be in agreement with the outgoing plane predicted by the LRB criterion (Figure 16d). The energy barrier for the slip transmission was $2.75 \times 10^{11}$ mJ/m$^3$.

The addition of hydrogen atoms along the GB distorts the underlying atomic structure, thereby decreasing the coincident sites along the GB. In the presence of hydrogen, the shear strain ($\gamma_{yz} = 8.8$ %) required to transmit the dislocation was much greater compared to the hydrogen free case (Figure 16e). The magnified view in Figure 16e shows the hydrogen atoms at the DGB site. The energy barrier for the dislocation increases from $2.75 \times 10^{11}$ mJ/m$^3$ for a hydrogen free case to $4.16 \times 10^{11}$ mJ/m$^3$ in the presence of hydrogen. This clearly shows the additional work done to transmit a dislocation across the GB in the presence of hydrogen.

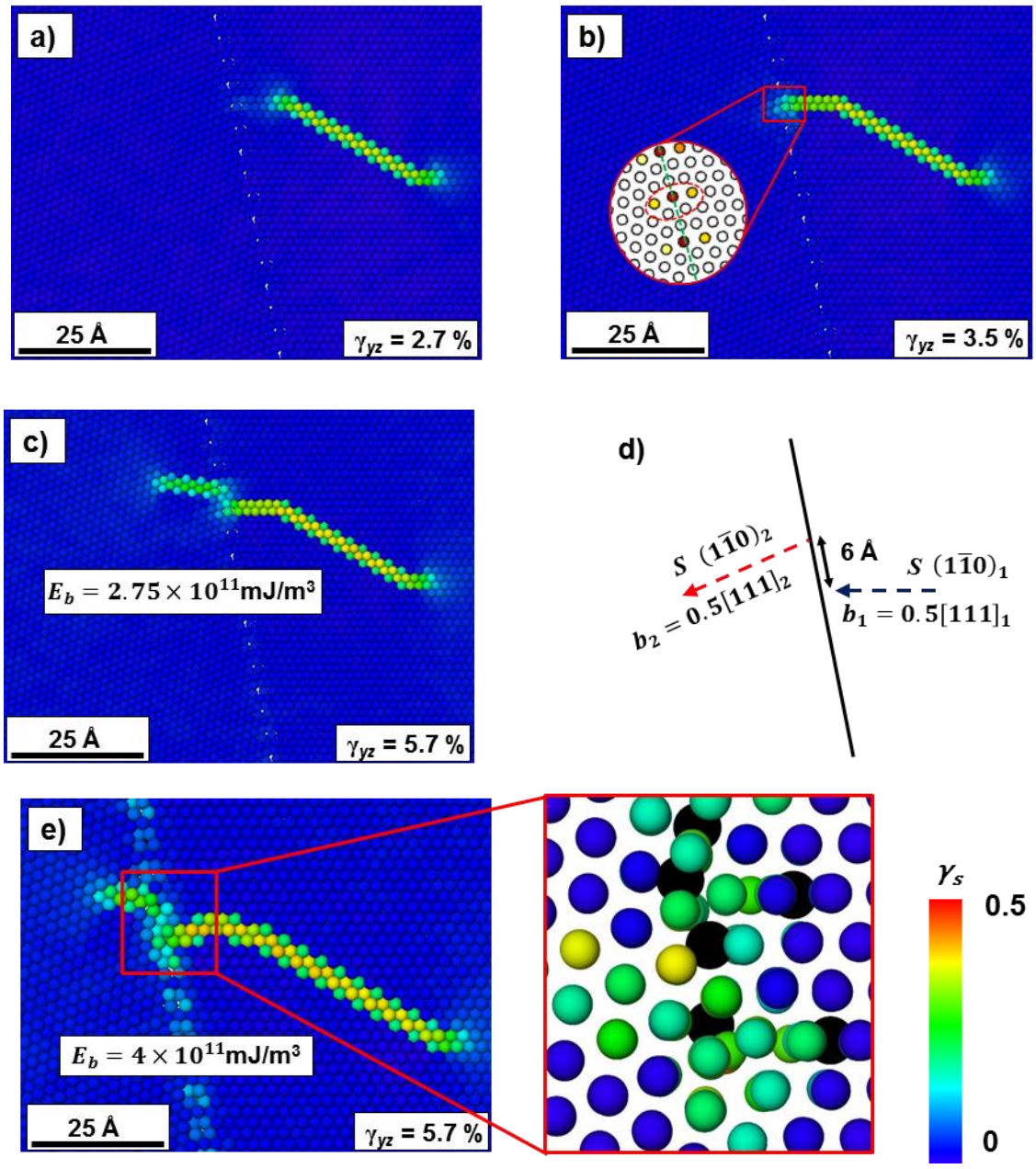


Figure 16: a-d) The interaction of a screw dislocation with the Σ7 (123) GB under the applied shear strain ($\gamma_{yz}$) along the Burgers vector direction. The inset b) shows the magnified GB structure colored according to the atomic volume estimated by Voronoi tessellation as described earlier. d) The schematic representation of the slip transmission mechanism. e) The influence of hydrogen atoms on the dislocation-grain boundary interaction. The magnified view in e) shows the hydrogen atom positions depicted by black circles. The atoms were colored according to the local atomic shear strain invariant ($\gamma_s$) on a scale of 0 to 0.5.

### 5.4.2 *Σ13 (134) STGB*

We now focus on the influence of hydrogen on the atomic events during the slip transmission across the Σ13 (134) STGB. Here the observed slip transmission for both scenarios (with and without hydrogen) occurred on the slip plane $(1\bar{1}0)_2$ that was not the maximum resolved shear stress slip plane $(10\bar{1})_2$ (refer to Table 5), thereby violating the LRB criterion. In the case of a hydrogen free environment, the screw dislocation was absorbed in the GB near the site of coincidence (Figure 17a). Subsequently, the dislocation was transmitted along the $(1\bar{1}0)_2$ by overcoming an energy barrier of $1.2 \times 10^{11}$ mJ/m$^3$ (Figure 17b). The dislocation was transmitted from the absorption site at the GB without requiring significant atomic rearrangement of the GB (direct transmission) (Figure 17b). The addition of hydrogen along the GB region shows that the energy barrier for slip-transmission increases to $3.5 \times 10^{11}$ mJ/m$^3$ (Figure 17c). The absorbed dislocation was accommodated within the GB up to an applied shear strain of 8.0% transmitting from a site 8 Å away from the initial GB site (Figure 17c). The presence of hydrogen clearly modifies the dislocation-grain boundary interaction (Figure 17c-d) by changing the transmission mechanism and increasing the energy barrier.

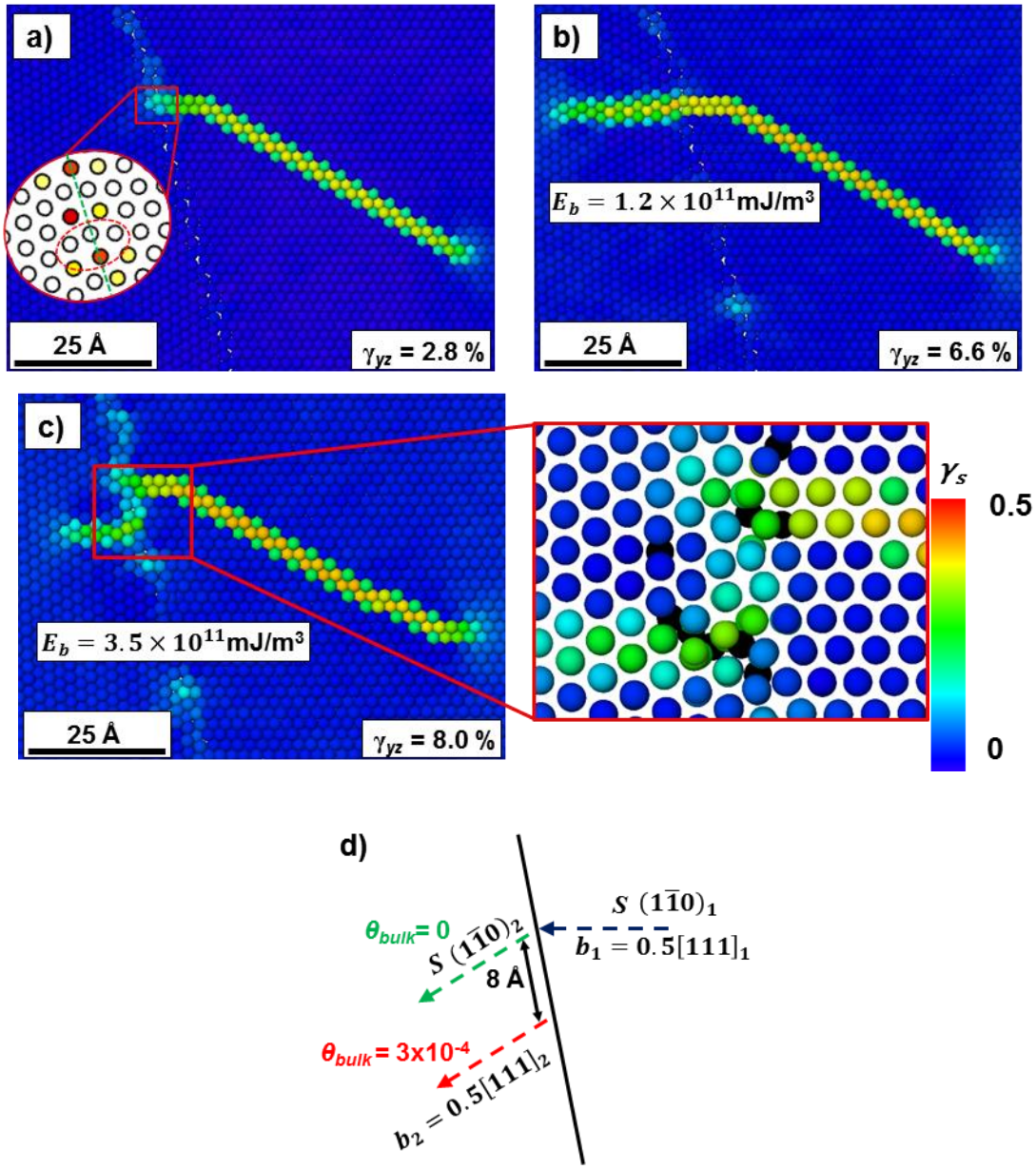


Figure 17: a-b) The interaction of a screw dislocation with the Σ13 (134) GB under the applied shear strain ($\gamma_{yz}$) along the Burgers vector direction. The inset a) shows the magnified GB structure colored according to the atomic volume estimated by Voronoi tessellation. c) The change in atomic events for the dislocation-grain boundary interaction in the presence of hydrogen. The atoms were colored according to the local atomic shear strain invariant ($\gamma_s$) on a scale of 0 to 0.5. d) The schematic representation of the change in slip transmission mechanism in the presence of hydrogen.

### 5.4.3 *Σ57 (178) STGB*

In the case of the Σ57 (178) GB, the predicted outcome for the DGB interaction was transmission along the $(10\bar{1})_2$ plane (Table 5). The screw dislocation was absorbed in the GB and with further shear strain moved along the GB to finally transmit by overcoming an energy barrier of $3.3 \times 10^{11}$ mJ/m$^3$ along the $(10\bar{1})_2$ (Figure 18a). The addition of hydrogen along the GB increases the slip transmission energy barrier to $5.1 \times 10^{11}$ mJ/m$^3$ (Figure 18b). The schematic representation in Figure 18c clearly highlights the influence of hydrogen which causes the dislocation to move further away from the absorption site before transmitting.

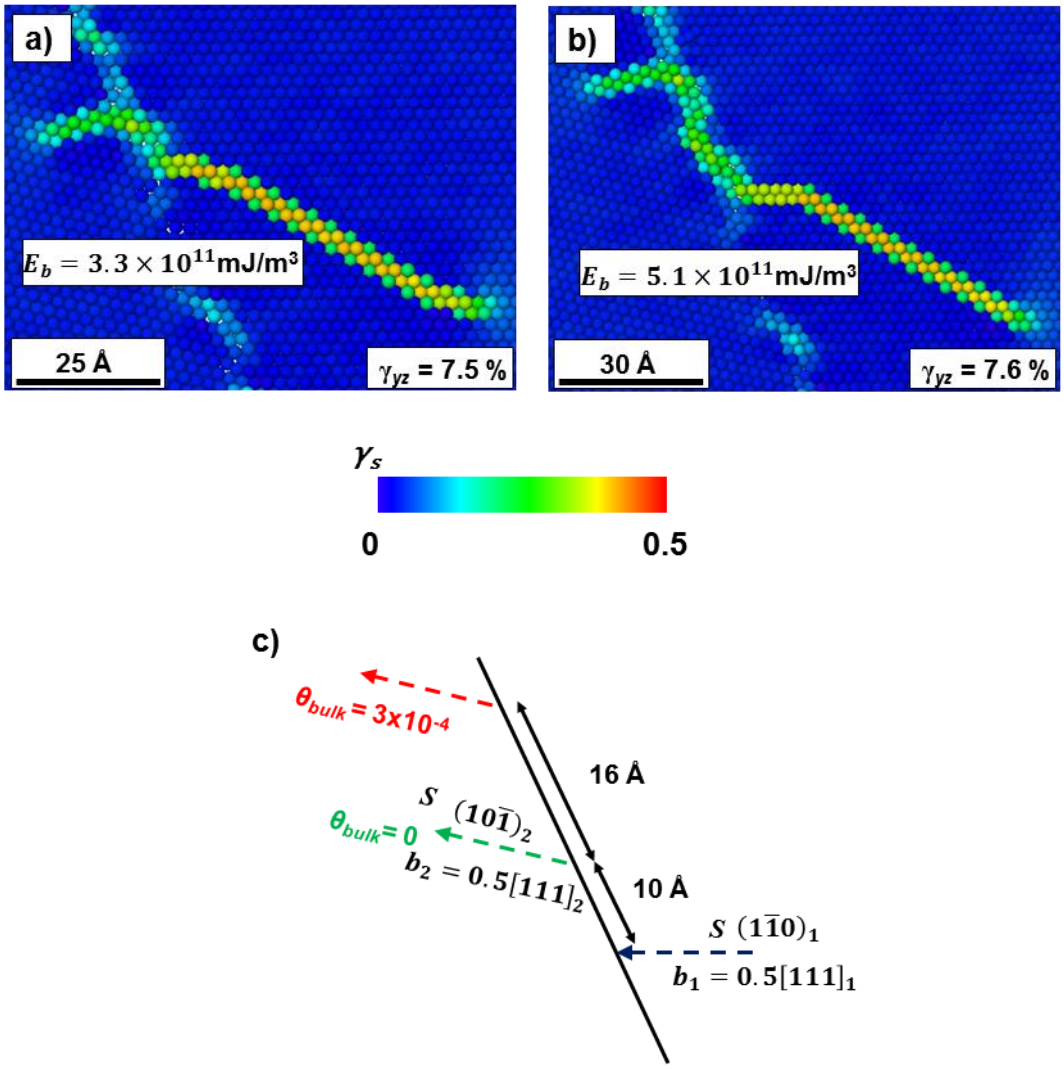


Figure 18: a) The interaction of a screw dislocation with the Σ57 (178) GB under the applied shear strain ($\gamma_{yz}$) along the Burgers vector direction. b) The atomic events of hydrogen on the slip transmission mechanism. The atoms were colored according to the local atomic shear strain invariant ($\gamma_s$) on a scale of 0 to 0.5. c) The schematic representation of influence of hydrogen on the slip transmission.

5.5 Discussion

The GBs are the primary strengthening mechanism in a crystalline material as they offer resistance to the easy glide of the dislocations. This phenomenon provides the required toughness and ductility to the polycrystalline material. However, during HE segregation of adequate hydrogen atoms along the GBs leads to a reduction in the

cohesive strength of the interface. In order to engineer microstructures less susceptible to fatigue crack initiation under the influence of hydrogen, it is important to understand the effect of hydrogen coupled with the GB structure on slip transmission. There have been several studies (Shih, Robertson, and Birnbaum 1988; S. Wang et al. 2014) that have observed an enhanced dislocation mobility in the presence of hydrogen. This has been primarily attributed to the shielding effect that the hydrogen atoms present when segregated around the dislocation core. In other words, the presence of hydrogen atoms modifies the stress field around the dislocation, thereby, decreasing the separation distances between the pile-up dislocations. Furthermore, this significantly decreases the stress required to overcome microstructural obstacles (precipitates and grain boundaries). On the other hand, the segregation of sufficient hydrogen concentration leads to a significant reduction in the cohesive strength of the interface (Masatake Yamaguchi et al. 2011; Solanki et al. 2012). However, there are several concerns related to the enhanced decohesion mechanism discussed elsewhere (S. Wang et al. 2014; Ian M. Robertson et al. 2015).

The energy balance for fatigue crack initiation in the presence of hydrogen was examined here. The energy balance takes into consideration the energy contributions of a) the persistent slip band structure under applied stress (Tanaka and Mura 1981; Sangid, Maier, and Sehitoglu 2011) and b) the interaction energy of the persistent slip band with GBs $(E_{pen})$. This physically represents a fraction of the dislocation density penetrating/transmitting across the GB. The energy barrier for slip transmission across the GB ($E_{barrier}$) is quantified at the atomic scale. In the case of fatigue crack initiation, the stored strain energy of the microstructure $(E_{int})$ must be greater than the energy

required to nucleate an intergranular crack at the GB $\left(E_{cleavage}\right)$. This can be formulated in the following manner:

$$E_{int} = E_{PSB}(\sigma_a, N, \rho, \tau_c, c) + E_{pen}(c, N, E_{GB}, E_{barrier}) \quad (14a)$$

$$E_{int} \geq E_{cleavage}(\gamma_s^{GB}, c) \quad (14b)$$

where, $\sigma_a$ is the applied stress , *N* is the number of fatigue cycles, $\rho$ is the dislocation density within the persistent slip band structure, $\tau_c$ is the Peierls stress, c is the hydrogen concentration at the GB given by Equation 12 and $E_{GB}$ is the GB energy. The presence of hydrogen increases the glissile dislocation density $\left(\rho_{0,H}\right)$ in comparison to the hydrogen free case $(\rho_0)$ because of the shielding effect afforded by the hydrogen environment surrounding a dislocation (S. Wang et al. 2014; Shih, Robertson, and Birnbaum 1988; P. Ferreira, Robertson, and Birnbaum 1998). This leads to an increased dislocation density in the persistent slip band, thereby increasing the energy contribution $(E_{PSB})$ in the energy balance equation (Equation 14a). In general, it was found that the energy barrier for slip transmission of the dislocation $(E_{barrier})$ increased in the presence of hydrogen at the GB (refer to Figure 19) for the several scenarios examined here. The energy barrier for slip transmission $(E_{barrier})$ was found to have a strong relationship to the initial GB energy (Figure 19). In other words, GBs with lower interfacial energy demonstrated a higher barrier for slip transmission these findings are in agreement with the previous study (Sangid et al. 2011). An inverse power law fit was found to best describe this relation.

$$E_{barrier} = 2.54 \times 10^{17}(E_{GB})^{-1.94} \quad (15)$$

The presence of hydrogen along the GB consistently increases the energy barrier for slip transmission across the <111> STGBs (Figure 19). The key finding being that the energy barrier for slip transmission was still best described by an inverse power law fit expression as derived earlier (Equation 15).

$$E_{barrier} = 1.29 \times 10^{17} (E_{GB})^{-1.82} \quad (16)$$

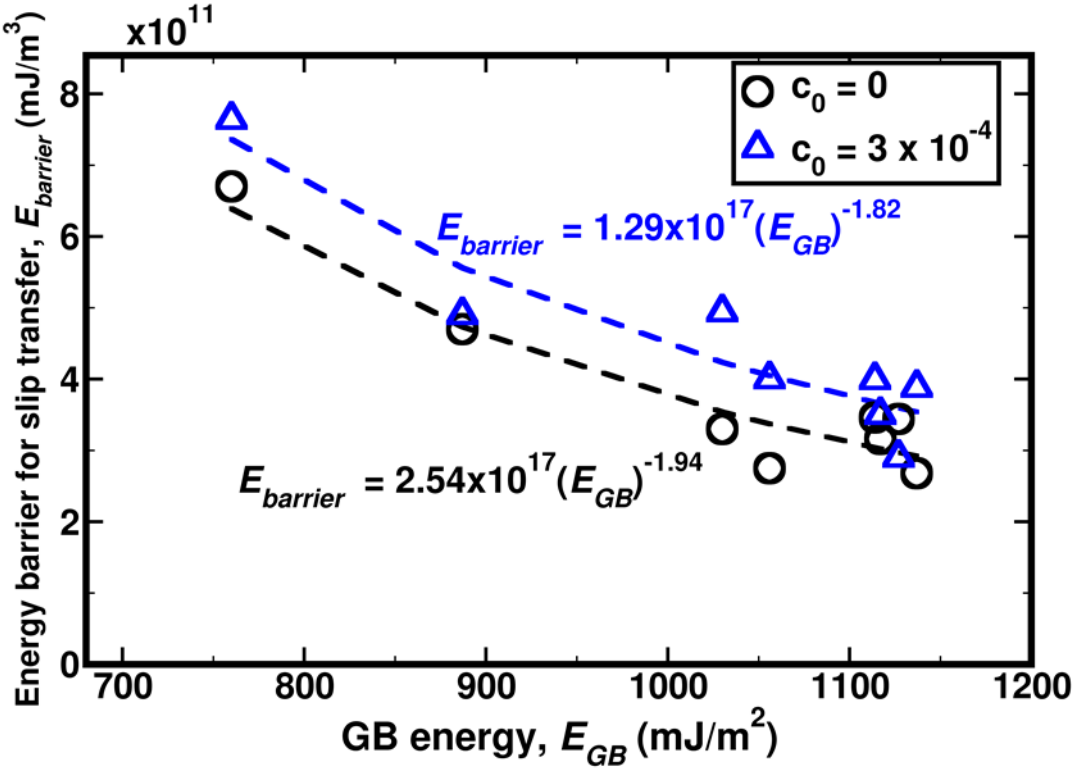


Figure 19: The effect of hydrogen on the slip transmission barrier through <111> symmetric tilt grain boundaries.

Thus, the presence of hydrogen increases the strain energy stored within the GB promoting alternative relief mechanisms, consequently, increasing the interaction energy between the persistent slip band and the GB $(E_{pen})$ (Equation 14a). These cascading events due to the presence of hydrogen lead to an increase in the strain energy accumulated at the persistent slip band GB interaction site. Furthermore, the glissile dislocations would carry along the hydrogen atmospheres responsible for the enhanced

mobility, thereby continuously depositing hydrogen at the GB. This effective transport mechanism of hydrogen in turn causes a decrease in the cohesive strength of the GB interface, as noted by previous studies (Masatake Yamaguchi et al. 2011; Solanki et al. 2012). This provides an opportunity for intergranular crack initiation in the absence of an effective release of the trapped dislocations within the GBs. Therefore, based on the results and the examination of the energy balance for fatigue crack initiation we highlight the role of plastic events in hydrogen-induced intergranular failure. These findings provide further evidence to the mechanism proposed by Wang et al (S. Wang et al. 2014). The effect of hydrogen on the increased susceptibility of the microstructure to intergranular fatigue crack initiation can be summarized in terms of the schematic in Figure 20.

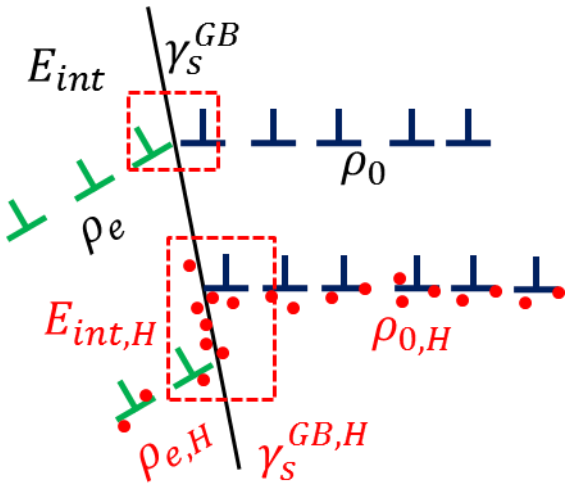


Figure 20: Schematic representation of the effect of hydrogen on the intergranular fatigue crack initiation. The top half shows the hydrogen free interaction of incident dislocation density of $\rho_0$ and the emitted dislocation density is $\rho_e$. In presence of hydrogen, the incident dislocation density $(\rho_{0,H})$ increases in comparison to hydrogen free because of the shielding effect afforded by the hydrogen environment surrounding a dislocation. The emitted dislocation density $(\rho_{e,H})$ is lower than in the hydrogen free case $(\rho_{e,H} < \rho_e)$.

## 5.6 Conclusions

In this work, the influence of hydrogen on the DGB interaction was examined for several <111> STGBs in Fe using atomistic simulations. The primary objective was to quantify the influence of hydrogen on the DGB interactions and reexamine the fatigue crack initiation criterion in light of these findings. The significant contributions of this study are as follows:

1. The outcome of the DGB interaction was strongly dependent on the GB character.
2. The segregated hydrogen atoms along the GB distorts the underlying structure, thereby increasing the energy barrier for slip transmission. In terms of fatigue loading, this would lead to an increase in the dislocations with the persistent band structure.

3. The energy required for the dislocation to transmit across the GB was found to be inversely related to the GB energy.
4. Based on the findings in this work and previous studies (P. Ferreira, Robertson, and Birnbaum 1998; Troiano 1960; R. A. Oriani 1972; Masatake Yamaguchi, Shiga, and Kaburaki 2004; Solanki et al. 2013) the fatigue crack initiation was examined by considering the various interaction energies under the influence of hydrogen. The presence of hydrogen was found to increase the energy barrier for the dislocations trapped at the dislocation to transmit across. In addition, the plasticity provides an effective transport medium for hydrogen to be deposited at the GB (P. J. Ferreira, Robertson, and Birnbaum 1999; S. Wang et al. 2014). In the absence of a feasible mechanism for the trapped dislocation intergranular crack initiation becomes a viable option.

# CHAPTER 6

# 6 THE EFFECT OF HYDROGEN ON DISLOCATION MOBILITY IN IRON

## 6.1 Introduction

The plastic deformation of BCC metals is well known to be significantly different than other close-packed metals (Christian 1983). The lattice resistance (Peierl's barrier) for the screw dislocation motion is large enough that it results in a temperature and strain rate dependent behavior (Christian 1983; Caillard and Martins 2003; Argon 2008). These metals also exhibit noticeable tension-compression asymmetry in flow stress in the low temperature regime (Taylor 1928), which has been attributed to the lattice resistance (Duesbery, Vitek, and Bowen 1973). In the case of face-centered-cubic metals, the plastic behavior is controlled by the obstacles in the dislocation motion at low temperatures. However, in BCC metals the lattice resistance dictates the plastic behavior in the low temperature regime. In contrast, the edge dislocation in BCC metals and the dislocations in face-centered-cubic metals exhibit low lattice resistance (Christopher R. Weinberger, Tucker, and Foiles 2013; Duesbery and Vitek 1998; Bhatia, Groh, and Solanki 2014).

In the case of BCC metals there is ambiguity regarding the preferred slip plane among {110}, {112} and {123} that correspond to the <111> slip direction (C R Weinberger, Boyce, and Battaile 2013). The slip along the {123} plane has only been observed at high temperatures or the presence of impurities. Therefore, it appear slip can take place along the {110} or the {112} planes. However, modelling and experimental efforts have observed that at low temperature slip happens along the {110} plane (Christian 1983; Wasserbäch et al. 2002; C R Weinberger, Boyce, and Battaile 2013). The non-planar configuration of the screw dislocation has been attributed with the high lattice resistance

(Ito and Vitek 2001; C R Weinberger, Boyce, and Battaile 2013). This non-planar dislocation core structure brings about a non-Schmid effect on the yield behavior (for details refer (Christian 1983). Therefore, it is critical to understand the slip behavior of screw dislocations for the comprehensive understanding of the plastic flow.

However, there are additional complications involved in studying the role of hydrogen on the dislocation mobility. In general, the presence of solutes in solid solution is a commonly used method to attain strengthening in alloys. The strength comes from modifications to the elastic, chemical and electronic interactions between the dislocations (Cottrell 1948; Hirth and Lothe 1966). In the presence of hydrogen, it has been suggested that hydrogen reduces the stress required for dislocations to multiply and glide (Beachem 1972). This concept was further examined by Lynch (S. P. Lynch 1984; S. P. Lynch 1988) from the perspective of adsorbed hydrogen atoms weakening the interatomic bonds leading to localized plasticity. However, Birnbaum, Robertson and coworkers (Birnbaum and Sofronis 1994; P. Ferreira, Robertson, and Birnbaum 1998; I. Robertson 1999; Sofronis, Liang, and Aravas 2001a) proposed that hydrogen forms an atmosphere around the dislocation by redistribution of the hydrogen atoms leading to the modification of the elastic interactions between dislocations and microstructural obstacles. Consequently, the dislocations glide at lower levels of applied stress.

Atomistic and first principle simulations have provided valuable insights into the plastic behavior of BCC metals. These studies have been able to establish the non-planar nature of the <111> screw dislocation core (Duesbery, Vitek, and Bowen 1973; Duesbery and Vitek 1998; Ito and Vitek 2001; Itakura, Kaburaki, and Yamaguchi 2012). Further, these simulations have reported the existence of two possible equilibrium core structures

(Vitek and Paidar 2008) both having D3 symmetry along the <111> zone (Gordon, Neeraj, and Mendelev 2011; Itakura, Kaburaki, and Yamaguchi 2012; Ashwin Ramasubramaniam, Itakura, and Carter 2009a) (Figure 21a-b). The existence of an unstable split-core configuration is observed in the motion of the dislocation across the lattice (Itakura, Kaburaki, and Yamaguchi 2012; Ventelon et al. 2013; Christopher R. Weinberger, Tucker, and Foiles 2013) as seen in Figure 21c. These studies have led to the development of crystal plasticity formulations which take into account the temperature and strain rate effects (Gröger et al. 2008; Gröger and Vitek 2008; Christopher R. Weinberger et al. 2012; Lim et al. 2015). However, the choice of interatomic potential for the atomistic simulations has a large influence on the stable dislocation configuration and the shape of the Peierls energy barrier (single hump vs. camel hump) (Ventelon and Willaime 2010; Christopher R. Weinberger, Tucker, and Foiles 2013; Hale, Zimmerman, and Weinberger 2014). In order to overcome this limitation, the first principle methods (density functional theory and quantum mechanics/ molecular mechanics method) (Zhao and Lu 2011a; Itakura, Kaburaki, and Yamaguchi 2012; Christopher R. Weinberger, Tucker, and Foiles 2013; Ventelon et al. 2013) can be employed. However, the computational cost involved with this method makes it unfeasible for the development of crystal plasticity formulation. Hence, the atomistic simulations employing an interatomic potential that can accurately predict the equilibrium dislocation core structure and the Peierls barrier curve can be employed to study the effect of hydrogen on the dislocation mobility.

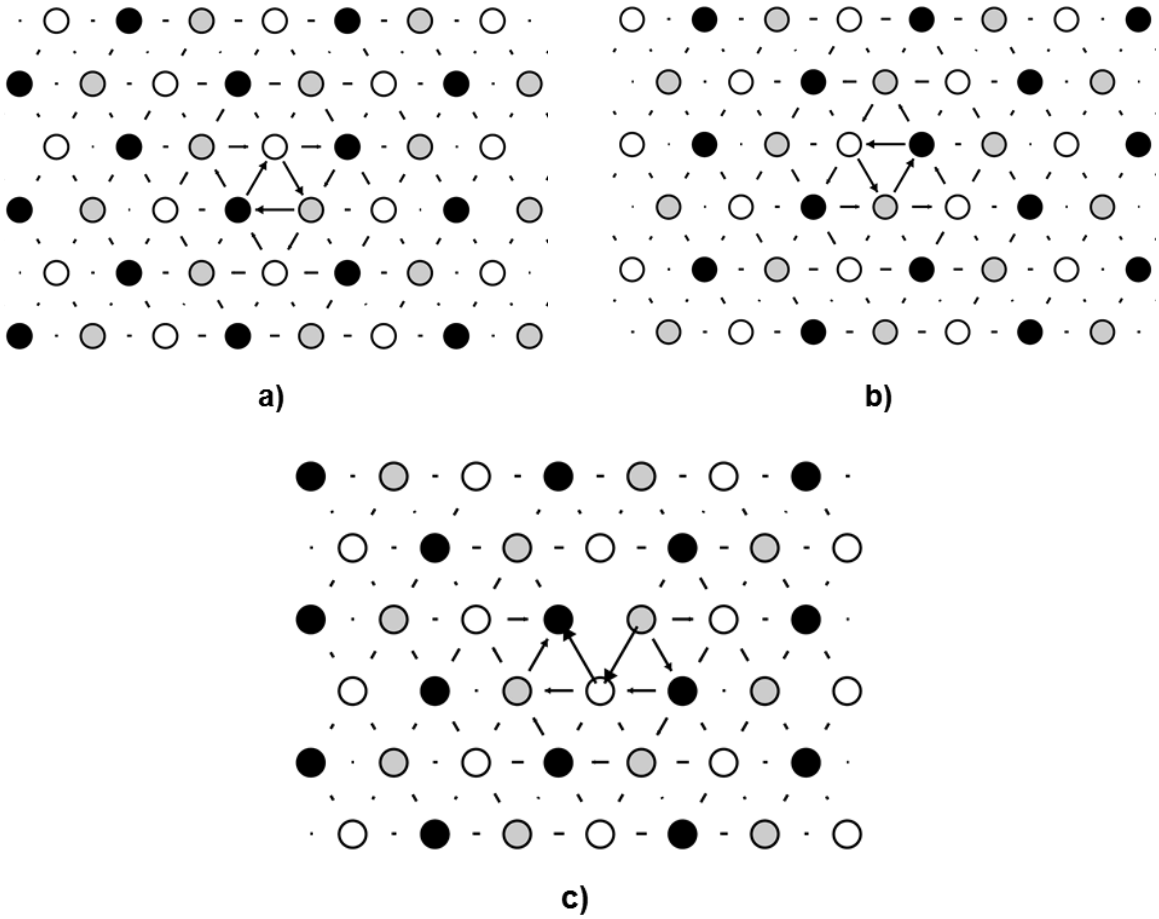


Figure 21: Differential displacement maps for the anisotropic linear elasticity solution for a) the easy-core, b) hard-core and c) split-core configurations. The atomic positions are represented by different colors to emphasize the distinct {111} planes.

In this chapter, we will present a systematic investigation that will focus on the effect of stress state on the $\frac{a}{2}\langle 111\rangle$ screw dislocation mobility in iron under the influence of hydrogen at 0 K. We start by calculating the stacking fault energies for the <111> Burger's vector along various planes ({110}, {112} and {123}), and found that the {110} plane has the lowest stacking fault energy followed by the {112} then the {123} in agreement with previous findings. Next, we examined the ability of the Fe-H interatomic potential (Ashwin Ramasubramaniam, Itakura, and Carter 2009a) to correctly predict the dislocation cores in pure Fe. It was found that the interatomic potential predicts a metastable state in the dislocation migration path (camel hump shaped), but for BCC

metals it has been established that during the dislocation motion there are no metastable configurations (Ventelon et al. 2013; Proville, Rodney, and Marinica 2012; Christopher R. Weinberger, Tucker, and Foiles 2013; Hale, Zimmerman, and Weinberger 2014; Itakura, Kaburaki, and Yamaguchi 2012). Nonetheless, we developed a consistent framework to quantify the effect of stress state on the critical resolved shear stress (CRSS) at which the dislocation overcomes the frictional resistance. It was found that the sense of shearing revealed a twinning-antitwinning asymmetry (Christian 1983; Duesbery and Vitek 1998; Gröger et al. 2008) for pure iron with the help of the interatomic potential of Chamati et al. (Chamati et al. 2006). This clearly illustrates that the CRSS was dependent on the orientation of the maximum resolved sheared stress plane (MRSSP) that does not obey the Schmid law. Therefore, the methodology developed in this chapter represents a significant contribution in development of a crystal plasticity framework that accurately describes the effect of hydrogen on dislocation mobility.

## 6.2 Methodology

In this section, the simulation technique to quantify the non-Schmid behavior associated with the effect of stress state of the screw dislocation is described. This work was performed using the LAMMPS molecular dynamics package (Plimpton 1995). The atomistic simulations were constructed with a perfect BCC lattice of Fe atoms with the crystallographic orientations $[\bar{1}2\bar{1}]$ (X), $[\bar{1}01]$ (Y) and $[111]$ (Z) (Figure 22). The simulation cell dimensions were $24a[\bar{1}2\bar{1}] \times 40a[\bar{1}0\bar{1}] \times 4a[111]$, where *a* is the lattice constant for iron. The screw dislocation was inserted using Stroh's anisotropic solution (Stroh 1958). The Burgers vector direction (Z) was periodic, while the outer layer of atoms along the X and Y directions were held fixed. The angle between the MRSSP and

the $(\bar{1}01)$ plane is defined by $\chi$ (measured in a clockwise sense) (Figure 22). Due to the crystal symmetry, $\chi$ was only varied in the range $-30° \leq \chi \leq 30°$ representing the {112} planes in BCC crystal. It is worth mentioning that the positive (twinning) and negative (anti-twinning) angles of $\chi$ are not equivalent.

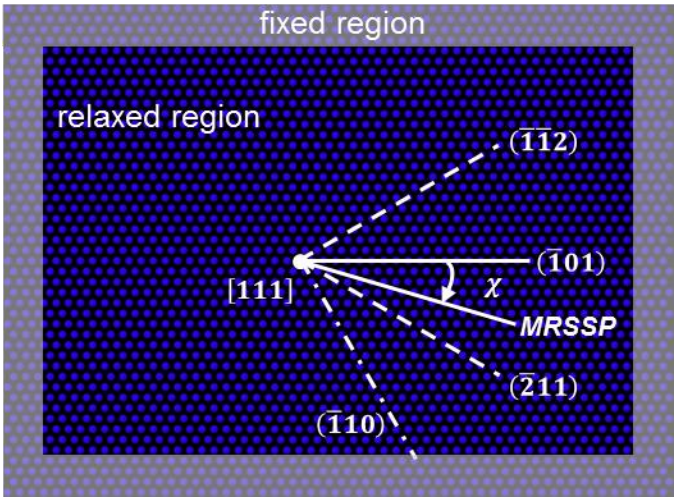


Figure 22: The schematic representation of the simulation cell. The fixed region (gray) atoms are held fixed through the minimization and the relaxed region (blue) atoms are allowed to relax during the minimization process. The angle between the MRSSP and the $(\bar{1}01)$ plane is defined by $\chi$ (measured in a clockwise sense).

In the right-handed coordinate system with the normal to the MRSSP aligned along the Y axis, the Z axis parallel to the Burgers vector. The stress tensor for applying shear stress parallel $(\sigma)$ and perpendicular $(\tau)$ to the Burgers vector is given as follows:

$$\Sigma^{MRSSP} = \begin{bmatrix} -\tau & 0 & 0 \\ 0 & \tau & \sigma \\ 0 & \sigma & 0 \end{bmatrix} \tag{17a}$$

The stress tensor mentioned above can be transformed by rotation of $-\chi$ about the Burger vector direction (Z) to obtain various MRSSP.

$$\Sigma^{(\bar{1}01)} = \begin{bmatrix} -\tau\cos 2\chi & \tau\sin 2\chi & \sigma\sin\chi \\ \tau\sin 2\chi & \tau\cos 2\chi & \sigma\cos\chi \\ \sigma\sin\chi & \sigma\cos\chi & 0 \end{bmatrix} \tag{17b}$$

The transformed stress tensor was then used to apply load to the atomistic simulation cell (Figure 21). The atoms within the relaxed region were minimized using a nonlinear conjugate gradient scheme. The CRSS was obtained by measuring the shear stress acting on the MRSSP in the slip direction that is required to initiate slip. The CRSS was calculated by incrementally applying the shear stress acting on the MRSSP $(5 \times 10^{-5} \times C_{44} \approx 5.7\ MPa)$ until the dislocation moves by at least one periodic unit cell.

## 6.3 Results

The Peierls energy barrier for a screw dislocation was measured using the nudge elastic band (NEB) method (Henkelman, Uberuaga, and Jónsson 2000) for the interatomic potentials developed by Chamati et al. (Chamati et al. 2006) and Ramasubramaniam et al. (Ashwin Ramasubramaniam, Itakura, and Carter 2009b) (Figure 23). The NEB calculations require the initial and final dislocation core positions to predict the energy pathway (camel hump shaped). The embedded atom description by Ramasubramaniam et al. (Ashwin Ramasubramaniam, Itakura, and Carter 2009b) clearly predicts a metastable dislocation configuration in the middle of the reaction pathway, corresponding to the split-core (Figure 21c and 30). On the other hand, the interatomic potential description by Chamati et al. (Chamati et al. 2006) predicts single hump sinusoidal shaped Peierls barrier that was found to be in agreement with previous findings (Ventelon et al. 2013; Itakura, Kaburaki, and Yamaguchi 2012) (Figure 23). It has been established by various previous studies that during the dislocation motion in BCC metals, there is a lack of metastable configurations (Ventelon et al. 2013; Proville, Rodney, and Marinica 2012; Christopher R. Weinberger, Tucker, and Foiles 2013; Hale,

Zimmerman, and Weinberger 2014; Itakura, Kaburaki, and Yamaguchi 2012). The Fe-H interatomic potential by Ramasubramaniam et al. (Ashwin Ramasubramaniam, Itakura, and Carter 2009b) fails to accurately predict the Peierls energy barrier. Therefore, the methodology developed here to examine the non-Schmid effect was applied in α-Fe.

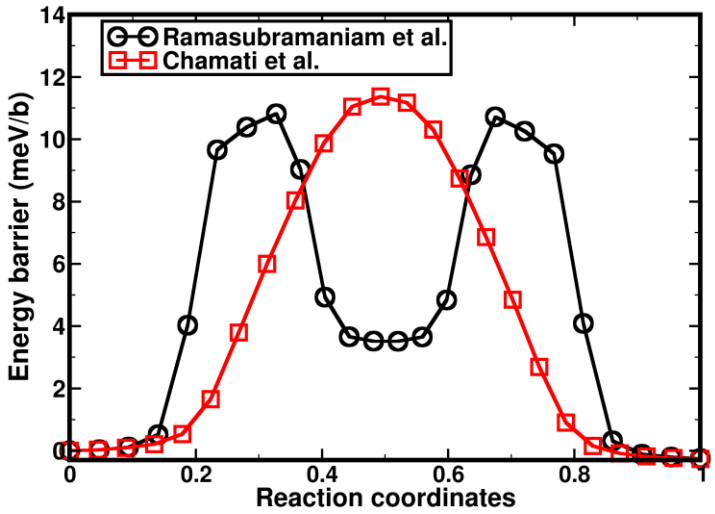


Figure 23: The Peierls potentials for various interatomic potentials for Fe using molecular dynamics. The energy barrier for dislocation motion was calculated by moving an isolated dislocation by one periodic length using the NEB method.

The generalized stacking fault energy along the <111> direction for {110}, {112} and {123} slip planes was measured using the interatomic potential by Chamati et al. (Chamati et al. 2006) as shown in Figure 24. The generalized stacking fault energy curve is defined as the change in energy per unit area obtained by gliding atomic planes past each other. The shape of the generalized stacking fault curve was found to be very similar for the three slip planes examined here (Figure 24). Furthermore, no intermediate minima were found along all the slip planes and maximum fault energy was obtained at 0.5b. This results in an absence of partial dislocation dissociations, which is consistent with previous findings on BCC materials (Christian 1983). Finally, based on the stacking fault

energy curve the {110} planes would be the energetically favorable for dislocation activity in the low temperature regime followed by the {112} and {123} planes.

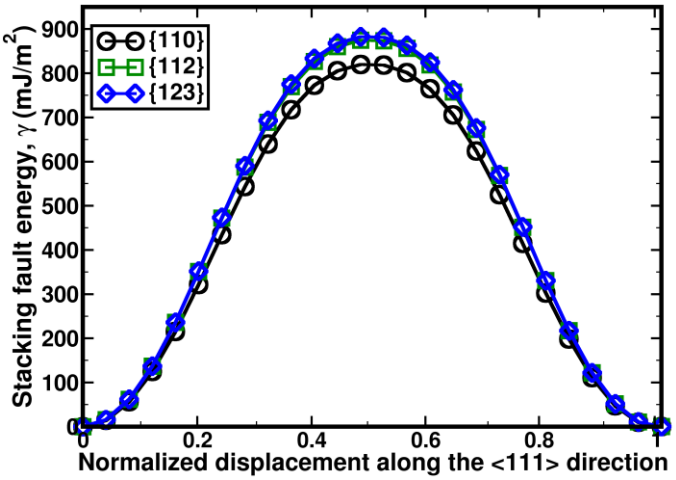


Figure 24: The generalized stacking fault energy curve by displacing along the <111> direction over {110}, {112} and {123} planes. The displacement is normalized by the magnitude of the Burgers vector $\left(\frac{a}{2}[111]\right)$.

6.3.1 *Loading by Applying Pure Shear Stress along the Burgers Vector Direction*

The evolution of Peierls stress as a function of variation in orientation of the MRSSP was examined. $\tau = 0$ MPa was substituted in Equation 17b. The shear stress along the Burgers vector direction ($\sigma$) was increased until the dislocation overcomes the internal resistance. According to the Schmid law, dislocation glide begins when the shear stress parallel to the Burgers vector on any given slip plane overcomes the Peierls stress. This implies that the orientation of the MRSSP and stress state play no role in the deformation behavior. The MRSSP was varied by changing the angle ($\chi$) between the MRSSP and the $(\bar{1}01)$ plane (Figure 22) in Equation 17b. As the $\chi$ increased from -25 to 25 the CRSS value consistently increased causing an asymmetry due to the change in shear direction in agreement with previous findings (Christian 1983; Duesbery, Vitek, and Bowen 1973;

Duesbery and Vitek 1998; Lim et al. 2015) (Figure 25). In the case of $\chi < -10°$ the dislocation was found to glide along the $(0\bar{1}1)$ plane; for the other cases the dislocation glide took place along the $(\bar{1}01)$ plane.

### 6.3.2 *Loading by Combined Application of Shear Stress Perpendicular and Parallel to the Burgers Vector Direction*

The effect of shear stress perpendicular to the Burgers vector on the Peierls stress was examined. The effect of these complicated stress states on the dislocation mobility cannot be examined experimentally, but with the help of simulations the effect of each of the components of the stress tensor (Equation 17b) can be quantified. In this case, $\tau = 114$ MPa was substituted in Equation 17b and the corresponding elastic displacement was applied. The shear stress perpendicular to the Burger vector $(\tau)$ was held constant, and the shear stress along the Burgers vector was increased incrementally until the dislocation glide was observed. The application of positive shear stress perpendicular to the Burgers vector $(\tau > 0)$ reduces the Peierls stress for dislocation glide (Figure 25), similar to the previous results (Christian 1983; Duesbery, Vitek, and Bowen 1973; Duesbery and Vitek 1998; Lim et al. 2015). In the case of $\chi = -25°$, the dislocation was found to glide along the $(0\bar{1}1)$ plane. For the other cases the dislocation glide took place along the $(\bar{1}01)$ plane. The application of negative shear stress perpendicular to the Burgers vector $(\tau < 0)$ was found to increase the CRSS for dislocation glide (Figure 25). It was found that for $\chi \leq -10°$, the dislocation was found to glide along the $(0\bar{1}1)$ plane. For the remaining cases dislocation glide was found along the $(\bar{1}01)$ plane.

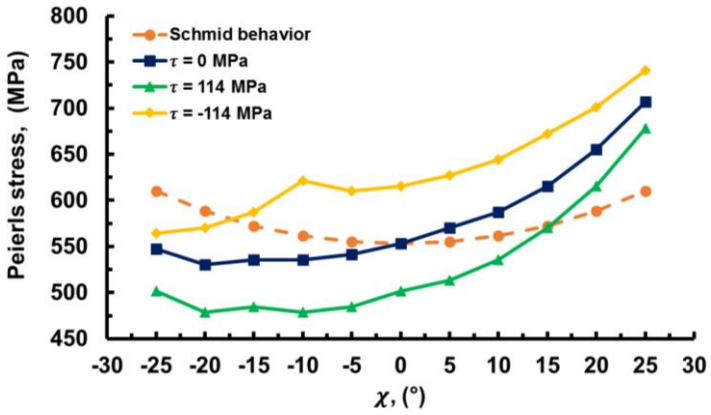


Figure 25: A comparison between the Schmid behavior and the observed Peierls stress for $\tau = 0$ MPa, $\tau = 114$ MPa and $\tau = -114$ MPa (Equation 17b) for various MRSSP orientations.

6.4 Summary

In this work, we have developed a comprehensive atomistic approach to study the dislocation behavior in BCC metals and shown initial results that are in agreement with the recent study by Lim et al. (Lim et al. 2015) on developing a multi-scale model for dislocation plasticity in iron. Unfortunately, the effect of hydrogen on the non-Schmid behavior cannot be carried out with the interatomic potential available (A. Ramasubramaniam et al. 2008). The Peierls energy barrier curve (Figure 23) predicts a metastable configuration in the dislocation reaction pathway that has been found to be inaccurate for BCC metals (Ventelon et al. 2013; Proville, Rodney, and Marinica 2012; Christopher R. Weinberger, Tucker, and Foiles 2013; Hale, Zimmerman, and Weinberger 2014; Itakura, Kaburaki, and Yamaguchi 2012). Nonetheless, the methodology developed can be employed to accurately describe the effect of hydrogen on plasticity at the continuum scale.

# CHAPTER 7

# 7 ENERGETICS, STABILITY AND INTERACTION OF GRAIN BOUNDARY TRIPLE JUNCTIONS WITH POINT DEFECTS

## 7.1 Introduction

Nanocrystalline (NC) materials (mean grain size, d < 100 nm) often have enhanced mechanical properties compared to coarse-grained materials ($d > 1$ μm). Therefore NC alloys are very attractive for multiple engineering applications, including for load-bearing structures (Valiev, Xia, and Langdon 2009). The challenge with broader applicability of NC materials has been the stability of the non-equilibrium microstructure during processing and deformation. It has been long established that the structural stability, mechanical behavior and fracture of NC materials is often driven by GBs (GBs, planar defects), triple junctions (TJs, line defects) and their underlying structures (Meyers, Mishra, and Benson 2006; Gleiter 2000). Hence a fundamental understanding of the relationship between the line/planar defect structures and the associated properties is important to develop interface-dominant materials. This is especially true in the case of NC materials where TJs constitute a large volume fraction and the properties have been found to be very different from the neighboring grains (Gleiter 2000).

In NC materials, the grain growth behavior is typically characterized with the help of classical (2D) approaches such as the original von Neumann-Mullins relation (Mullins 1956). However, such a model provides an incomplete description of the grain growth kinetics in NC materials as it ignores the TJ contribution in this behavior. In fact, Czubayko et al. (Czubayko et al. 1998) experimentally showed that a low TJ mobility can

induce a significant drag effect on the grain growth and subsequently proposed a modified von Neumann-Mullins relationship that, to some extent, captures the interplay between the GB and TJ kinetics on the grain growth behavior (Czubayko et al. 1998). Nevertheless, such models were derived with the help of applying geometric and thermodynamic constraints on TJs. Therefore, these models fail to account for the varying TJ structures and the distinct intrinsic properties and the effect of TJs on the grain growth behavior of NC materials (Gottstein, King, and Shvindlerman 2000; Moneesh Upmanyu et al. 1999; M Upmanyu et al. 2002; Gottstein, Ma, and Shvindlerman 2005). The structural stability of TJs has been linked to several thermodynamic variables, such as the excess free energy, the resolved line tension and the resolved line force of TJs (Gottstein, King, and Shvindlerman 2000; Srinivasan et al. 1999; King 1999). For instance, Gottstein et al. have shown that the excess Gibbs energy at the TJ can serve as a measure of the TJ mobility (Gottstein, King, and Shvindlerman 2000). Nonetheless, there is a lack of systematic investigations exploring various thermodynamic properties of TJs formed by commonly observed GBs (Fortier et al. 1991; Fortier, Miller, and Aust 1997; Schuh, Kumar, and King 2005; Kremer et al. 2005; Rohrer et al. 2010) and their links to the structural stability of NC materials, i.e., defect migrations.

The presence of trace amounts of solutes at microstructural sinks (GB and TJs) can bring about drastic change in mechanical properties of structural materials (Ullmaier 1984; Stoller 1990; Bloom et al. 2007). This issue becomes increasingly critical during the design of NC microstructures for structural applications. Thus, the interaction of solute atoms with defects is critical in understanding the material response under harsh

conditions, such as radiation and corrosion damage. During these processes, spatial rearrangement of point defects and solute atoms takes place. The incoming flux of defects towards GBs and TJs leads to the segregation of solute atoms. Atomistic simulations have been used to understand the underlying mechanisms with GB-solute interaction (Rajagopalan, Tschopp, and Solanki 2014; N. R. Rhodes, Tschopp, and Solanki 2013; M. Yamaguchi, Nishiyama, and Kaburaki 2007). In these works, it has been observed that trace amounts of solute atoms at the GB can cause a drastic decrease in interface strength (H, He, P and Ga). On the other hand, the presence of solute atoms, such as B, V and C provides increased interfacial strength and ductility.

In this work, atomistic simulations were used to study the intrinsic properties associated with GB TJs in Fe. The sink efficiency of TJs for various point defects (vacancies and self-interstitials (SIA)) and solute atom (H) configurations was examined. The TJs were formed by the intersection of <110> symmetric tilt GBs in BCC Fe. The TJs have a distinct atomistic structure compared to those of their constituent GBs and, therefore, distinct properties (King 2010). Hence, the solute drag phenomena was examined for a range of special TJs that involve the Σ3 GB (these TJs have been shown to occur frequently (Fortier et al. 1991; Fortier, Miller, and Aust 1997; Rohrer et al. 2010)) (Table 6).

7.2 Methodology

Molecular statics simulations using LAMMPS (Plimpton 1995) were employed in this work to investigate the structural stability of TJs. The Fe-H atomic interactions in this work were described using the EAM potential of Ramasubramaniam et al. (Ashwin Ramasubramaniam, Itakura, and Carter 2009a), which is based on the Fe EAM potential of Hepburn and Ackland (Hepburn and Ackland 2008). The Fe-H potential was parameterized using an extensive database of energies and configurations from DFT calculations of dissolution and diffusion of hydrogen in bulk α-Fe, the binding of hydrogen to free surfaces, vacancies and dislocations, as well as other cross interactions between hydrogen and Fe. In this work TJs were constructed using <110> symmetric tilt GBs (see Table 6). These GBs were generated using the methodology described in Chapter 4. Circular wedges were then cut from the GBs along the stitch plane, i.e. {001}/{011} planes (see Figure 26) (Kremer et al. 2005; Wu, Zhou, and Nazarov 2007).

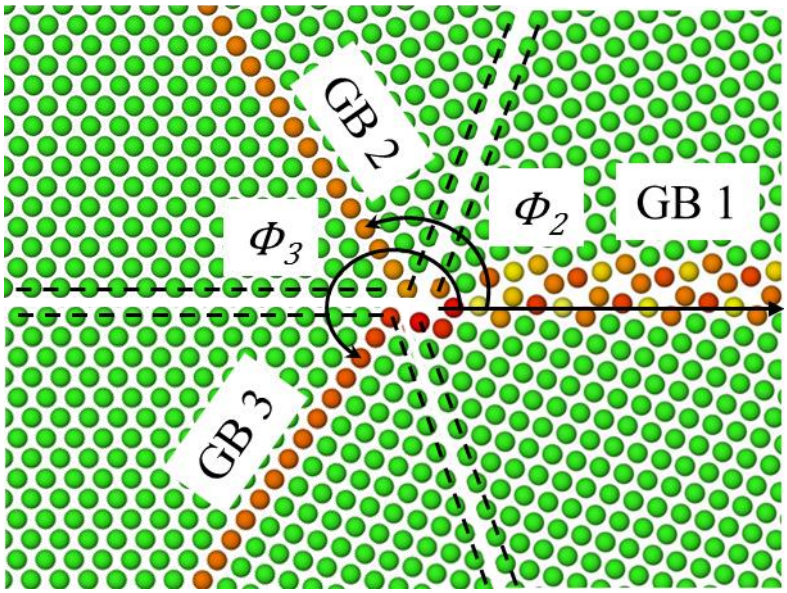


Figure 26: Schematic showing construction of a GB TJ configuration. The GBs were minimized separately and a wedge was carved out along the {001}/{011} plane represented by dashed lines.

Table 6: Details of grain boundary triple junctions along with the CSL and the misorientation ($\theta$) for each GB interface.

| **Triple Junction** | **GB #1 ($\Sigma$, $\theta$)** | **GB #2 ($\Sigma$, $\theta$)** | **GB #3 ($\Sigma$, $\theta$)** |
|---|---|---|---|
| Σ3-Σ3-Σ9 | Σ9 (114), 38.94° | Σ3 (112), 70.53° | Σ3 (112), 70.53° |
| Σ3-Σ9-Σ27 | Σ9 (221), 141.06° | Σ9 (221), 141.06° | Σ3 (112), 70.53° |
| Σ3-Σ11-Σ33 | Σ33 (225), 58.99° | Σ11 (332), 129.52° | Σ3 (112), 70.53° |
| Σ3-Σ19-Σ57 | Σ57 (558), 82.95° | Σ19 (116), 26.52° | Σ3 (112), 70.53° |
| Σ3-Σ27-Σ81 | Σ81(778), 102.12° | Σ27 (115), 31.59° | Σ3 (112), 70.53 |
| Σ3-Σ33-Σ99 | Σ99 (7710), 89.42° | Σ33 (118), 20.05° | Σ3 (112), 70.53° |

Subsequently, GBs labelled 2 and 3 were rotated by $\phi_2$ and $\phi_3$ about the GB tilt axis, as shown in Figure 26. Lastly, the three wedges were brought together, the overlapping atoms were removed and the energy minimization carried out at 0 K. According to the Herring's relation the TJ attempts to minimize the resolved surface tension during formation. The resolved line tension acting at the TJ was approximated at the atomic scale using the following relation:

$$\gamma_r = \sum_{i=1}^{3} \gamma_i \, l_x^i \tag{18}$$

where, the periodic length of each GB interface ($l_x^i$) was used to weigh the surface tension contribution of each interface. The surface tension for the intersecting GBs ($\gamma_i$) was defined by averaging the normal and tangential components of stress acting over a region of ±20 Å normal to the interfaces. The resolved line force was another quantity used to understand the energetics of TJs. This was defined as:

$$F_i = \Delta E_i l_x^i \tag{19a}$$

$$F_{TJ} = \sqrt{\left(\sum_{i=1}^{3} F_i \cos\phi_i\right)^2 + \left(\sum_{i=1}^{3} F_i \sin\phi_i\right)^2} \quad (19b)$$

The excess energy per unit GB area ($\Delta E_i$) subsequent to the formation of the TJ was defined over a region of ±20 Å normal to the GB. The line force for all the GBs was resolved at the TJ ($F_{TJ}$) to obtain the line force at the TJ.

The vacancy formation energy at an atomic site α ($E_f^{\alpha}$) is defined as:

$$E_f^{\alpha} = E_{TJ}^{\alpha} - E_{TJ} + E_{coh} \quad (20a)$$

The defect formation energy at an interstitial site $\beta$ (H and SIA) is defined as:

$$E_f^{\beta} = E_{TJ}^{\beta} - E_{TJ} - E_{coh} \quad (20b)$$

where, $E_{coh}$ is the cohesive energy per atom of the defect in the pristine lattice and $E_{TJ}^{\alpha}$, $E_f^{\beta}$ and $E_{TJ}$ are the total energies of the TJ simulation cell in the presence of a vacancy, interstitial solute atom and the bulk respectively. It is useful to relate the defect formation energy in the TJ configuration ($E_f^{\alpha,\beta}$) with that in the bulk ($E_f^0$) to quantify the vacancy binding energy at an atomic site α:

$$E_b^{\alpha,\beta} = E_f^0 - E_f^{\alpha,\beta} \quad (21)$$

## 7.3 Results

The atomic hydrostatic stress for various TJs has been shown in Figure 27. The buildup of hydrostatic stress near the Σ3-Σ3-Σ9 (Figure 27a) was far greater in contrast to the Σ3-Σ9-Σ27 (Figure 27b). Similarly, the buildup of hydrostatic stress for the Σ3-Σ19-Σ57 and Σ3-Σ27-Σ81 outlines the underlying GB dislocation structure. In some cases, Σ3-Σ3-Σ9 and Σ3-Σ11-Σ33, the stress accumulation far exceeds the stress along the constituent GBs. This implies that the TJ has a greater amount of elastic strain energy stored. In contrast to Σ3-Σ27-Σ81 and other TJs, the stress accumulated was far less when compared to the constituent GBs. This variation of atomic hydrostatic stress near the TJ was further used to characterize the resolved line tension that will be discussed later.

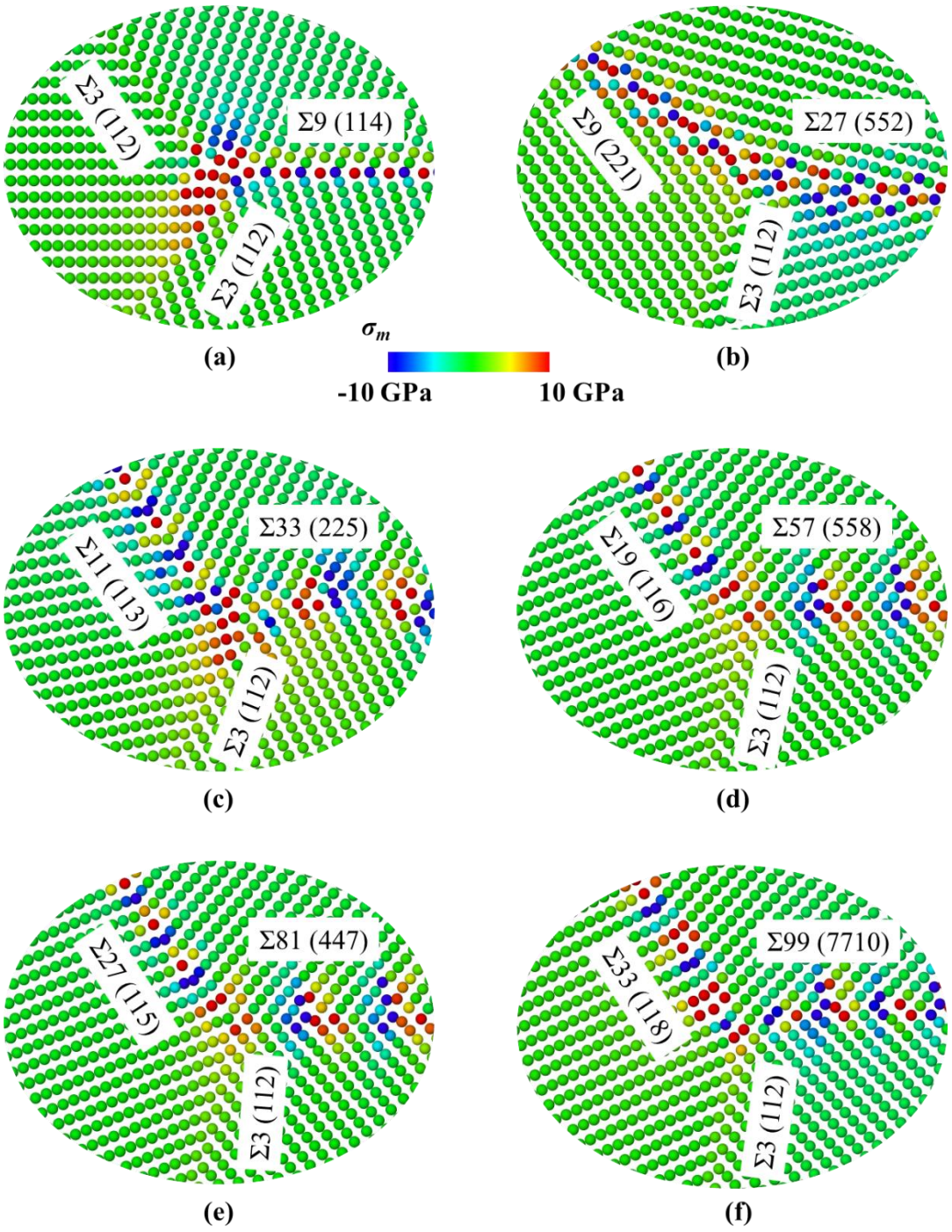


Figure 27: The minimized atomic configuration of: a) Σ3-Σ3-Σ9, b) Σ3-Σ9-Σ27, c) Σ3-Σ11-Σ33, d) Σ3-Σ19-Σ57, e) Σ3-Σ27-Σ81 and f) Σ3-Σ33-Σ99 TJs. Atoms were colored according to the local variation in hydrostatic stress from -10 to 10 GPa.

The net change in volume due to the formation of the TJ was computed using the following relation to comprehend the misfit strain induced during the formation of TJ.

$$\Delta V_{TJ} = \pi r_{TJ}^2 - \frac{n\omega_{bulk}}{r_{TJ}} - \sum_{i=1}^{3} l_x^i \Delta V_{GB}^i \tag{22a}$$

$$r_{TJ} = max(l_x^i) \tag{22b}$$

Here $r_{TJ}$ is the radius for the TJ for calculating net change in volume, $\omega_{bulk}$ is the atomic volume in a pristine BCC lattice at 0 K, and $\Delta V_{GB}^i$ is the volume expansion along the GB plane per unit of the GB area for the $i^{th}$ interface.

The net change in normalized volume follows a clear trend that TJs with high Σ GBs undergo greater volumetric expansion in contrast to other TJs (see Figure 28a). This suggests that the high Σ GBs would form a more diffused TJ which was found to be in agreement with previous findings (Costantini et al. 2000). As discussed previously, the line tension can significantly affect the mobility of the TJ; hence, we computed the line tension for various TJs. According to Herring's relation the TJ attempts to minimize the resolved surface tension during formation. The resolved line tension acting at the TJ was approximated at the atomic scale using the following relation:

$$\gamma_r = \sum_{i=1}^{3} \gamma_i \, l_x^i \tag{23}$$

The surface tension for the intersecting GBs ($\gamma_i$) was defined by averaging normal and tangential stresses acting over a region of ±20 Å normal to the interfaces. The excess energy due to the formation of TJs can also be described as the elastic strain energy stored due to the formation of TJs and is defined as:

$$\Delta E_{TJ} = \left( E_{TJ} - nE_{coh} - \sum_{i=1}^{3} E_{GB}^{i} l_x^i l_z \right) / l_z \quad (24)$$

where $E_{TJ}$ is the energy of the defected structure with TJ and GB interfaces, $E_{coh}$ is the cohesive energy of each atom at 0 K in a pristine BCC lattice, $E_{GB}^{i}$ is the GB formation energy per unit area for the $i^{th}$ interface and $l_x^i$ is the length of the unit vector tangential to the GB plane. The net excess energy was normalized by the line length ($l_z$) of the TJ. These results were found by summation of atomic energies within a distance of 19 nm from the TJ. The resolved line tension followed a trend similar (Figure 28b) to the net change in volume at the TJ with a local maxima for the Σ3-Σ9-Σ27. In the case of the resolved line tension, the Σ3-Σ33-Σ99 had a high line tension compared to other TJs.

The trend for excess energy at the TJ (Figure 28c) was maximum for Σ3-Σ9-Σ27 the rest of the TJs have similar energies except Σ3-Σ3-Σ9 that had the lowest excess energy of $3 \times 10^{-8}$ J/m. The values for excess energy due to the formation of the TJ were found to be in close agreement with previous findings (Shekhar and King 2008; Costantini et al. 2000; Fortier et al. 1991).

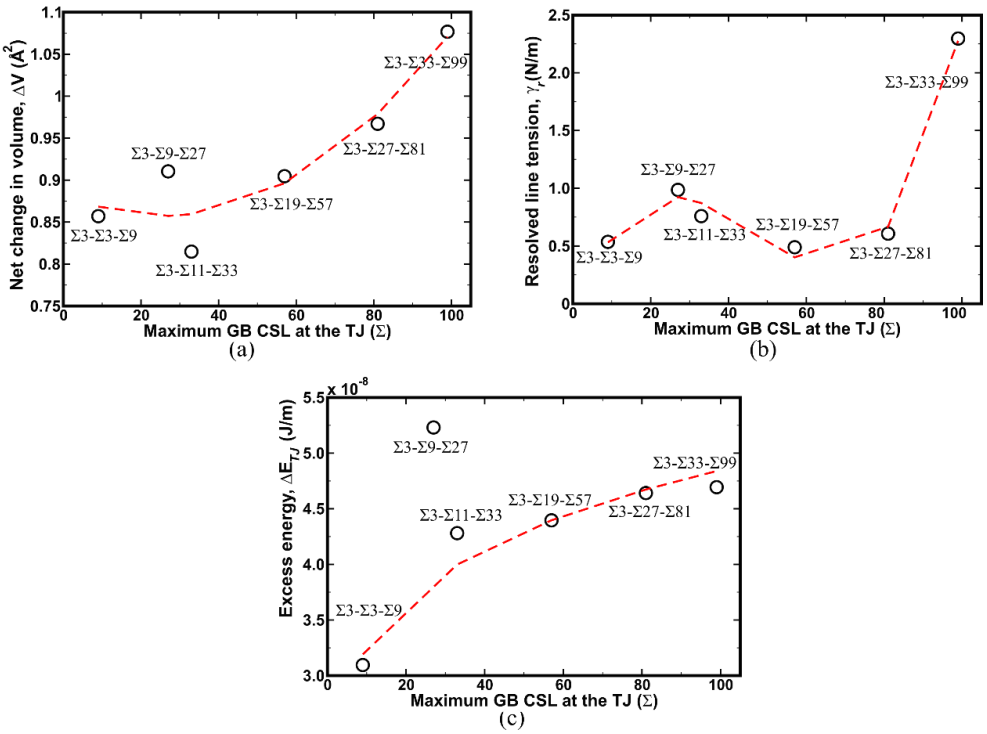


Figure 28: (a) The net change in volume at the TJ. In general, a clear trend can be observed that high CSL GB TJs underwent large volume change during formation of the TJ. (b) The resolved line tension acting along the TJ. c) The excess energy due to formation of the TJ.

Furthermore, equipped with the understanding of key intrinsic properties of various TJs the energetic interactions of various TJs with solute atoms/point defects were examined. The segregation/binding potency for solute atoms/point defects was computed at various atomic sites in the vicinity of the TJ (≤ 2 nm) as shown in Figure 29. The binding energy ($E_b$) is essentially the extra energy required to form a defect at a specific site near the defect region in comparison to the bulk formation energy of the defect ($E_b^{TJ} = E_f^{TJ} - E_f^{bulk}$, where $E_f^{bulk}$ for H vacancy and SIA was 0.28, 1.75, 3.5 eV, respectively, refer to (Solanki et al. 2012; Bhatia and Solanki 2013; Rajagopalan, Tschopp, and Solanki 2014)). Similarly, the segregation energy is opposite of the binding energy ($E_{seg}^{TJ} = -E_b^{TJ}$) .

### 7.3.1 *Vacancy*

The vacancies play a key role during mass-transport towards/away from the TJs. Thus, in this section we explore the effect of atomic structure surrounding the TJs on the vacancy binding behavior. The atomic sites with higher binding energy were found to be clustered near regions of high hydrostatic stress within the atomic structure (Figure 27). The effect of TJ on the binding tendency for atomic sites within the grains was found to be negligible, i.e., the atoms far away from the TJs are white (0 eV vacancy binding energy) indicating that there is no energy difference over the bulk lattice (see Figure 29). There is a clear difference between the number of minimum energy sites in the vicinity of the TJ between the Σ3-Σ3-Σ9 and Σ3-Σ33-Σ99 TJs (Figure 29a and 29b). The Σ3-Σ3-Σ9 TJ has minimum energy sites concentrated in a very small region around the TJ (3 Å radially) indicating the extent of the TJ elastic strain field (Figure 29a). On the other hand, the Σ3-Σ33-Σ99 TJ has more stable vacancy sites away from the TJ along the constituent GBs (Figure 29b). This clearly indicates that vacancies have a strong bias towards the defected structures with the greatest compressive strain field.
Furthermore, the role of constituent GBs and the TJ on vacancy binding was examined by plotting the mean binding energy as a function of radial distance from the TJ (Figure 29c). The vacancy binding energy for a majority of TJs converged to the bulk vacancy formation energy at a length of approximately 1.5 nm from the TJ. The Σ3-Σ3-Σ9 TJ had the maximum binding energy near the TJ (< 5 Å) of all the TJs followed by the Σ3-Σ33-Σ99 TJ. At first glance these TJs seem to be at odds with the measured intrinsic properties of the various TJs as both of these TJs represent opposite ends of the excess stored energy.

However, when investigated from the perspective of the underlying interplay between GB and TJ dominated binding behavior for point defects, the above mentioned behavior seems clear.

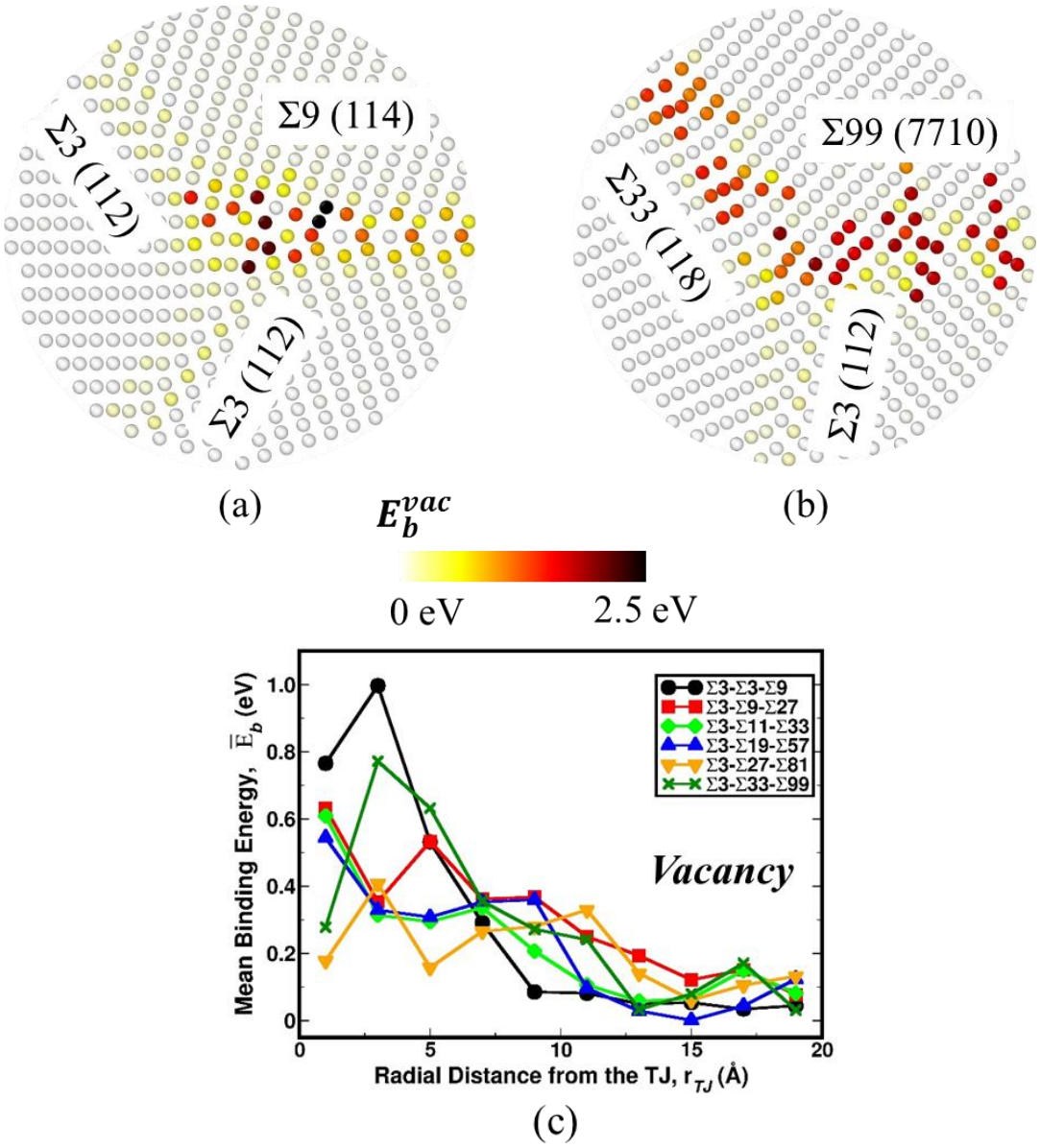


Figure 29: The atomic variation in vacancy binding energy near a) Σ3-Σ3-Σ9 and b) Σ3-Σ33-Σ99 TJs. The atoms were colored based on the vacancy binding energy at each site. c) The mean vacancy binding energy as a function of radial distance from the TJ. A total of 10 concentric bins were defined ($r_{i-1} \leq r \leq r_i$ ) up to 2 nm from the TJ. White atoms correspond to the bulk binding energy (~ 0 eV) and black atoms represent the minimum vacancy binding energy of 2.5 eV.

### 7.3.2 *Self-Interstitial Atom (SIA)*

Radiation damage creates lattice point defects (vacancies and interstitials) which can alter the physical and mechanical properties of the material through the nucleation of defects such as defect clusters, defect-impurity complexes, voids and defect-solute clusters. The stability of a nuclear material depends on its effectiveness in absorbing point defects through various microstructural sinks (GBs and TJs). Thus, in this section we explore the effect of the SIA on various TJs.

The variation in binding strength of SIA in the vicinity of the TJ was found by plotting the mean binding energy as a function of radial distance from the TJ core for various TJ (Figure 30). This clearly gives a measure of the interplay between GB and TJ strain fields. The Σ3-Σ3-Σ9 and Σ3-Σ11-Σ33 TJs have high binding strength for SIA in comparison to the other TJs (Figure 30). The TJ influence on the SIA binding was around 12-15 Å as the binding energy converges towards bulk beyond that distance. There seems to be a higher preference for absorbing SIA in contrast to vacancy around the TJs. These findings are consistent with results for GB sink efficiency for point defects (Tschopp et al. 2012a).

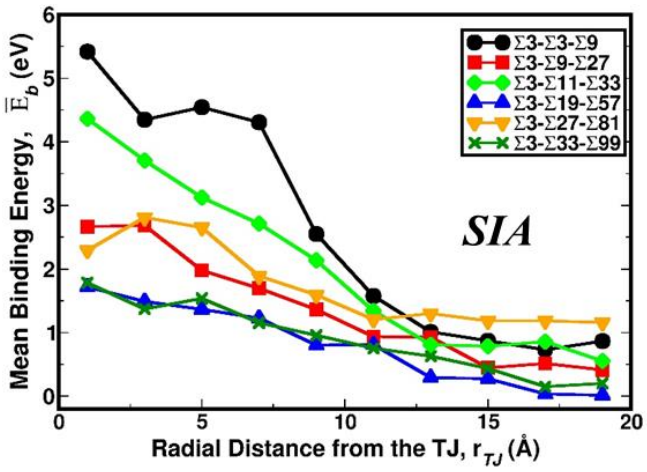


Figure 30: The mean binding energy for a self-interstitial atom as a function of radial distance from the TJ. A total of 10 concentric bins were defined ($r_{i-1} \leq r \leq r_i$ ) up to 2 nm from the TJ.

7.3.3 *Hydrogen*

The influence of the atomic structure surrounding the TJ was analyzed by visualizing the site to site variation in H binding energy variation (Figure 31a-b). The atomic sites with higher binding energy were found to be clustered near regions of high hydrostatic stress within the atomic structures of the Σ3-Σ3-Σ9 and Σ3-Σ11-Σ33 TJs. The influence of GB on the binding strength in the Σ3-Σ11-Σ33 TJ can be interpreted by looking at the far-field binding energies along the GB. The mean binding energy versus the radial distance from the TJ gives a measure of the TJs that have a larger selection of stable sites near the core for the Σ3-Σ3-Σ9, Σ3-Σ11-Σ33 and Σ3-Σ27-Σ81 TJs (Figure 31c).

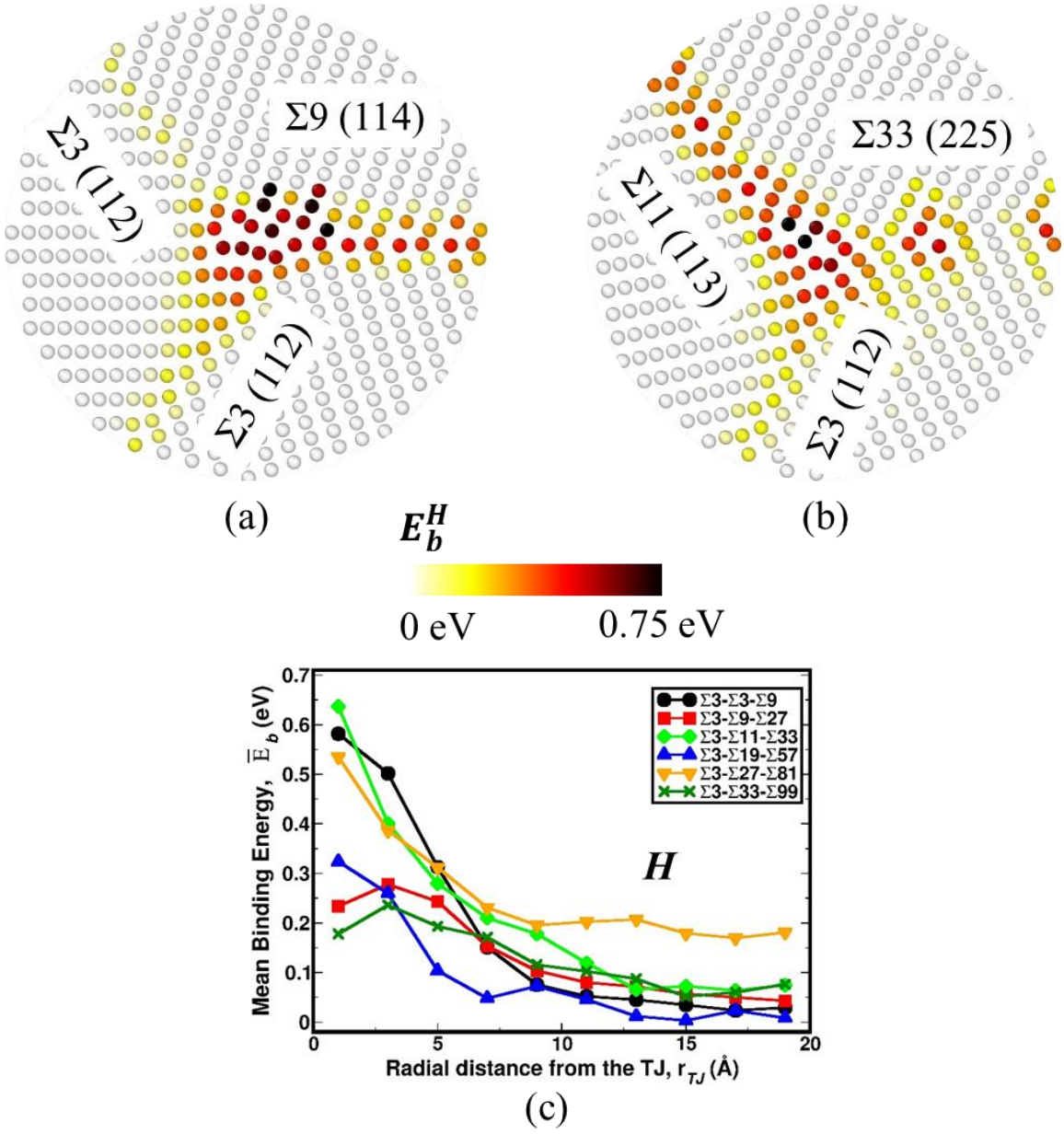


Figure 31: The atomic variation in vacancy binding energy near a) Σ3-Σ3-Σ9 and b) Σ3-Σ11-Σ33 TJs. The atoms were colored based on the vacancy binding energy at each site. c) The mean vacancy binding energy as a function of radial distance from the TJ. A total of 10 concentric bins were defined ($r_{i-1} \leq r \leq r_i$ ) up to 2 nm from the TJ. White atoms correspond to the bulk binding energy (~ 0 eV) and black atoms represent the minimum vacancy binding energy of 0.75 eV.

The physical ramifications of the distinctive properties of TJs compared to the constituent GBs was highlighted in terms of hydrogen concentration using the Langmuir-McLean (McLean 1957) relation (Figure 32). The concentration of solute (hydrogen) at the TJ ($X_{TJ}$) was expressed in terms of the nominal bulk concentration ($X_b = 0.28\%$), the binding energy for the solute atoms ($E_b$) in the vicinity of the defect and the temperature ($T$) in the following manner:

$$X_{TJ} = \left(1 + \left(\frac{1 - X_b}{X_b}\right) \exp(-E_b/k_B T\right)^{-1} \quad (25)$$

The Σ3-Σ3-Σ9 TJ was selected for the comparison between the TJ and GB hydrogen concentration profile (Figure 32). It has the least measured intrinsic properties but on the other hand shows the highest sink efficiency for point defects and solute atoms in this work (Figure 31). The Σ3-Σ3-Σ9 TJ was found to have a 100% sink efficiency for the nominal hydrogen concentration up to a temperature of 500 K, and beyond this temperature the sink efficiency of the TJ falls to 40% at 1000 K. On the other hand, the Σ3 and Σ9 GBs saw sharp drop in the hydrogen concentrations with increasing temperature. These findings clearly show that despite the limited segregation potency of the Σ3 GBs, these interfaces can create TJs in NC material that have a much higher tendency for solute segregation. This leads to increased susceptibility of decohesion at the TJ due to extremely rich environments of hydrogen.

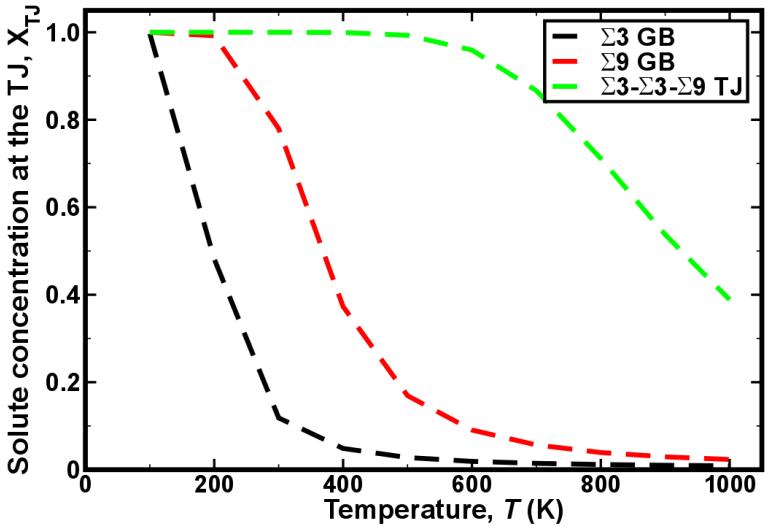


Figure 32: The unique behavior of the Σ3-Σ3-Σ9 TJ in comparison to the constituent GBs, in terms of variations in hydrogen concentration for a range of temperatures (Equation 25, $X_b^H = 0.28$ %).

7.4 Conclusions

In summary, the various intrinsic quantities pertinent to the structural stability of TJs and GB network in Fe were systematically quantified. This work provides insights regarding the structural stability of NC materials. The hydrostatic stress field and the net volume change can be used to measure the degree of variability in the TJ local structural arrangement, which influences the mechanical behavior of NC materials. For instance, the TJ misfit strain is a function of the net volume change during the formation of the TJ (Figure 28). The variation in atomic scale hydrostatic stress build up at the TJ allows visualization of the fact that TJ strain energy is not directly correlated to the constituent GBs but depends on other factors such as the location of the TJ with regard to the constituent GB structures. There is a strong energetic preference for SIA around the TJ over a vacancy defect (Figure 29 and 30). This is similar to the results observed for GBs in Fe (Tschopp et al. 2011). The hydrogen concentration across a wide range of

temperature for the Σ3-Σ3-Σ9 TJ was found to be distinctly higher in comparison to the constituent GBs (Figure 32); similar conclusions were drawn by King (King 2010). Overall, in this work a methodology to investigate the role of TJs with regard to the structural stability of NC material was developed and preliminary results on this have been presented.

# REFERENCES


Abell, G. C. 1985. “Empirical Chemical Pseudopotential Theory of Molecular and Metallic Bonding.” *Physical Review B* 31 (10): 6184–96. doi:10.1103/PhysRevB.31.6184.

Abraham, Daniel P., and Carl J. Altstetter. 1995a. “Hydrogen-Enhanced Localization of Plasticity in an Austenitic Stainless Steel.” *Metallurgical and Materials Transactions A* 26 (11): 2859–71.

———. 1995b. “The Effect of Hydrogen on the Yield and Flow Stress of an Austenitic Stainless Steel.” *Metallurgical and Materials Transactions A* 26 (11): 2849–58. doi:10.1007/BF02669643.

Adlakha, I., M. A. Bhatia, M. A. Tschopp, and K. N. Solanki. 2014. “Atomic Scale Investigation of Grain Boundary Structure Role on Intergranular Deformation in Aluminium.” *Philosophical Magazine* 94 (30): 3445–66. doi:10.1080/14786435.2014.961585.

Adlakha, I., and K. N. Solanki. 2015. “Structural Stability and Energetics of Grain Boundary Triple Junctions in Face Centered Cubic Materials.” *Scientific Reports* 5 (March). doi:10.1038/srep08692.

Andersen, Hans C. 1980. “Molecular Dynamics Simulations at Constant Pressure And/or Temperature.” *The Journal of Chemical Physics* 72 (4): 2384–93. doi:10.1063/1.439486.

Andrew, J. H. 1914. “The Embrittling of Iron by Caustic Soda.” *Transactions of the Faraday Society* 9 (0): 316–29. doi:10.1039/TF9140900316.

Apostol, F., and Y. Mishin. 2011. “Interatomic Potential for the Al-Cu System.” *Physical Review B* 83 (5): 054116. doi:10.1103/PhysRevB.83.054116.

Argon, Ali S. 2008. *Strengthening Mechanisms in Crystal Plasticity. Oxford: Oxford University*. Oxford.

Asano, S., and R. Otsuka. 1976. “The Lattice Hardening due to Dissolved Hydrogen in Iron and Steel.” *Scripta Metallurgica* 10 (11): 1015–20.

Aust, K. T., U. Erb, and G. Palumbo. 1994. “Interface Control for Resistance to Intergranular Cracking.” *Materials Science and Engineering: A* 176 (1–2): 329–34. doi:10.1016/0921-5093(94)90995-4.

Bachurin, D. V., D. Weygand, and P. Gumbsch. 2010. “Dislocation–grain Boundary Interaction in 〈1 1 1〉 Textured Thin Metal Films.” *Acta Materialia* 58 (16): 5232–41. doi:10.1016/j.actamat.2010.05.037.

Balluffi, R. W. 1977. “Grain Boundary Structure and Segregation.” *Interfacial Segregation*, 193–237.

Banerji, Samir K., Charles J. McMahon, and Howard C. Feng. 1978. “Intergranular Fracture in 4340-Type Steels: Effects of Impurities and Hydrogen.” *Metallurgical Transactions A* 9 (2): 237–47.

Barnoush, Afrooz, and Horst Vehoff. 2010. “Recent Developments in the Study of Hydrogen Embrittlement: Hydrogen Effect on Dislocation Nucleation.” *Acta Materialia* 58 (16): 5274–85.

Baskes, M. I. 1992. “Modified Embedded-Atom Potentials for Cubic Materials and Impurities.” *Physical Review B* 46 (5): 2727–42. doi:10.1103/PhysRevB.46.2727.

Beachem, C. D. 1972. “A New Model for Hydrogen-Assisted Cracking (hydrogen ‘embrittlement’).” *Metallurgical Transactions* 3 (2): 441–55. doi:10.1007/BF02642048.

Bechtle, S., M. Kumar, B. P. Somerday, M. E. Launey, and R. O. Ritchie. 2009. “Grain-Boundary Engineering Markedly Reduces Susceptibility to Intergranular Hydrogen Embrittlement in Metallic Materials.” *Acta Materialia* 57 (14): 4148–57. doi:10.1016/j.actamat.2009.05.012.

Bernstein, I. M. 1970. “The Role of Hydrogen in the Embrittlement of Iron and Steel.” *Materials Science and Engineering* 6 (1): 1–19. doi:10.1016/0025-5416(70)90073-X.

Bhatia, M. A., S. Groh, and K. N. Solanki. 2014. “Atomic-Scale Investigation of Point Defects and Hydrogen-Solute Atmospheres on the Edge Dislocation Mobility in Alpha Iron.” *Journal of Applied Physics* 116 (6): 064302. doi:10.1063/1.4892630.

Bhatia, M. A., and K. N. Solanki. 2013. “Energetics of Vacancy Segregation to Symmetric Tilt Grain Boundaries in Hexagonal Closed Pack Materials.” *Journal of Applied Physics* 114 (24): 244309. doi:10.1063/1.4858401.

Bieler, T. R., A. Fallahi, B. C. Ng, D. Kumar, M. A. Crimp, B. A. Simkin, A. Zamiri, F. Pourboghrat, and D. E. Mason. 2005. “Fracture Initiation/propagation Parameters for Duplex TiAl Grain Boundaries Based on Twinning, Slip, Crystal Orientation, and Boundary Misorientation.” *Intermetallics*, 2nd IRC International TiAl Workshop, 13 (9): 979–84. doi:10.1016/j.intermet.2004.12.013.

Birnbaum, H. K. 1984. “Mechanical Properties of Metal Hydrides.” *Journal of the Less Common Metals* 104 (1): 31–41. doi:10.1016/0022-5088(84)90433-8.

Birnbaum, H. K., and P. Sofronis. 1994. “Hydrogen-Enhanced Localized Plasticity—a Mechanism for Hydrogen-Related Fracture.” *Materials Science and Engineering: A* 176 (1): 191–202.

Bishop, G.H., and B. Chalmers. 1968. “A Coincidence — Ledge — Dislocation Description of Grain Boundaries.” *Scripta Metallurgica* 2 (2): 133–39. doi:10.1016/0036-9748(68)90085-9.

Blöchl, P. E. 1994. “Projector Augmented-Wave Method.” *Physical Review B* 50 (24): 17953–79. doi:10.1103/PhysRevB.50.17953.

Bloom, E. E., J. T. Busby, C. E. Duty, P. J. Maziasz, T. E. McGreevy, B. E. Nelson, B. A. Pint, P. F. Tortorelli, and S. J. Zinkle. 2007. “Critical Questions in Materials Science and Engineering for Successful Development of Fusion Power.” *Journal of Nuclear Materials* 367: 1–10.

Bonakdar, A., F. Wang, J. J. Williams, and N. Chawla. 2012. “Environmental Effects on Fatigue Crack Growth in 7075 Aluminum Alloy.” *Metallurgical and Materials Transactions A* 43 (8): 2799–2809. doi:10.1007/s11661-011-0810-0.

Bragg, Lawrence, and J. F. Nye. 1947. “A Dynamical Model of a Crystal Structure.” *Proceedings of the Royal Society of London. Series A, Mathematical and Physical Sciences*, 474–81.

Brandl, C., E. Bitzek, P. M. Derlet, and H. Van Swygenhoven. 2007. “Slip Transfer through a General High Angle Grain Boundary in Nanocrystalline Aluminum.” *Applied Physics Letters* 91 (11): 111914. doi:10.1063/1.2784939.

Brandon, D. G. 1966. “The Structure of High-Angle Grain Boundaries.” *Acta Metallurgica* 14 (11): 1479–84.

Brenner, Donald W. 1990. “Empirical Potential for Hydrocarbons for Use in Simulating the Chemical Vapor Deposition of Diamond Films.” *Physical Review B* 42 (15): 9458–71. doi:10.1103/PhysRevB.42.9458.

Brenner, Donald W., Olga A. Shenderova, Judith A. Harrison, Steven J. Stuart, Boris Ni, and Susan B. Sinnott. 2002. “A Second-Generation Reactive Empirical Bond Order (REBO) Potential Energy Expression for Hydrocarbons.” *Journal of Physics: Condensed Matter* 14 (4): 783. doi:10.1088/0953-8984/14/4/312.

Brenner, D.w. 2000. “The Art and Science of an Analytic Potential.” *Physica Status Solidi (b)* 217 (1): 23–40. doi:10.1002/(SICI)1521-3951(200001)217:1<23::AID-PSSB23>3.0.CO;2-N.

Bristowe, P. D., and A. G. Crocker. 1978. “The Structure of High-Angle (001) CSL Twist Boundaries in F.c.c. Metals.” *Philosophical Magazine A* 38 (5): 487–502. doi:10.1080/01418617808239249.

Britton, T. B., D. Randman, and A. J. Wilkinson. 2009. “Nanoindentation Study of Slip Transfer Phenomenon at Grain Boundaries.” *Journal of Materials Research* 24 (3): 607–15.

B., Sunil Kumar, Balla Sai Prasad, Vivekanand Kain, and Jayanth Reddy. 2013. “Methods for Making Alloy 600 Resistant to Sensitization and Intergranular Corrosion.” *Corrosion Science* 70 (May): 55–61. doi:10.1016/j.corsci.2012.12.021.

Buckingham, R. A. 1938. “The Classical Equation of State of Gaseous Helium, Neon and Argon.” *Proceedings of the Royal Society A: Mathematical, Physical and Engineering Sciences* 168 (933): 264–83. doi:10.1098/rspa.1938.0173.

Bulatov, Vasily V., Bryan W. Reed, and Mukul Kumar. 2014. “Grain Boundary Energy Function for Fcc Metals.” *Acta Materialia* 65 (February): 161–75. doi:10.1016/j.actamat.2013.10.057.

Burgers, J. M. 1940. “Geometrical Considerations Concerning the Structural Irregularities to Be Assumed in a Crystal.” *Proceedings of the Physical Society* 52 (1): 23.

Caillard, Daniel, and Jean-Luc Martins. 2003. *Thermally Activated Mechanisms in Crystal Plasticity*. Vol. 8.

Carneiro, Rogério Augusto, Rajindra Clement Ratnapuli, and Vanessa de Freitas Cunha Lins. 2003. “The Influence of Chemical Composition and Microstructure of API Linepipe Steels on Hydrogen Induced Cracking and Sulfide Stress Corrosion Cracking.” *Materials Science and Engineering: A* 357 (1–2): 104–10. doi:10.1016/S0921-5093(03)00217-X.

Chamati, H., N. I. Papanicolaou, Y. Mishin, and D. A. Papaconstantopoulos. 2006. “Embedded-Atom Potential for Fe and Its Application to Self-Diffusion on Fe(1 0 0).” *Surface Science* 600 (9): 1793–1803. doi:10.1016/j.susc.2006.02.010.

Cheng, Y., M. Mrovec, and P. Gumbsch. 2008. “Atomistic Simulations of Interactions between the 1 / 2⟨111⟩ Edge Dislocation and Symmetric Tilt Grain Boundaries in Tungsten.” *Philosophical Magazine* 88 (4): 547–60. doi:10.1080/14786430801894577.

Cheung, C., U. Erb, and G. Palumbo. 1994. “Application of Grain Boundary Engineering Concepts to Alleviate Intergranular Cracking in Alloys 600 and 690.” *Materials Science and Engineering: A* 185 (1–2): 39–43. doi:10.1016/0921-5093(94)90925-3.

Christian, J. W. 1983. “Some Surprising Features of the Plastic Deformation of Body-Centered Cubic Metals and Alloys.” *Metallurgical Transactions A* 14 (7): 1237–56. doi:10.1007/BF02664806.

Clark, W.A.T., R.H. Wagoner, Z.Y. Shen, T.C. Lee, I.M. Robertson, and H.K. Birnbaum. 1992. “On the Criteria for Slip Transmission across Interfaces in Polycrystals.” *Scripta Metallurgica et Materialia* 26 (2): 203–6. doi:10.1016/0956-716X(92)90173-C.

Clausius, Rudolf. 1870. “XVI. On a Mechanical Theorem Applicable to Heat.” *The London, Edinburgh, and Dublin Philosophical Magazine and Journal of Science* 40 (265): 122–27.

Clouet, Emmanuel, Lisa Ventelon, and F. Willaime. 2009. “Dislocation Core Energies and Core Fields from First Principles.” *Physical Review Letters* 102 (5): 055502. doi:10.1103/PhysRevLett.102.055502.

Cormier, J., J. M. Rickman, and T. J. Delph. 2001. “Stress Calculation in Atomistic Simulations of Perfect and Imperfect Solids.” *Journal of Applied Physics* 89 (1): 99–104. doi:10.1063/1.1328406.

Costantini, Sonia, Paola Alippi, Luciano Colombo, and Fabrizio Cleri. 2000. “Triple Junctions and Elastic Stability of Polycrystalline Silicon.” *Physical Review B* 63 (4): 045302.

Cotterill, P. 1961. “The Hydrogen Embrittlement of Metals.” *Progress in Materials Science* 9 (4): 205–301. doi:10.1016/0079-6425(61)90005-6.

Cottrell, A. H. 1948. “Report on Strength of Solids.” *The Physical Society* 30.

Coulson, C. A. 1939. “The Electronic Structure of Some Polyenes and Aromatic Molecules. VII. Bonds of Fractional Order by the Molecular Orbital Method.” *Proceedings of the Royal Society of London. Series A, Mathematical and Physical Sciences* 169 (938): 413–28.

Crawford, Douglas C., and Gary S. Was. 2013. “The Role of Grain Boundary Misorientation in Intergranular Cracking of Ni-16Cr-9Fe in 360 °C Argon and High-Purity Water.” *Metallurgical Transactions A* 23 (4): 1195–1206. doi:10.1007/BF02665051.

Cyrot-Lackmann, F. 1967. “On the Electronic Structure of Liquid Transitional Metals.” *Advances in Physics* 16 (63): 393–400. doi:10.1080/00018736700101495.

Czubayko, U., V. G. Sursaeva, G. Gottstein, and L. S. Shvindlerman. 1998. “Influence of Triple Junctions on Grain Boundary Motion.” *Acta Materialia* 46 (16): 5863–71. doi:10.1016/S1359-6454(98)00241-9.

Davenport, J.W., and P.H. Estrup. 1990. “Hydrogen on Transition Metals.” In *The Chemical Physics of Solid Surfaces and Heterogeneous Catalysis*, 3A:1–38. Amsterdam: Elsevier.

Daw, M. S., and M. I. Baskes. 1984. “Embedded-Atom Method: Derivation and Application to Impurities, Surfaces, and Other Defects in Metals.” *Physical Review B* 29 (12): 6443.

Daw, M. S., M. I. Baskes, C. L. Bisson, and W. G. Wolfer. 1985. "Application of the Embedded Atom Method to Fracture, Dislocation Dynamics, and Hydrogen Embrittlement." *Modeling Environmental Effects on Crack Growth Processes*, 99–124.

Daw, Murray S., and M. I. Baskes. 1983. "Semiempirical, Quantum Mechanical Calculation of Hydrogen Embrittlement in Metals." *Physical Review Letters* 50 (17): 1285.

Daw, Murray S., Stephen M. Foiles, and Michael I. Baskes. 1993. "The Embedded-Atom Method: A Review of Theory and Applications." *Materials Science Reports* 9 (7–8): 251–310. doi:10.1016/0920-2307(93)90001-U.

Dewald, M. P., and W. A. Curtin. 2007a. "Multiscale Modelling of Dislocation/grain Boundary Interactions. II. Screw Dislocations Impinging on Tilt Boundaries in Al." *Philosophical Magazine* 87 (30): 4615–41. doi:10.1080/14786430701297590.

———. 2007b. "Multiscale Modelling of Dislocation/grain-Boundary Interactions: I. Edge Dislocations Impinging on Σ11 (1 1 3) Tilt Boundary in Al." *Modelling and Simulation in Materials Science and Engineering* 15 (1): S193. doi:10.1088/0965-0393/15/1/S16.

Differt, K., U. Esmann, and H. Mughrabi. 1986. "A Model of Extrusions and Intrusions in Fatigued Metals II. Surface Roughening by Random Irreversible Slip." *Philosophical Magazine A* 54 (2): 237–58.

Drautz, Ralf, and D. G. Pettifor. 2006. "Valence-Dependent Analytic Bond-Order Potential for Transition Metals." *Physical Review B* 74 (17): 174117. doi:10.1103/PhysRevB.74.174117.

Duesbery, M. S., and V. Vitek. 1998. "Plastic Anisotropy in B.c.c. Transition Metals." *Acta Materialia* 46 (5): 1481–92. doi:10.1016/S1359-6454(97)00367-4.

Duesbery, M. S., V. Vitek, and D. K. Bowen. 1973. "The Effect of Shear Stress on the Screw Dislocation Core Structure in Body-Centred Cubic Lattices." *Proceedings of the Royal Society of London A: Mathematical, Physical and Engineering Sciences* 332 (1588): 85–111. doi:10.1098/rspa.1973.0014.

During, E.D.D. 1997. "Corrosion Atlas: A Collection of Illustrated Case Histories." *Elsevier*.

Eastman, J., F. Heubaum, T. Matsumoto, and H. K. Birnbaum. 1982. "The Effect of Hydrogen on the Solid Solution Strengthening and Softening of Nickel." *Acta Metallurgica* 30 (8): 1579–86.

Energy, Board on, Environmental Systems National Research Council, Division on Engineering, Physical Sciences National Research Council, and Washington

National Academy of Engineering. 2004. *The Hydrogen Economy: Opportunities, Costs, Barriers, and R&D Needs*. National Academies Press.

Essmann, U., U. Gösele, and H. Mughrabi. 1981. "A Model of Extrusions and Intrusions in Fatigued Metals I. Point-Defect Production and the Growth of Extrusions." *Philosophical Magazine A* 44 (2): 405–26.

Farkas, D., H. Van Swygenhoven, and PM Derlet. 2002. "Intergranular Fracture in Nanocrystalline Metals." *Physical Review B.Condensed Matter and Materials Physics* 66 (6): 060101.1–060101.4.

Ferreira, PJ, IM Robertson, and HK Birnbaum. 1998. "Hydrogen Effects on the Interaction between Dislocations." *Acta Materialia* 46 (5): 1749–57.

Ferreira, P.J., I.M. Robertson, and H.K. Birnbaum. 1998. "Hydrogen Effects on the Interaction between Dislocations." *Acta Materialia* 46 (5): 1749–57. doi:10.1016/S1359-6454(97)00349-2.

Ferreira, P. J., I. M. Robertson, and H. K. Birnbaum. 1999. "Hydrogen Effects on the Character of Dislocations in High-Purity Aluminum." *Acta Materialia* 47 (10): 2991–98.

Foiles, Stephen M., and Michael I. Baskes. 2012. "Contributions of the Embedded-Atom Method to Materials Science and Engineering." *MRS Bulletin* 37 (05): 485–91. doi:10.1557/mrs.2012.93.

Fortier, P., W. A. Miller, and K. T. Aust. 1997. "Triple Junction and Grain Boundary Character Distributions in Metallic Materials." *Acta Materialia* 45 (8): 3459–67. doi:10.1016/S1359-6454(97)00004-9.

Fortier, P, G Palumbo, G. D Bruce, W. A Miller, and K. T Aust. 1991. "Triple Line Energy Determination by Scanning Tunneling Microscopy." *Scripta Metallurgica et Materialia* 25 (1): 177–82. doi:10.1016/0956-716X(91)90376-C.

Gahr, S., M. L. Grossbeck, and H. K. Birnbaum. 1977. "Hydrogen Embrittlement of Nb I—Macroscopic Behavior at Low Temperatures." *Acta Metallurgica* 25 (2): 125–34.

Gangloff, RP, and B. P. Somerday. 2012. *Gaseous Hydrogen Embrittlement of Materials in Energy Technologies: Mechanisms, Modelling and Future Developments*. Vol. 2. Elsevier. https://books-google-com.ezproxy1.lib.asu.edu/books/about/Gaseous_Hydrogen_Embrittlement_of_Materi.html?id=9YBwAgAAQBAJ.

Gemperle, A., J. Gemperlová, and N. Zárubová. 2004. "Interaction of Slip Dislocations with Grain Boundaries in Body-Centered Cubic Bicrystals." *Materials Science and*

*Engineering: A*, 13th International Conference on the Strength of Materials, 387–389 (December): 46–50. doi:10.1016/j.msea.2004.03.081.

Gerberich, W. W., P. Marsh, J. Hoehn, S. Venkataraman, and H. Huang. 1993. "Hydrogen/plasticity Interactions in Stress Corrosion Cracking." *Corrosion-Deformation Interactions (CDI'92), T. Magnin and JM Gras (eds.), Les Editions de Physique, Les Ulis*, 325–53.

Gerberich, W. W., P. Marsh, J. Hoehn, S. Venkataraman, H. Huang, T. Magnin, and J. M. Gras. 1993. "Corrosion-Deformation Interactions." *Les Edition de Physique, Les Ulis, France*, 325.

Girshick, A., A. M. Bratkovsky, D. G. Pettifor, and V. Vitek. 1998. "Atomistic Simulation of Titanium. I. A Bond-Order Potential." *Philosophical Magazine A* 77 (4): 981–97. doi:10.1080/01418619808221223.

Gleiter, H. 2000. "Nanostructured Materials: Basic Concepts and Microstructure." *Acta Materialia* 48 (1): 1–29. doi:10.1016/S1359-6454(99)00285-2.

Gordon, P.A., T. Neeraj, and M.I. Mendelev. 2011. "Screw Dislocation Mobility in BCC Metals: A Refined Potential Description for A-Fe." *Philosophical Magazine* 91 (30): 3931–45. doi:10.1080/14786435.2011.597947.

Gottstein, G, A. H King, and L. S Shvindlerman. 2000. "The Effect of Triple-Junction Drag on Grain Growth." *Acta Materialia* 48 (2): 397–403. doi:10.1016/S1359-6454(99)00373-0.

Gottstein, G., Y. Ma, and L. S. Shvindlerman. 2005. "Triple Junction Motion and Grain Microstructure Evolution." *Acta Materialia* 53 (5): 1535–44. doi:10.1016/j.actamat.2004.12.006.

Grimmer, H., W. Bollmann, and D. H. Warrington. 1974. "Coincidence-Site Lattices and Complete Pattern-Shift in Cubic Crystals." *Acta Crystallographica Section A: Crystal Physics, Diffraction, Theoretical and General Crystallography* 30 (2): 197–207.

Groeber, M. A., B. K. Haley, M. D. Uchic, D. M. Dimiduk, and S. Ghosh. 2006. "3D Reconstruction and Characterization of Polycrystalline Microstructures Using a FIB–SEM System." *Materials Characterization* 57 (4–5): 259–73. doi:10.1016/j.matchar.2006.01.019.

Gröger, R., A. G. Bailey, and V. Vitek. 2008. "Multiscale Modeling of Plastic Deformation of Molybdenum and Tungsten: I. Atomistic Studies of the Core Structure and Glide of 1/2 〈1 1 1〉 Screw Dislocations at 0 K." *Acta Materialia* 56 (19): 5401–11. doi:10.1016/j.actamat.2008.07.018.

Gröger, R., V. Racherla, J. L. Bassani, and V. Vitek. 2008. “Multiscale Modeling of Plastic Deformation of Molybdenum and Tungsten: II. Yield Criterion for Single Crystals Based on Atomistic Studies of Glide of Screw Dislocations.” *Acta Materialia* 56 (19): 5412–25. doi:10.1016/j.actamat.2008.07.037.

Gröger, R., and V. Vitek. 2008. “Multiscale Modeling of Plastic Deformation of Molybdenum and Tungsten. III. Effects of Temperature and Plastic Strain Rate.” *Acta Materialia* 56 (19): 5426–39. doi:10.1016/j.actamat.2008.07.027.

Gu, B., J. Luo, and X. Mao. 1999. “Hydrogen-Facilitated Anodic Dissolution-Type Stress Corrosion Cracking of Pipeline Steels in Near-Neutral pH Solution.” *Corrosion* 55 (1): 96–106. doi:10.5006/1.3283971.

Hack, J. E., and G. R. Leverant. 1982. “The Influence of Microstructure on the Susceptibility of Titanium Alloys to Internal Hydrogen Embrittlement.” *Metallurgical Transactions A* 13 (10): 1729–38. doi:10.1007/BF02647828.

Hale, Lucas M., Hojun Lim, Jonathan A. Zimmerman, Corbett C. Battaile, and Christopher R. Weinberger. 2015. “Insights on Activation Enthalpy for Non-Schmid Slip in Body-Centered Cubic Metals.” *Scripta Materialia* 99 (April): 89–92. doi:10.1016/j.scriptamat.2014.11.035.

Hale, Lucas M., Jonathan A. Zimmerman, and Christopher R. Weinberger. 2014. “Simulations of Bcc Tantalum Screw Dislocations: Why Classical Inter-Atomic Potentials Predict {1 1 2} Slip.” *Computational Materials Science* 90 (July): 106–15. doi:10.1016/j.commatsci.2014.03.064.

Hall, E. O. 1951. “The Deformation and Ageing of Mild Steel: III Discussion of Results.” *Proceedings of the Physical Society. Section B* 64 (9): 747. doi:10.1088/0370-1301/64/9/303.

Hayward, Erin, and Chaitanya Deo. 2011a. “Energetics of Small Hydrogen–vacancy Clusters in Bcc Iron.” *Journal of Physics: Condensed Matter* 23 (42): 425402. doi:10.1088/0953-8984/23/42/425402.

———. 2011b. “Energetics of Small Hydrogen–vacancy Clusters in Bcc Iron.” *Journal of Physics: Condensed Matter* 23 (42): 425402. doi:10.1088/0953-8984/23/42/425402.

He, Bingling, Wei Xiao, Wei Hao, and Zhixue Tian. 2013. “First-Principles Investigation into the Effect of Cr on the Segregation of Multi-H at the Fe Σ3 (1 1 1) Grain Boundary.” *Journal of Nuclear Materials* 441 (1–3): 301–5. doi:10.1016/j.jnucmat.2013.06.015.

Henkelman, Graeme, Blas P. Uberuaga, and Hannes Jónsson. 2000. “A Climbing Image Nudged Elastic Band Method for Finding Saddle Points and Minimum Energy Paths.” *The Journal of Chemical Physics* 113 (22): 9901–4.

Hepburn, Derek J., and Graeme J. Ackland. 2008. “Metallic-Covalent Interatomic Potential for Carbon in Iron.” *Physical Review B* 78 (16): 165115. doi:10.1103/PhysRevB.78.165115.

Herzberg, E.F., E.D. Ambrogio, and C.L. Barker. 2006. “The Annual Cost of Corrosion for Army Ground Vehicles and Navy Ships.” SKT50T1. LMI report.

Hirth, J.P. 1974. “Defect Structures in Grain Boundaries.” *Acta Metallurgica* 22 (8): 1023–31. doi:10.1016/0001-6160(74)90027-3.

Hirth, J.P, and R.W Balluffi. 1973. “On Grain Boundary Dislocations and Ledges.” *Acta Metallurgica* 21 (7): 929–42. doi:10.1016/0001-6160(73)90150-8.

Hirth, J. P., and P. C. Gehlen. 1969. “Dislocation Displacement Fields in Anisotropic Media.” *Journal of Applied Physics* 40 (5): 2177–81. doi:10.1063/1.1657954.

Hirth, J. P., and J. Lothe. 1966. *Dislocation Theory*. McGraw-Hill.

Holm, Elizabeth A., Gregory S. Rohrer, Stephen M. Foiles, Anthony D. Rollett, Herbert M. Miller, and David L. Olmsted. 2011. “Validating Computed Grain Boundary Energies in Fcc Metals Using the Grain Boundary Character Distribution.” *Acta Materialia* 59 (13): 5250–56.

Hondros, E. D., M. P. Seah, S. Hofmann, and P. Lejček. 1996. “Chapter 13 - Interfacial and Surface Microchemistry.” In *Physical Metallurgy (Fourth Edition)*, edited by Robert W. CahnPeter Haasen, 1201–89. Oxford: North-Holland. http://www.sciencedirect.com/science/article/pii/B9780444898753500181.

Hoover, William G. 1986. “Constant-Pressure Equations of Motion.” *Physical Review A* 34 (3): 2499–2500. doi:10.1103/PhysRevA.34.2499.

Hwang, C., and I. M. Bernstein. 1983. “A Demonstration of Dislocation Transport of Hydrogen in Iron.” *Scripta Metallurgica* 17 (11): 1299–1304. doi:10.1016/0036-9748(83)90220-X.

Ingle, K. W., and A. G. Crocker. 1980. “On the Structure of High-Angle (110) CSL Twist Boundaries in F.c.c. Metals.” *Philosophical Magazine A* 41 (5): 713–21. doi:10.1080/01418618008239344.

Irving, J. H., and John G. Kirkwood. 1950. “The Statistical Mechanical Theory of Transport Processes. IV. The Equations of Hydrodynamics.” *The Journal of Chemical Physics* 18 (6): 817–29. doi:10.1063/1.1747782.

Itakura, M., H. Kaburaki, and M. Yamaguchi. 2012. “First-Principles Study on the Mobility of Screw Dislocations in Bcc Iron.” *Acta Materialia* 60 (9): 3698–3710. doi:10.1016/j.actamat.2012.03.033.

Ito, K., and V. Vitek. 2001. “Atomistic Study of Non-Schmid Effects in the Plastic Yielding of Bcc Metals.” *Philosophical Magazine A* 81 (5): 1387–1407. doi:10.1080/01418610108214447.

Jiang, D.E, and Emily A Carter. 2003. “Adsorption and Diffusion Energetics of Hydrogen Atoms on Fe(1 1 0) from First Principles.” *Surface Science* 547 (1–2): 85–98. doi:10.1016/j.susc.2003.10.007.

Jiang, D. E., and Emily A. Carter. 2004. “First Principles Assessment of Ideal Fracture Energies of Materials with Mobile Impurities: Implications for Hydrogen Embrittlement of Metals.” *Acta Materialia* 52 (16): 4801–7.

Jiao, Z., and G. S. Was. 2008. “Localized Deformation and IASCC Initiation in Austenitic Stainless Steels.” *Journal of Nuclear Materials*, Microstructural Processes in Irradiated Materials Proceedings of the Symposium on Microstructural Processes in Irradiated Materials, as part of the annual meeting of The Minerals, Metals & Materials Society, 382 (2–3): 203–9. doi:10.1016/j.jnucmat.2008.08.032.

Jin, Z.-H., P. Gumbsch, E. Ma, K. Albe, K. Lu, H. Hahn, and H. Gleiter. 2006. “The Interaction Mechanism of Screw Dislocations with Coherent Twin Boundaries in Different Face-Centred Cubic Metals.” *Scripta Materialia* 54 (6): 1163–68. doi:10.1016/j.scriptamat.2005.11.072.

Johnson, William H. 1874. “On Some Remarkable Changes Produced in Iron and Steel by the Action of Hydrogen and Acids.” *Proceedings of the Royal Society of London* 23 (156-163): 168–79.

Jones, J. E. 1924a. “On the Determination of Molecular Fields. I. From the Variation of the Viscosity of a Gas with Temperature.” *Proceedings of the Royal Society A: Mathematical, Physical and Engineering Sciences* 106 (738): 441–62. doi:10.1098/rspa.1924.0081.

———. 1924b. “On the Determination of Molecular Fields. II. From the Equation of State of a Gas.” *Proceedings of the Royal Society A: Mathematical, Physical and Engineering Sciences* 106 (738): 463–77. doi:10.1098/rspa.1924.0082.

Kacher, Josh, B. P. Eftink, B. Cui, and I. M. Robertson. 2014. “Dislocation Interactions with Grain Boundaries.” *Current Opinion in Solid State and Materials Science*, Slip Localization and Transfer in Deformation and Fatigue of Polycrystals, 18 (4): 227–43. doi:10.1016/j.cossms.2014.05.004.

Kane, RD. 2006. “Corrosion in Petroleum Refining and Petrochemical Operations.” *ASM Handbook Volume 13C, Corrosion: Environments and Industries*, 981.

Kashinath, A., A. Misra, and M. J. Demkowicz. 2013. “Stable Storage of Helium in Nanoscale Platelets at Semicoherent Interfaces.” *Physical Review Letters* 110 (8): 086101. doi:10.1103/PhysRevLett.110.086101.

Kelchner, Cynthia L., S. J. Plimpton, and J. C. Hamilton. 1998. “Dislocation Nucleation and Defect Structure during Surface Indentation.” *Physical Review B* 58 (17): 11085.

Kim, Hyungjun, Julius T. Su, and William A. Goddard. 2011. “High-Temperature High-Pressure Phases of Lithium from Electron Force Field (eFF) Quantum Electron Dynamics Simulations.” *Proceedings of the National Academy of Sciences* 108 (37): 15101–5. doi:10.1073/pnas.1110322108.

Kimura, H., and H. Matsui. 1987. “Mechanism of Hydrogen-Induced Softening and Hardening in Iron.” *Scripta Metallurgica* 21 (3): 319–24. doi:10.1016/0036-9748(87)90221-3.

King, Alexander H. 1999. “The Geometric and Thermodynamic Properties of Grain Boundary Junctions.” *Interface Science* 7 (3-4): 251–71.

———. 2010. “Triple Lines in Materials Science and Engineering.” *Scripta Materialia* 62 (12): 889–93. doi:10.1016/j.scriptamat.2010.02.020.

Kobayashi, Shigeaki, Masashi Hirata, Sadahiro Tsurekawa, and Tadao Watanabe. 2011. “Grain Boundary Engineering for Control of Fatigue Crack Propagation in Austenitic Stainless Steel.” *Procedia Engineering*, 11th International Conference on the Mechanical Behavior of Materials (ICM11), 10: 112–17. doi:10.1016/j.proeng.2011.04.021.

Kobayashi, Shigeaki, Toshiyuki Inomata, Hiroyuki Kobayashi, Sadahiro Tsurekawa, and Tadao Watanabe. 2008. “Effects of Grain Boundary-and Triple Junction-Character on Intergranular Fatigue Crack Nucleation in Polycrystalline Aluminum.” *Journal of Materials Science* 43 (11): 3792–99.

Ko, Won-Seok, Jong Bae Jeon, Chang-Hoon Lee, Jae-Kon Lee, and Byeong-Joo Lee. 2013. “Intergranular Embrittlement of Iron by Phosphorus Segregation: An Atomistic Simulation.” *Modelling and Simulation in Materials Science and Engineering* 21 (2): 025012.

Kremer, R., R. Narayanan, S. Shekhar, and A. H. King. 2005. “On the Design of Controlled Tricrystal Specimens for the Systematic Investigation of Static Grain Boundary Triple Junction Properties.” *Journal of Materials Science* 40 (11): 2795–2802.

Kresse, G., and J. Furthmüller. 1996a. “Efficiency of Ab-Initio Total Energy Calculations for Metals and Semiconductors Using a Plane-Wave Basis Set.” *Computational Materials Science* 6 (1): 15–50. doi:10.1016/0927-0256(96)00008-0.

———. 1996b. “Efficient Iterative Schemes for Ab Initio Total-Energy Calculations Using a Plane-Wave Basis Set.” *Physical Review B* 54 (16): 11169–86. doi:10.1103/PhysRevB.54.11169.

Kresse, G., and J. Hafner. 1993. “Ab Initio Molecular Dynamics for Open-Shell Transition Metals.” *Physical Review B* 48 (17): 13115–18. doi:10.1103/PhysRevB.48.13115.

Kresse, G., and D. Joubert. 1999. “From Ultrasoft Pseudopotentials to the Projector Augmented-Wave Method.” *Physical Review B* 59 (3): 1758–75. doi:10.1103/PhysRevB.59.1758.

Kumar, Mukul, Wayne E. King, and Adam J. Schwartz. 2000. “Modifications to the Microstructural Topology in F.c.c. Materials through Thermomechanical Processing.” *Acta Materialia* 48 (9): 2081–91. doi:10.1016/S1359-6454(00)00045-8.

Kumar, Mukul, Adam J. Schwartz, and Wayne E. King. 2002. “Microstructural Evolution during Grain Boundary Engineering of Low to Medium Stacking Fault Energy Fcc Materials.” *Acta Materialia* 50 (10): 2599–2612. doi:10.1016/S1359-6454(02)00090-3.

Kwon, Dong-Il, and R.J. Asaro. 1990. “Hydrogen-Assisted Ductile Fracture in Spheroidized 1518 Steel.” *Acta Metallurgica et Materialia* 38 (8): 1595–1606. doi:10.1016/0956-7151(90)90127-3.

Lanczos, Cornelius. 1950. *An Iteration Method for the Solution of the Eigenvalue Problem of Linear Differential and Integral Operators*. United States Governm. Press Office.

Lassila, D. H., and H. K. Birnbaum. 1986. “The Effect of Diffusive Hydrogen Segregation on Fracture of Polycrystalline Nickel.” *Acta Metallurgica* 34 (7): 1237–43. doi:10.1016/0001-6160(86)90010-6.

———. 1987. “Intergranular Fracture of Nickel: The Effect of Hydrogen-Sulfur Co-Segregation.” *Acta Metallurgica* 35 (7): 1815–22.

———. 1988. “The Effect of Diffusive Segregation on the Fracture of Hydrogen Charged Nickel.” *Acta Metallurgica* 36 (10): 2821–25. doi:10.1016/0001-6160(88)90128-9.

Lee, Byeong-Joo, Won-Seok Ko, Hyun-Kyu Kim, and Eun-Ha Kim. 2010. “The Modified Embedded-Atom Method Interatomic Potentials and Recent Progress in Atomistic Simulations.” *Calphad* 34 (4): 510–22. doi:10.1016/j.calphad.2010.10.007.

Lee, T. C., I. M. Robertson, and H. K. Birnbaum. 1989. “Prediction of Slip Transfer Mechanisms across Grain Boundaries.” *Scripta Metallurgica* 23 (5): 799–803.

Lee, T. D., T. Goldenberg, and J. P. Hirth. 1979. “Effect of Hydrogen on Fracture of U-Notched Bend Specimens of Spheroidized AISI 1095 Steel.” *Metallurgical Transactions A* 10 (2): 199–208. doi:10.1007/BF02817629.

Lejček, Pavel, and Siegfried Hofmann. 1995. "Thermodynamics and Structural Aspects of Grain Boundary Segregation." *Critical Reviews in Solid State and Materials Sciences* 20 (1): 1–85. doi:10.1080/10408439508243544.

Lejček, Pavel, Siegfried Hofmann, and Václav Paidar. 2003. "Solute Segregation and Classification of [100] Tilt Grain Boundaries in A-Iron: Consequences for Grain Boundary Engineering." *Acta Materialia* 51 (13): 3951–63. doi:10.1016/S1359-6454(03)00219-2.

Liang, Tao, Tzu-Ray Shan, Yu-Ting Cheng, Bryce D. Devine, Mark Noordhoek, Yangzhong Li, Zhize Lu, Simon R. Phillpot, and Susan B. Sinnott. 2013. "Classical Atomistic Simulations of Surfaces and Heterogeneous Interfaces with the Charge-Optimized Many Body (COMB) Potentials." *Materials Science and Engineering: R: Reports* 74 (9): 255–79. doi:10.1016/j.mser.2013.07.001.

Liang, Y., and P. Sofronis. 2003. "Toward a Phenomenological Description of Hydrogen-Induced Decohesion at Particle/matrix Interfaces." *Journal of the Mechanics and Physics of Solids* 51 (8): 1509–31.

Lim, H., L. M. Hale, J. A. Zimmerman, C. C. Battaile, and C. R. Weinberger. 2015. "A Multi-Scale Model of Dislocation Plasticity in -Fe: Incorporating Temperature, Strain Rate and Non-Schmid Effects." *International Journal of Plasticity*. Accessed January 19. doi:10.1016/j.ijplas.2014.12.005.

Liu, X., W. Xie, W. Chen, and H. Zhang. 2011. "Effects of Grain Boundary and Boundary Inclination on Hydrogen Diffusion in A-Iron." *Journal of Materials Research* 26 (21): 2735–43.

Livingston, J.D, and B Chalmers. 1957. "Multiple Slip in Bicrystal Deformation." *Acta Metallurgica* 5 (6): 322–27. doi:10.1016/0001-6160(57)90044-5.

Louthan Jr, MR, GR Caskey Jr, JA Donovan, and DE Rawl Jr. 1972. "Hydrogen Embrittlement of Metals." *Materials Science and Engineering* 10: 357–68.

Louthan Jr., M.R, G.R Caskey Jr., J.A Donovan, and D.E Rawl Jr. 1972. "Hydrogen Embrittlement of Metals." *Materials Science and Engineering* 10: 357–68. doi:10.1016/0025-5416(72)90109-7.

Lufrano, J., P. Sofronis, and HK Birnbaum. 1998. "Elastoplastically Accommodated Hydride Formation and Embrittlement." *Journal of the Mechanics and Physics of Solids* 46 (9): 1497–1520.

Lutsko, J. F. 1988. "Stress and Elastic Constants in Anisotropic Solids: Molecular Dynamics Techniques." *Journal of Applied Physics* 64 (3): 1152–54. doi:10.1063/1.341877.

Lynch, S. P. 1984. “A Fractographic Study of Gaseous Hydrogen Embrittlement and Liquid-Metal Embrittlement in a Tempered-Martensitic Steel.” *Acta Metallurgica* 32 (1): 79–90. doi:10.1016/0001-6160(84)90204-9.

———. 1988. “Environmentally Assisted Cracking: Overview of Evidence for an Adsorption-Induced Localised-Slip Process.” *Acta Metallurgica* 36 (10): 2639–61.

———. 2013. “Mechanisms and Kinetics of Environmentally Assisted Cracking: Current Status, Issues, and Suggestions for Further Work.” *Metallurgical and Materials Transactions A* 44 (3): 1209–29. doi:10.1007/s11661-012-1359-2.

Lynch, Stan. 2012. “Hydrogen Embrittlement Phenomena and Mechanisms.” http://www.degruyter.com.ezproxy1.lib.asu.edu/view/j/corrrev.2012.30.issue-3-4/corrrev-2012-0502/corrrev-2012-0502.xml.

Matsui, H., H. Kimura, and S. Moriya. 1979. “The Effect of Hydrogen on the Mechanical Properties of High Purity Iron I. Softening and Hardening of High Purity Iron by Hydrogen Charging during Tensile Deformation.” *Materials Science and Engineering* 40 (2): 207–16.

Matsumoto, Ryosuke, Shinya Taketomi, Sohei Matsumoto, and Noriyuki Miyazaki. 2009. “Atomistic Simulations of Hydrogen Embrittlement.” *International Journal of Hydrogen Energy* 34 (23): 9576–84. doi:10.1016/j.ijhydene.2009.09.052.

McLean, D. 1957. “Grain Boundary Segregation in Metals.”

McMahon, CJ. 2001. “Hydrogen-Induced Intergranular Fracture of Steels.” *Engineering Fracture Mechanics* 68 (6): 773–88.

McMahon Jr, C. J., and V. Vitek. 1979. “The Effects of Segregated Impurities on Intergranular Fracture Energy.” *Acta Metallurgica* 27 (4): 507–13.

McMurtrey, M. D., G. S. Was, L. Patrick, and D. Farkas. 2011. “Relationship between Localized Strain and Irradiation Assisted Stress Corrosion Cracking in an Austenitic Alloy.” *Materials Science and Engineering: A* 528 (10–11): 3730–40. doi:10.1016/j.msea.2011.01.073.

Melchionna, S., G. Ciccotti, and B. L. Holian. 1993. “Hoover NPT Dynamics for Systems Varying in Shape and Size.” *Molecular Physics* 78 (3): 533–44.

Merkle, K. L., and D. Wolf. 1992. “Low-Energy Configurations of Symmetric and Asymmetric Tilt Grain Boundaries †.” *Philosophical Magazine A* 65 (2): 513–30. doi:10.1080/01418619208201536.

Merrick, R. D. 1989. “An Overview of Hydrogen Damage to Steels at Low Temperatures.” *Mater. Performance;(United States)* 28 (2). http://www.osti.gov/scitech/biblio/6266605.

Meyers, M. A., A. Mishra, and D. J. Benson. 2006. “Mechanical Properties of Nanocrystalline Materials.” *Progress in Materials Science* 51 (4): 427–556.

Mishin, Y., M.J. Mehl, and D.A. Papaconstantopoulos. 2005. “Phase Stability in the Fe-Ni System: Investigation by First-Principles Calculations and Atomistic Simulations.” *Acta Materialia* 53 (15): 4029–41. doi:10.1016/j.actamat.2005.05.001.

Mrovec, M., C. Elsässer, and P. Gumbsch. 2009. “Interactions between Lattice Dislocations and Twin Boundaries in Tungsten: A Comparative Atomistic Simulation Study.” *Philosophical Magazine* 89 (34-36): 3179–94. doi:10.1080/14786430903246346.

Mrovec, M., D. Nguyen-Manh, D. G. Pettifor, and V. Vitek. 2004. “Bond-Order Potential for Molybdenum: Application to Dislocation Behavior.” *Physical Review B* 69 (9): 094115. doi:10.1103/PhysRevB.69.094115.

Mullins, William W. 1956. “Two-Dimensional Motion of Idealized Grain Boundaries.” *Journal of Applied Physics* 27 (8): 900–904.

Myers, S. Mo, M. I. Baskes, H. K. Birnbaum, Jo Wo Corbett, G. G. DeLeo, S. K. Estreicher, Eo E. Haller, Po Jena, No M. Johnson, and Ro Kirchheim, others. 1992. “Hydrogen Interactions with Defects in Crystalline Solids.” *Reviews of Modern Physics* 64 (2): 559.

Nelson, Howard G. 1994. “Effect of High Temperature Hydrogen on Titanium Base Alloys.” In *Hydrogen Effects in Materials*, edited by Anthony W. Thompson and Neville R. Moody, 697–718. John Wiley & Sons, Inc. http://onlinelibrary.wiley.com.ezproxy1.lib.asu.edu/doi/10.1002/9781118803363.ch61/summary.

Nelson, Howard G., Dell P. Williams, and James E. Stein. 1972. “Environmental Hydrogen Embrittlement of an A-B Titanium Alloy: Effect of Microstructure.” *Metallurgical Transactions* 3 (2): 473–79. doi:10.1007/BF02642051.

Nickerson, B. 2015. “Operational Airframe Experience with Combined Environmental and Mechanical Loading.” *Corrosion Review* to appear.

Noordhoek, Mark J., Tao Liang, Zizhe Lu, Tzu-Ray Shan, Susan B. Sinnott, and Simon R. Phillpot. 2013. “Charge-Optimized Many-Body (COMB) Potential for Zirconium.” *Journal of Nuclear Materials* 441 (1–3): 274–79. doi:10.1016/j.jnucmat.2013.06.004.

Nosé, Shuichi. 1984. “A Unified Formulation of the Constant Temperature Molecular Dynamics Methods.” *The Journal of Chemical Physics* 81 (1): 511–19. doi:10.1063/1.447334.

Nosé, Shūichi. 1986. “An Extension of the Canonical Ensemble Molecular Dynamics Method.” *Molecular Physics* 57 (1): 187–91. doi:10.1080/00268978600100141.

Nosé, Shuichi, and M. L. Klein. 1983. “Constant Pressure Molecular Dynamics for Molecular Systems.” *Molecular Physics* 50 (5): 1055–76. doi:10.1080/00268978300102851.

Novak, P., R. Yuan, B. P. Somerday, P. Sofronis, and R. O. Ritchie. 2010. “A Statistical, Physical-Based, Micro-Mechanical Model of Hydrogen-Induced Intergranular Fracture in Steel.” *Journal of the Mechanics and Physics of Solids* 58 (2): 206–26. doi:10.1016/j.jmps.2009.10.005.

Oda, Y., and H. Noguchi. 2005. “Observation of Hydrogen Effects on Fatigue Crack Growth Behaviour in an 18Cr-8Ni Austenitic Stainless Steel.” *International Journal of Fracture* 132 (2): 99–113.

Olmsted, David L., Stephen M. Foiles, and Elizabeth A. Holm. 2009. “Survey of Computed Grain Boundary Properties in Face-Centered Cubic Metals: I. Grain Boundary Energy.” *Acta Materialia* 57 (13): 3694–3703.

Oriani, R. A. 1972. “A Mechanistic Theory of Hydrogen Embrittlement of Steels.” *Berichte Der Bunsengesellschaft Für Physikalische Chemie* 76 (8): 848–57.

Oriani, R A. 1978. “Hydrogen Embrittlement of Steels.” *Annual Review of Materials Science* 8 (1): 327–57. doi:10.1146/annurev.ms.08.080178.001551.

Oriani, R. A., and P. H. Josephic. 1974. “Equilibrium Aspects of Hydrogen-Induced Cracking of Steels.” *Acta Metallurgica* 22 (9): 1065–74.

Oriani, R.A., and P.H. Josephic. 1979. “Hydrogen-Enhanced Load Relaxation in a Deformed Medium-Carbon Steel.” *Acta Metallurgica* 27 (6): 997–1005. doi:10.1016/0001-6160(79)90187-1.

Oriani, Richard A. 1970. “The Diffusion and Trapping of Hydrogen in Steel.” *Acta Metallurgica* 18 (1): 147–57.

Palin-Luc, Thierry, Rubén Pérez-Mora, Claude Bathias, Gonzalo Domínguez, Paul C. Paris, and Jose Luis Arana. 2010. “Fatigue Crack Initiation and Growth on a Steel in the Very High Cycle Regime with Sea Water Corrosion.” *Engineering Fracture Mechanics*, International Conference on Crack Paths 2009, 77 (11): 1953–62. doi:10.1016/j.engfracmech.2010.02.015.

Palumbo, G., D. M. Doyle, A. M. El-Sherik, U. Erb, and K. T. Aust. 1991. “Intercrystalline Hydrogen Transport in Nanocrystalline Nickel.” *Scripta Metallurgica et Materialia* 25 (3): 679–84.

Palumbo, G., P. J. King, K. T. Aust, U. Erb, and P. C. Lichtenberger. 1991. "Grain Boundary Design and Control for Intergranular Stress-Corrosion Resistance." *Scripta Metallurgica et Materialia* 25 (8): 1775–80. doi:10.1016/0956-716X(91)90303-I.

Parkins, Redvers N. 2000. "A Review of Stress Corrosion Cracking of High Pressure Gas Pipelines." *CORROSION 2000*.

Parrinello, M., and A. Rahman. 1982. "Strain Fluctuations and Elastic Constants." *The Journal of Chemical Physics* 76 (5): 2662–66. doi:10.1063/1.443248.

Parr, Robert G., Robert A. Donnelly, Mel Levy, and William E. Palke. 1978. "Electronegativity: The Density Functional Viewpoint." *The Journal of Chemical Physics* 68 (8): 3801–7. doi:10.1063/1.436185.

Parthasarathy, T. A., H. F. Lopez, and P. G. Shewmon. 1985. "Hydrogen Attack Kinetics of 2.25 Cr-1 Mo Steel Weld Metals." *Metallurgical Transactions A* 16 (6): 1143–49. doi:10.1007/BF02811683.

Perdew, John P., Kieron Burke, and Matthias Ernzerhof. 1997. "Generalized Gradient Approximation Made Simple [Phys. Rev. Lett. 77, 3865 (1996)]." *Physical Review Letters* 78 (7): 1396–1396. doi:10.1103/PhysRevLett.78.1396.

Petch, N. J. 1954. "The Fracture of Metals." *Progress in Metal Physics* 5: 1–52. doi:10.1016/0502-8205(54)90003-9.

Pettifor, D. G. 1989. "New Many-Body Potential for the Bond Order." *Physical Review Letters* 63 (22): 2480–83. doi:10.1103/PhysRevLett.63.2480.

Pettifor, D. G., and I. I. Oleinik. 2002. "Analytic Bond-Order Potential for Open and Close-Packed Phases." *Physical Review B* 65 (17): 172103. doi:10.1103/PhysRevB.65.172103.

Pettifor, D. G., I. I. Oleinik, D. Nguyen-Manh, and V. Vitek. 2002. "Bond-Order Potentials: Bridging the Electronic to Atomistic Modelling Hierarchies." *Computational Materials Science* 23 (1–4): 33–37. doi:10.1016/S0927-0256(01)00204-X.

Pfeil, L. B. 1926. "The Effect of Occluded Hydrogen on the Tensile Strength of Iron." *Proceedings of the Royal Society of London. Series A, Containing Papers of a Mathematical and Physical Character* 112 (760): 182–95.

Plimpton, S. 1995. "Fast Parallel Algorithms for Short-Range Molecular Dynamics." *Journal of Computational Physics* 117 (1): 1–19.

Polcarova, M., J. Gemperlova, J. Bradler, A. Jacques, A. George, and L. Priester. 1998. "In-Situ Observation of Plastic Deformation of Fe-Si Bicrystals by White-Beam

Synchrotron Radiation Topography." *Philosophical Magazine A* 78 (1): 105–30. doi:10.1080/014186198253705.

Pond, R. C. 1977. "Periodic Grain Boundary Structures in Aluminium. II. A Geometrical Method for Analysing Periodic Grain Boundary Structure and Some Related Transmission Electron Microscope Observations." *Proceedings of the Royal Society of London. A. Mathematical and Physical Sciences* 357 (1691): 471–83.

———. 1979. "On the Symmetry and Structure of (001) Twist Boundaries in F.c.c. Metals." *Philosophical Magazine A* 39 (5): 679–83. doi:10.1080/01418617908239298.

Pond, R. C., D. A. Smith, and V. Vitek. 1979. "Computer Simulation Of< 110> Tilt Boundaries: Structure and Symmetry." *Acta Metallurgica* 27 (2): 235–41.

Pouillier, E., A. -F. Gourgues, D. Tanguy, and E. P. Busso. 2012. "A Study of Intergranular Fracture in an Aluminium Alloy due to Hydrogen Embrittlement." *International Journal of Plasticity* 34 (July): 139–53. doi:10.1016/j.ijplas.2012.01.004.

Proville, Laurent, David Rodney, and Mihai-Cosmin Marinica. 2012. "Quantum Effect on Thermally Activated Glide of Dislocations." *Nature Materials* 11 (10): 845–49. doi:10.1038/nmat3401.

Rajagopalan, M., M. A. Bhatia, M. A. Tschopp, D. J. Srolovitz, and K. N. Solanki. 2014. "Atomic-Scale Analysis of Liquid-Gallium Embrittlement of Aluminum Grain Boundaries." *Acta Materialia* 73 (July): 312–25. doi:10.1016/j.actamat.2014.04.011.

Rajagopalan, M., M. A. Tschopp, and K. N. Solanki. 2014. "Grain Boundary Segregation of Interstitial and Substitutional Impurity Atoms in Alpha-Iron." *JOM* 66 (1): 129–38.

Ramasubramaniam, A., M. Itakura, M. Ortiz, and E. A. Carter. 2008. "Effect of Atomic Scale Plasticity on Hydrogen Diffusion in Iron: Quantum Mechanically Informed and on-the-Fly Kinetic Monte Carlo Simulations." *J. Mater. Res* 23 (10): 2758.

Ramasubramaniam, Ashwin, Mitsuhiro Itakura, and Emily A. Carter. 2009a. "Interatomic Potentials for Hydrogen in A–iron Based on Density Functional Theory." *Physical Review B* 79 (17): 174101.

———. 2009b. "Interatomic Potentials for Hydrogen in A–iron Based on Density Functional Theory." *Physical Review B* 79 (17): 174101. doi:10.1103/PhysRevB.79.174101.

Read, W. T., and W. Shockley. 1950. "Dislocation Models of Crystal Grain Boundaries." *Physical Review* 78 (3): 275.

Rhodes, N. R., M.A. Tschopp, and K. N. Solanki. 2013. "Quantifying the Energetics and Length Scales of Carbon Segregation to A-Fe Symmetric Tilt Grain Boundaries Using Atomistic Simulations." *Modelling and Simulation in Materials Science and Engineering* 21 (3): 035009.

Rhodes, P. R., L. A. Skogsberg, and R. N. Tuttle. 2007. "Pushing the Limits of Metals in Corrosive Oil and Gas Well Environments." *Corrosion* 63 (1): 63–100.

Rice, J. R. 1992. "Dislocation Nucleation from a Crack Tip: An Analysis Based on the Peierls Concept." *Journal of the Mechanics and Physics of Solids* 40 (2): 239–71.

Rice, J. R., and J. S. Wang. 1989. "Embrittlement of Interfaces by Solute Segregation." *Materials Science and Engineering: A* 107: 23–40.

Ringdalen Vatne, Inga, Alexander Stukowski, Christian Thaulow, Erling Østby, and Jaime Marian. 2013. "Three-Dimensional Crack Initiation Mechanisms in Bcc-Fe under Loading Modes I, II and III." *Materials Science and Engineering: A* 560 (January): 306–14. doi:10.1016/j.msea.2012.09.071.

Rittner, JD, and DN Seidman. 1996. "< 110> Symmetric Tilt Grain-Boundary Structures in Fcc Metals with Low Stacking-Fault Energies." *Physical Review B* 54 (10): 6999.

Robertson, Ian M., P. Sofronis, A. Nagao, M. L. Martin, S. Wang, D. W. Gross, and K. E. Nygren. 2015. "Hydrogen Embrittlement Understood." *Metallurgical and Materials Transactions B*, March, 1–19. doi:10.1007/s11663-015-0325-y.

Robertson, IM. 1999. "The Effect of Hydrogen on Dislocation Dynamics." *Engineering Fracture Mechanics* 64 (5): 649–73.

Robertson, I.M. 2001. "The Effect of Hydrogen on Dislocation Dynamics." *Engineering Fracture Mechanics* 68 (6): 671–92. doi:10.1016/S0013-7944(01)00011-X.

Robertson, IM, and HK Birnbaum. 1986. "An HVEM Study of Hydrogen Effects on the Deformation and Fracture of Nickel." *Acta Metallurgica* 34 (3): 353–66.

Rodney, D., and G. Martin. 2000. "Dislocation Pinning by Glissile Interstitial Loops in a Nickel Crystal: A Molecular-Dynamics Study." *Physical Review B* 61 (13): 8714.

Rogers, H. C. 1968. "Hydrogen Embrittlement of Metals Atomic Hydrogen from a Variety of Sources Reduces the Ductility of Many Metals." *Science* 159 (3819): 1057–64.

Rohrer, Gregory S., Elizabeth A. Holm, Anthony D. Rollett, Stephen M. Foiles, Jia Li, and David L. Olmsted. 2010. "Comparing Calculated and Measured Grain Boundary Energies in Nickel." *Acta Materialia* 58 (15): 5063–69.

Rozenak, P., and D. Eliezer. 1987. “Phase Changes Related to Hydrogen-Induced Cracking in Austenitic Stainless Steel.” *Acta Metallurgica* 35 (9): 2329–40. doi:10.1016/0001-6160(87)90081-2.

Sadananda, K., and A. K. Vasudevan. 2011. “Review of Environmentally Assisted Cracking.” *Metallurgical and Materials Transactions A* 42 (2): 279–95.

Sanderson, R. T. 1983. “Electronegativity and Bond Energy.” *Journal of the American Chemical Society* 105 (8): 2259–61. doi:10.1021/ja00346a026.

Sangid, Michael D., Tawhid Ezaz, Huseyin Sehitoglu, and Ian M. Robertson. 2011. “Energy of Slip Transmission and Nucleation at Grain Boundaries.” *Acta Materialia* 59 (1): 283–96. doi:10.1016/j.actamat.2010.09.032.

Sangid, Michael D., Hans J. Maier, and Huseyin Sehitoglu. 2011. “The Role of Grain Boundaries on Fatigue Crack Initiation – An Energy Approach.” *International Journal of Plasticity* 27 (5): 801–21. doi:10.1016/j.ijplas.2010.09.009.

Saraev, D., and S. Schmauder. 2003. “Atomic-Scale Simulations of the Interaction between Dislocations and Tilt Grain Boundaries in A-Iron.” *Physica Status Solidi (b)* 240 (1): 81–90. doi:10.1002/pssb.200301883.

Scamans, G.M. 1978. “Hydrogen Bubbles in Embrittled Al-Zn-Mg Alloys.” *Journal of Materials Science* 13 (1): 27–36. doi:10.1007/BF00739268.

Schuh, C. A., M. Kumar, and W. E. King. 2005. “Universal Features of Grain Boundary Networks in FCC Materials.” *Journal of Materials Science* 40 (4): 847–52.

Shan, Tzu-Ray, Bryce D. Devine, Travis W. Kemper, Susan B. Sinnott, and Simon R. Phillpot. 2010. “Charge-Optimized Many-Body Potential for the Hafnium/hafnium Oxide System.” *Physical Review B* 81 (12): 125328. doi:10.1103/PhysRevB.81.125328.

Shekhar, Shashank, and Alexander H. King. 2008. “Strain Fields and Energies of Grain Boundary Triple Junctions.” *Acta Materialia* 56 (19): 5728–36. doi:10.1016/j.actamat.2008.07.053.

Shen, Z., R.H. Wagoner, and W.A.T. Clark. 1986. “Dislocation Pile-up and Grain Boundary Interactions in 304 Stainless Steel.” *Scripta Metallurgica* 20 (6): 921–26. doi:10.1016/0036-9748(86)90467-9.

Shen, Z., R. H. Wagoner, and W. A. T. Clark. 1988. “Dislocation and Grain Boundary Interactions in Metals.” *Acta Metallurgica* 36 (12): 3231–42.

Shih, D. S., I. M. Robertson, and H. K. Birnbaum. 1988. “Hydrogen Embrittlement of A Titanium:< I> In Situ</i> Tem Studies.” *Acta Metallurgica* 36 (1): 111–24.

Shimada, M., H. Kokawa, Z. J. Wang, Y. S. Sato, and I. Karibe. 2002. “Optimization of Grain Boundary Character Distribution for Intergranular Corrosion Resistant 304 Stainless Steel by Twin-Induced Grain Boundary Engineering.” *Acta Materialia* 50 (9): 2331–41.

Smith, D.A., V. Vitek, and R.C. Pond. 1977. “Computer Simulation of Symmetrical High Angle Boundaries in Aluminium.” *Acta Metallurgica* 25 (5): 475–83. doi:10.1016/0001-6160(77)90187-0.

Soer, W. A., and J. Th. M. De Hosson. 2005. “Detection of Grain-Boundary Resistance to Slip Transfer Using Nanoindentation.” *Materials Letters* 59 (24–25): 3192–95. doi:10.1016/j.matlet.2005.03.075.

Sofronis, P., and H.K. Birnbaum. 1995a. “Mechanics of the Hydrogendashdislocationdashimpurity interactions—I. Increasing Shear Modulus.” *Journal of the Mechanics and Physics of Solids* 43 (1): 49–90. doi:10.1016/0022-5096(94)00056-B.

———. 1995b. “Mechanics of the Hydrogendashdislocationdashimpurity interactions—I. Increasing Shear Modulus.” *Journal of the Mechanics and Physics of Solids* 43 (1): 49–90. doi:10.1016/0022-5096(94)00056-B.

Sofronis, P., Y. Liang, and N. Aravas. 2001a. “Hydrogen Induced Shear Localization of the Plastic Flow in Metals and Alloys.” *European Journal of Mechanics-A/Solids* 20 (6): 857–72.

———. 2001b. “Hydrogen Induced Shear Localization of the Plastic Flow in Metals and Alloys.” *European Journal of Mechanics - A/Solids* 20 (6): 857–72. doi:10.1016/S0997-7538(01)01179-2.

———. 2001c. “Hydrogen Induced Shear Localization of the Plastic Flow in Metals and Alloys.” *European Journal of Mechanics - A/Solids* 20 (6): 857–72. doi:10.1016/S0997-7538(01)01179-2.

Solanki, Kiran N., Mark A. Tschopp, Mehul A. Bhatia, and Nathan R. Rhodes. 2012. “Atomistic Investigation of the Role of Grain Boundary Structure on Hydrogen Segregation and Embrittlement in A-Fe.” *Metallurgical and Materials Transactions A* 44 (3): 1365–75. doi:10.1007/s11661-012-1430-z.

———. 2013. “Atomistic Investigation of the Role of Grain Boundary Structure on Hydrogen Segregation and Embrittlement in A-Fe.” *Metallurgical and Materials Transactions A* 44 (3): 1365–75. doi:10.1007/s11661-012-1430-z.

Somerday, B. P., and P. Sofronis. 2013. “Hydrogen-Materials Interactions.” In . Materials Park, OH.

Song, J., and W. A. Curtin. 2014. “Mechanisms of Hydrogen-Enhanced Localized Plasticity: An Atomistic Study Using A-Fe as a Model System.” *Acta Materialia* 68 (April): 61–69. doi:10.1016/j.actamat.2014.01.008.

Song, J., M. Soare, and W. A. Curtin. 2010. “Testing Continuum Concepts for Hydrogen Embrittlement in Metals Using Atomistics.” *Modelling and Simulation in Materials Science and Engineering* 18 (4): 045003.

Song, Jun, and W. A. Curtin. 2011. “A Nanoscale Mechanism of Hydrogen Embrittlement in Metals.” *Acta Materialia* 59 (4): 1557–69.

———. 2012. “Atomic Mechanism and Prediction of Hydrogen Embrittlement in Iron.” *Nature Materials*. http://www.nature.com.ezproxy1.lib.asu.edu/nmat/journal/vaop/ncurrent/full/nmat3479.html.

Spearot, Douglas E., M.A. Tschopp, Karl I. Jacob, and David L. McDowell. 2007. “Tensile Strength Of< 100> And< 110> Tilt Bicrystal Copper Interfaces.” *Acta Materialia* 55 (2): 705–14.

Srinivasan, S. G., J. W. Cahn, H. Jónsson, and G. Kalonji. 1999. “Excess Energy of Grain-Boundary Trijunctions: An Atomistic Simulation Study.” *Acta Materialia* 47 (9): 2821–29. doi:10.1016/S1359-6454(99)00120-2.

Stoller, Roger E. 1990. “The Influence of Helium on Microstructural Evolution: Implications for DT Fusion Reactors.” *Journal of Nuclear Materials* 174 (2): 289–310.

Stroh, A. N. 1958. “Dislocations and Cracks in Anisotropic Elasticity.” *Philosophical Magazine* 3 (30): 625–46. doi:10.1080/14786435808565804.

Stuart, Steven J., Alan B. Tutein, and Judith A. Harrison. 2000. “A Reactive Potential for Hydrocarbons with Intermolecular Interactions.” *The Journal of Chemical Physics* 112 (14): 6472–86. doi:10.1063/1.481208.

Su, Julius T., and William A. Goddard. 2007. “Excited Electron Dynamics Modeling of Warm Dense Matter.” *Physical Review Letters* 99 (18): 185003. doi:10.1103/PhysRevLett.99.185003.

Sutton, AP. 1982. “On the Structure of (001) Twist Boundaries in Fcc Metals.” *Philosophical Magazine A* 46 (1): 171–76.

———. 1989. “On the Structural Unit Model of Grain Boundary Structure.” *Philosophical Magazine Letters* 59 (2): 53–59.

Sutton, A. P., and V. Vitek. 1980. “On the Coincidence Site Lattice and DSC Dislocation Network Model of High Angle Grain Boundary Structure.” *Scripta Metallurgica* 14 (1): 129–32.

Sutton, AP, and V. Vitek. 1983. “On the Structure of Tilt Grain Boundaries in Cubic Metals I. Symmetrical Tilt Boundaries.” *Philosophical Transactions of the Royal Society of London.Series A, Mathematical and Physical Sciences* 309 (1506): 1–36.

Taheri, Mitra L., Anthony D. Rollett, and Hasso Weiland. 2004. “In-Situ Quantification of Solute Effects on Grain Boundary Mobility and Character in Aluminum Alloys during Recrystallization.” *Materials Science Forum* 467-470: 997–1002. doi:10.4028/www.scientific.net/MSF.467-470.997.

Taheri, Mitra L., Jason T. Sebastian, Bryan W. Reed, David N. Seidman, and Anthony D. Rollett. 2010. “Site-Specific Atomic Scale Analysis of Solute Segregation to a Coincidence Site Lattice Grain Boundary.” *Ultramicroscopy* 110 (4): 278–84. doi:10.1016/j.ultramic.2009.11.006.

Taketomi, Shinya, Ryosuke Matsumoto, and Noriyuki Miyazaki. 2008. “Atomistic Study of Hydrogen Distribution and Diffusion around a {1 1 2}<1 1 1> Edge Dislocation in Alpha Iron.” *Acta Materialia* 56 (15): 3761–69. doi:10.1016/j.actamat.2008.04.011.

———. 2010. “Atomistic Study of the Effect of Hydrogen on Dislocation Emission from a Mode II Crack Tip in Alpha Iron.” *International Journal of Mechanical Sciences* 52 (2): 334–38. doi:10.1016/j.ijmecsci.2009.09.042.

Taketomi, S., R. Matsumoto, and N. Miyazaki. 2010. “Atomistic Study of the Effect of Hydrogen on Dislocation Emission from a Mode II Crack Tip in Alpha Iron.” *International Journal of Mechanical Sciences* 52 (2): 334–38.

Tanaka, K., and T. Mura. 1981. “A Dislocation Model for Fatigue Crack Initiation.” *Journal of Applied Mechanics* 48 (1): 97–103.

Tang, Xiangyun, and Anthony W. Thompson. 1994. “Hydrogen Effects on Slip Character and Ductility in Ni□Co Alloys.” *Materials Science and Engineering: A* 186 (1–2): 113–19. doi:10.1016/0921-5093(94)90309-3.

Tapasa, K., Y. N. Osetsky, and D. J. Bacon. 2007. “Computer Simulation of Interaction of an Edge Dislocation with a Carbon Interstitial in A-Iron and Effects on Glide.” *Acta Materialia* 55 (1): 93–104.

Taylor, G. I. 1928. “The Deformation of Crystals of B -Brass.” *Proceedings of the Royal Society of London. Series A, Containing Papers of a Mathematical and Physical Character* 118 (779): 1–24.

Tersoff, J. 1986. “New Empirical Model for the Structural Properties of Silicon.” *Physical Review Letters* 56 (6): 632–35. doi:10.1103/PhysRevLett.56.632.

———. 1988a. “Empirical Interatomic Potential for Silicon with Improved Elastic Properties.” *Physical Review B* 38 (14): 9902–5. doi:10.1103/PhysRevB.38.9902.

———. 1988b. “Empirical Interatomic Potential for Carbon, with Applications to Amorphous Carbon.” *Physical Review Letters* 61 (25): 2879–82. doi:10.1103/PhysRevLett.61.2879.

Thompson, A. W. 1985. “Hydrogen-Assisted Fracture at Notches.” *Materials Science and Technology* 1 (9): 711–18. doi:10.1179/026708385790124260.

Troiano, Alexander R. 1960. “The Role of Hydrogen and Other Interstitials in the Mechanical Behavior of Metals.” *Trans. ASM* 52 (1): 54–80.

Tsai, D. H. 1979. “The Virial Theorem and Stress Calculation in Molecular Dynamics.” *The Journal of Chemical Physics* 70 (3): 1375–82. doi:doi:10.1063/1.437577.

Tschopp, M. A., F. Gao, L. Yang, and K. N. Solanki. 2014. “Binding Energetics of Substitutional and Interstitial Helium and Di-Helium Defects with Grain Boundary Structure in A-Fe.” *Journal of Applied Physics* 115 (3): 033503. doi:10.1063/1.4861719.

Tschopp, M.A., MF Horstemeyer, F. Gao, X. Sun, and M. Khaleel. 2011. “Energetic Driving Force for Preferential Binding of Self-Interstitial Atoms to Fe Grain Boundaries over Vacancies.” *Scripta Materialia* 64 (9): 908–11.

Tschopp, M.A., K. Solanki, F. Gao, X. Sun, M. Khaleel, and M. Horstemeyer. 2012a. “Probing Grain Boundary Sink Strength at the Nanoscale: Energetics and Length Scales of Vacancy and Interstitial Absorption by Grain Boundaries in A-Fe.” *Physical Review B* 85 (6). doi:10.1103/PhysRevB.85.064108.

Tschopp, M.A., KN Solanki, F. Gao, X. Sun, M. A. Khaleel, and MF Horstemeyer. 2012b. “Probing Grain Boundary Sink Strength at the Nanoscale: Energetics and Length Scales of Vacancy and Interstitial Absorption by Grain Boundaries in Iñ-Fe.” *Physical Review B* 85 (6): 064108.

Tschopp, M.A., Douglas E. Spearot, and David L. McDowell. 2008. “Influence of Grain Boundary Structure on Dislocation Nucleation in Fcc Metals.” *Dislocations in Solids* 14: 43–139.

Tschopp, M.A., G. J. Tucker, and D. L. McDowell. 2007. “Structure and Free Volume Of< 110> Symmetric Tilt Grain Boundaries with the E Structural Unit.” *Acta Materialia* 55 (11): 3959–69.

Ullmaier, H. 1984. “The Influence of Helium on the Bulk Properties of Fusion Reactor Structural Materials.” *Nuclear Fusion* 24 (8): 1039.

Ulmer, D. G., and C. J. Altstetter. 1991. “Hydrogen-Induced Strain Localization and Failure of Austenitic Stainless Steels at High Hydrogen Concentrations.” *Acta Metallurgica et Materialia* 39 (6): 1237–48. doi:10.1016/0956-7151(91)90211-I.

Upmanyu, Moneesh, D. J. Srolovitz, L. S. Shvindlerman, and G. Gottstein. 1999. “Triple Junction Mobility: A Molecular Dynamics Study.” *Interface Science* 7 (3-4): 307–19. doi:10.1023/A:1008781611991.

Upmanyu, M, D. J Srolovitz, L. S Shvindlerman, and G Gottstein. 2002. “Molecular Dynamics Simulation of Triple Junction Migration.” *Acta Materialia* 50 (6): 1405–20. doi:10.1016/S1359-6454(01)00446-3.

Valiev, Ruslan Z., Kenong Xia, and Terence G. Langdon. 2009. “Processing by Severe Plastic Deformation:an Ancient Skill Adapted for the Modern World.” *International Journal of Materials Research* 100 (12): 1623–31. doi:10.3139/146.110233.

Van Duin, Adri C. T., Siddharth Dasgupta, Francois Lorant, and William A. Goddard. 2001. “ReaxFF: A Reactive Force Field for Hydrocarbons.” *The Journal of Physical Chemistry A* 105 (41): 9396–9409. doi:10.1021/jp004368u.

Van Swygenhoven, H., PM Derlet, and seth FrA. 2004. “Stacking Fault Energies and Slip in Nanocrystalline Metals.” *Nature Materials* 3 (6): 399–403.

Vehoff, H., and W. Rothe. 1983. “Gaseous Hydrogen Embrittlement in FeSi-and Ni-Single Crystals.” *Acta Metallurgica* 31 (11): 1781–93.

Ventelon, Lisa, and F. Willaime. 2010. “Generalized Stacking-Faults and Screw-Dislocation Core-Structure in Bcc Iron: A Comparison between Ab Initio Calculations and Empirical Potentials.” *Philosophical Magazine* 90 (7-8): 1063–74. doi:10.1080/14786431003668793.

Ventelon, Lisa, F. Willaime, E. Clouet, and D. Rodney. 2013. “Ab Initio Investigation of the Peierls Potential of Screw Dislocations in Bcc Fe and W.” *Acta Materialia* 61 (11): 3973–85. doi:10.1016/j.actamat.2013.03.012.

Vitek, V., and V. Paidar. 2008. “Chapter 87 - Non-Planar Dislocation Cores: A Ubiquitous Phenomenon Affecting Mechanical Properties of Crystalline Materials.” In *Dislocations in Solids*, edited by J. P. Hirth, 14:439–514. A Tribute to F.R.N. Nabarro. Elsevier. http://www.sciencedirect.com/science/article/pii/S1572485907000071.

Vitek, V., DA Smith, and RC Pond. 1980. “Structure of Tilt Grain Boundaries in Bcc Metals.” *Philosophical Magazine A* 41 (5): 649–63.

Wang, L., Y. Yang, P. Eisenlohr, T. R. Bieler, M. A. Crimp, and D. E. Mason. 2009. "Twin Nucleation by Slip Transfer across Grain Boundaries in Commercial Purity Titanium." *Metallurgical and Materials Transactions A* 41 (2): 421–30. doi:10.1007/s11661-009-0097-6.

Wang, Shuai, Naoyuki Hashimoto, and Somei Ohnuki. 2013. "Hydrogen-Induced Change in Core Structures of {110}[111] Edge and {110}[111] Screw Dislocations in Iron." *Scientific Reports* 3 (September). doi:10.1038/srep02760.

Wang, Shuai, Naoyuki Hashimoto, Yongming Wang, and Somei Ohnuki. 2013. "Activation Volume and Density of Mobile Dislocations in Hydrogen-Charged Iron." *Acta Materialia* 61 (13): 4734–42. doi:10.1016/j.actamat.2013.05.007.

Wang, Shuai, May L. Martin, Petros Sofronis, Somei Ohnuki, Naoyuki Hashimoto, and Ian M. Robertson. 2014. "Hydrogen-Induced Intergranular Failure of Iron." *Acta Materialia* 69 (May): 275–82. doi:10.1016/j.actamat.2014.01.060.

Warner, DH, WA Curtin, and S. Qu. 2007. "Rate Dependence of Crack-Tip Processes Predicts Twinning Trends in Fcc Metals." *Nature Materials* 6 (11): 876–81.

Was, Gary S., Diana Farkas, and Ian M. Robertson. 2012. "Micromechanics of Dislocation Channeling in Intergranular Stress Corrosion Crack Nucleation." *Current Opinion in Solid State and Materials Science*, Material Challenges for Advanced Nuclear Power Systems, 16 (3): 134–42. doi:10.1016/j.cossms.2012.03.003.

Was, Gary S., Visit Thaveeprungsriporn, and Douglas C. Crawford. 1998. "Grain Boundary Misorientation Effects on Creep and Cracking in Ni-Based Alloys." *JOM* 50 (2): 44–49. doi:10.1007/s11837-998-0249-y.

Was *, G. S., and J. T. Busby. 2005. "Role of Irradiated Microstructure and Microchemistry in Irradiation-Assisted Stress Corrosion Cracking." *Philosophical Magazine* 85 (4-7): 443–65. doi:10.1080/02678370412331320224.

Wasserbäch, W., S. Sahling, R. O. Pohl, and E. Thompson. 2002. "Low-Temperature Internal Friction and Thermal Conductivity of Plastically Deformed, High-Purity Monocrystalline Niobium." *Journal of Low Temperature Physics* 127 (3-4): 121–51. doi:10.1023/A:1014848312572.

Watanabe, Tadao. 1994. "The Impact of Grain Boundary Character Distribution on Fracture in Polycrystals." *Materials Science and Engineering: A* 176 (1–2): 39–49. doi:10.1016/0921-5093(94)90957-1.

———. 2011. "Grain Boundary Engineering: Historical Perspective and Future Prospects." *Journal of Materials Science* 46 (12): 4095–4115. doi:10.1007/s10853-011-5393-z.

Watanabe, Tadao, and Sadahiro Tsurekawa. 1999. “The Control of Brittleness and Development of Desirable Mechanical Properties in Polycrystalline Systems by Grain Boundary Engineering.” *Acta Materialia* 47 (15): 4171–85.

———. 2004. “Toughening of Brittle Materials by Grain Boundary Engineering.” *Materials Science and Engineering: A*, 13th International Conference on the Strength of Materials, 387–389 (December): 447–55. doi:10.1016/j.msea.2004.01.140.

Watson, J. W., M. Meshii, and Y. Z. Shen. 1988. “Effect of Cathodic Charging on the Mechanical Properties of Aluminum.” *Metallurgical Transactions A* 19 (9): 2299–2304.

Weinberger, Christopher R., Corbett C. Battaile, Thomas E. Buchheit, and Elizabeth A. Holm. 2012. “Incorporating Atomistic Data of Lattice Friction into BCC Crystal Plasticity Models.” *International Journal of Plasticity* 37 (October): 16–30. doi:10.1016/j.ijplas.2012.03.012.

Weinberger, Christopher R., Garritt J. Tucker, and Stephen M. Foiles. 2013. “Peierls Potential of Screw Dislocations in Bcc Transition Metals: Predictions from Density Functional Theory.” *Physical Review B* 87 (5): 054114. doi:10.1103/PhysRevB.87.054114.

Weinberger, C R, B L Boyce, and C C Battaile. 2013. “Slip Planes in Bcc Transition Metals.” *International Materials Reviews* 58 (5): 296–314. doi:10.1179/1743280412Y.0000000015.

Woodtli, Jarmila, and Rolf Kieselbach. 2000. “Damage due to Hydrogen Embrittlement and Stress Corrosion Cracking.” *Engineering Failure Analysis* 7 (6): 427–50. doi:10.1016/S1350-6307(99)00033-3.

Wu, M. S., K. Zhou, and A. A. Nazarov. 2007. “Crack Nucleation at Disclinated Triple Junctions.” *Physical Review B* 76 (13): 134105.

Yamaguchi, Masatake. 2011. “First-Principles Study on the Grain Boundary Embrittlement of Metals by Solute Segregation: Part I. Iron (Fe)-Solute (B, C, P, and S) Systems.” *Metallurgical and Materials Transactions A* 42 (2): 319–29. doi:10.1007/s11661-010-0381-5.

Yamaguchi, Masatake, Ken-Ichi Ebihara, Mitsuhiro Itakura, Tomoko Kadoyoshi, Tomoaki Suzudo, and Hideo Kaburaki. 2011. “First-Principles Study on the Grain Boundary Embrittlement of Metals by Solute Segregation: Part II. Metal (Fe, Al, Cu)-Hydrogen (H) Systems.” *Metallurgical and Materials Transactions A* 42 (2): 330–39. doi:10.1007/s11661-010-0380-6.

Yamaguchi, Masatake, Motoyuki Shiga, and Hideo Kaburaki. 2004. “First-Principles Study on Segregation Energy and Embrittling Potency of Hydrogen in NiΣ5(012)

Tilt Grain Boundary." *Journal of the Physical Society of Japan* 73 (2): 441–49. doi:10.1143/JPSJ.73.441.

Yamaguchi, M., Y. Nishiyama, and H. Kaburaki. 2007. "Decohesion of Iron Grain Boundaries by Sulfur or Phosphorous Segregation: First-Principles Calculations." *Physical Review B* 76 (3): 035418.

Yamashita, M., T. Mimaki, S. Hashimoto, and S. Miura. 1991. "Stress Corrosion Cracking of [110] and [100] Tilt Boundaries of A-Cu-Al Alloy." *Philosophical Magazine A* 63 (4): 707–26. doi:10.1080/01418619108213909.

You, C. P., A. W. Thompson, and I. M. Bernstein. 1995. "Ductile Fracture Processes in 7075 Aluminum." *Metallurgical and Materials Transactions A* 26 (2): 407–15. doi:10.1007/BF02664677.

Yuasa, Motohiro, Kohei Masunaga, Mamoru Mabuchi, and Yasumasa Chino. 2014. "Interaction Mechanisms of Screw Dislocations with and Twin Boundaries in Mg." *Philosophical Magazine* 94 (3): 285–305. doi:10.1080/14786435.2013.853136.

Zhao, Yi, and Gang Lu. 2011a. "QM/MM Study of Dislocation—hydrogen/helium Interactions in A-Fe." *Modelling and Simulation in Materials Science and Engineering* 19 (6): 065004. doi:10.1088/0965-0393/19/6/065004.

———. 2011b. "QM/MM Study of Dislocation—hydrogen/helium Interactions in A-Fe." *Modelling and Simulation in Materials Science and Engineering* 19 (6): 065004. doi:10.1088/0965-0393/19/6/065004.

Zhevnenko, S. N., D. V. Vaganov, and E. I. Gershman. 2011. "Rapid Penetration of Bismuth from Solid Bi2Te3 along Grain Boundaries in Cu and Cu-Based Alloys." *Journal of Materials Science* 46 (12): 4248–53. doi:10.1007/s10853-010-5234-5.

Zhou, Min, and David L. McDowell. 2002. "Equivalent Continuum for Dynamically Deforming Atomistic Particle Systems." *Philosophical Magazine A* 82 (13): 2547–74. doi:10.1080/01418610208240052.

Zimmerman, J. A., E. B. WebbIII, J. J. Hoyt, R. E. Jones, P. A. Klein, and D. J. Bammann. 2004. "Calculation of Stress in Atomistic Simulation." *Modelling and Simulation in Materials Science and Engineering* 12 (4): S319. doi:10.1088/0965-0393/12/4/S03.

Zimmerman, Jonathan A., Huajian Gao, and Farid F. Abraham. 2000. "Generalized Stacking Fault Energies for Embedded Atom FCC Metals." *Modelling and Simulation in Materials Science and Engineering* 8 (2): 103. doi:10.1088/0965-0393/8/2/302.

Zimmermann, M. 2012. “Diversity of Damage Evolution during Cyclic Loading at Very High Numbers of Cycles.” *International Materials Reviews* 57 (2): 73–91. doi:10.1179/1743280411Y.0000000005.

# APPENDIX A

# OVERVIEW OF ATOMISTIC SIMULATIONS

## A.1 Introduction

Over the past few decades, the progress in computational resources and the resolution of experimental observations has motivated theoretical studies to understand the influence of the atomic arrangement of complex materials. The two primary approaches for the theoretical study at the atomic scale are (i) first-principle methods, based on finding the quantum mechanical solution for the atomic structures and (ii) atomistic methods comprised of molecular dynamics (MD), molecular statics (MS) and Monte Carlo (MC). The first-principle calculations can accurately predict the interatomic interactions of pure elements and complex alloy systems. However, the first-principle methods are computationally demanding thereby limiting the size of the atomic domain that can be examined to only a few hundred atoms. In order to examine mechanics of material deformation at the atomic scale the limitation of DFT methods hinders the ability to effectively study the critical crack, dislocation and grain boundary interactions. Therefore, in this section we will focus on employing atomistic simulation techniques with a particular interest in studying the application to mechanics.

## A.2 Molecular statics

The molecular statics (MS) approach considers athermal interactions (0 K); whereby, the minimum energy position of atoms is calculated solely based on the potential energy contribution. The conjugate gradient method is used to determine the positional rearrangement of the atoms. This works by following the direction of the steepest descent in the total potential energy of the atomic configuration that is conjugate to the previous atomic configuration. This method attempts to find the minimum energy configuration based on a pre-defined convergence criteria.

A.3 Molecular dynamics

The molecular dynamics approach consists of solving Newton's equations of motion for an N particle system evolving with time.

$$m\frac{d^2r_i}{dt^2} = -\frac{\partial U(r_i)}{\partial r_i} \tag{A1}$$

Here, $r_i$ represents the position vectors of the N atom system, $U(r_i)$ is the potential energy expressed in terms of the spatial arrangement of atoms, *m* is the atomic mass and *t* is the time. In this equation, $F = -\frac{\partial U(r_i)}{\partial r_i}$ is the interatomic force on atom *i* and $\frac{d^2r_i}{dt^2}$ is the acceleration.

A.4 Monte Carlo methods

The Monte Carlo approach relies on the statistical mechanics approach to estimate macroscopic quantities at thermal equilibrium using the Boltzmann's approach. For a microscopic quantity $A(\{\boldsymbol{r}_i, \boldsymbol{p}_i\})$ that depends on the atomic positions ($\boldsymbol{r}_i$) and momentum ($\boldsymbol{p}_i$), the ensemble average can be expressed as:

$$\langle A \rangle = \frac{1}{Z}\int \prod_{i=1}^{N} A(\{\boldsymbol{r}_i, \boldsymbol{p}_i\}) exp\big(-\beta H(\{\boldsymbol{r}_i, \boldsymbol{p}_i\})\big) d\boldsymbol{r}_i d\boldsymbol{p}_i$$

$$Z = \int \prod_{i=1}^{N} exp\big(-\beta H(\{\boldsymbol{r}_i, \boldsymbol{p}_i\})\big) d\boldsymbol{r}_i d\boldsymbol{p}_i \tag{A2}$$

$$H(\{\boldsymbol{r}_i, \boldsymbol{p}_i\}) = \sum_{i=1}^{N} \frac{|\boldsymbol{p}_i|^2}{2m} + V(\{\boldsymbol{r}_i\})$$

where $\beta = 1/(k_B T)$, $k_B$ is the Boltzmann's constant and $T$ is the temperature, $Z$ is the partition function which ensures the normalization of the probability distribution, $H$ is the Hamiltonian operator and $V(\{\boldsymbol{r}_i\})$ describes the interatomic potential energy. The direct integration of Equation A2 to obtain ensemble averages is not possible numerically. However, Monte Carlo methods make it possible to quantify the microscopic function that is only dependent on the atomic configuration **R**, $A = A(\boldsymbol{R})$.

$$\langle A \rangle = \int d\boldsymbol{R}\, A(\boldsymbol{R}) \rho(\boldsymbol{R})$$

$$\rho(\boldsymbol{R}) = \frac{1}{Z_{\boldsymbol{R}}} exp(-\beta V(\boldsymbol{R})) \tag{A3}$$

$$Z(\boldsymbol{R}) = \int d\boldsymbol{R}\, exp(-\beta V(\boldsymbol{R}))$$

Where, $\rho(\boldsymbol{R})$ is the Boltzmann's distribution function in the configurational sub-space, and $Z(\boldsymbol{R})$ is the configurational part of the partition function. After enough configurational states have been examined, the ensemble average can be estimated by Equation A3.

The chief difference between MD and MC methods is in the sampling approach utilized in the statistical mechanics framework (Equation A2) for the estimation of the macroscopic properties of interest. The MC method is based on the idea of sampling sufficient configurational states based on Boltzmann's distribution (Equation A3). In the case of MD, the new configuration is generated by advancing in time and finding the atom positions and velocities based on Newton's equation of motion (Equation A1).

A.5 Ensembles in MD Simulation

In MD simulations, the physical quantities measured are statistical averages for a chosen ensemble (microcanonical, canonical and isothermal-isobaric), as the total energy (*E*) is a constant of motion. The study of nano-mechanics of material behavior at the atomic length scale requires conditions that closely reflect the experimental setup. Thus, canonical and isothermal-isobaric ensembles offer a choice between two realistic conditions: a) thermal equilibrium at fixed temperature (canonical/NVT) ensemble; b) controlled pressure and temperature conditions (isothermal-isobaric/NPT) ensemble. There are two approaches to solve these ensembles: a) performing certain Monte Carlo moves during the Newtonian MD; b) employing reformulated Lagrangian equations of motion. Next, we present a brief overview of the most widely employed algorithms for performing the canonical and isothermal-isobaric ensembles in a MD framework.

A.5.1 Nosé-Hoover Thermostat

The Nosé approach is based on performing deterministic MD at constant temperature employing the extended Lagrangian. The extended Lagrangian contains the standard Lagrangian formulation of Newton's equation of motion and additionally artificial coordinates and velocities (Shuichi Nosé and Klein 1983; Shuichi Nosé 1984). This scheme was applied to the constant volume equation of motion proposed by Hoover (Hoover 1986). In the implementation of the constant volume ensemble, an artificial thermodynamic coefficient of friction ($\xi$) was introduced (Shūichi Nosé 1986). The equations of motion can be rewritten as following:

$$\dot{r}_i = \frac{\boldsymbol{p}_i}{m_i}$$

$$\dot{\boldsymbol{p}}_i = -\frac{\partial U(\boldsymbol{r}_i)}{\partial \boldsymbol{r}_i} - \xi \boldsymbol{p}_i \tag{A4}$$

$$\dot{\xi} = {v_T}^2 \left(\frac{T}{T_0} - 1\right)$$

where, $\boldsymbol{p}_i$ is the atomic momentum, $T_0$ is the temperature of the thermal reservoir and $v_T$ is the thermostating frequency. The thermodynamic friction coefficient dynamically rescales the velocities of the atoms to achieve the desired temperature ($T_0$).

A.5.2 Isothermal-Isobaric Ensemble

A number of models have been proposed to perform MD simulations in the NPT ensemble (Andersen 1980; Parrinello and Rahman 1982; Shuichi Nosé 1984; Hoover 1986). Each of these implementations are driven by the mismatch created between the desired and internal pressures to change the simulation box size. The NPT implementation has a close analogy to the NVT algorithm, as it also employs an isobaric friction coefficient ($\boldsymbol{\eta}$) similar to the thermodynamic friction coefficient. The following equations are a few modifications proposed by Melchionna et al. (Melchionna, Ciccotti, and Holian 1993) to Hoover's equations of motion for constant pressure (Hoover 1986) to accurately implement the NPT ensemble:

$$\dot{\boldsymbol{r}}_i = \frac{\boldsymbol{p}_i}{m_i} + \boldsymbol{\eta}(\boldsymbol{r}_i - R_0)$$

$$\dot{\boldsymbol{p}}_i = -\frac{\partial U(\boldsymbol{r}_i)}{\partial \boldsymbol{r}_i} - (\boldsymbol{\eta} + \xi \boldsymbol{I})\boldsymbol{p}_i \tag{A5}$$

$$\dot{\boldsymbol{\eta}} = \frac{{v_P}^2}{N k_B T_0} V(\boldsymbol{\sigma} - \boldsymbol{P_0})$$

$$\dot{\boldsymbol{h}} = \boldsymbol{\eta h}$$

where, $\boldsymbol{P_0}$ is the desired pressure and $v_P$ is the pressure dampening coefficient. The simulation cell boundaries are defined by $\boldsymbol{h}$. The internal stress state of the system ($\boldsymbol{\sigma}$) is calculated using the virial definition discussed later.

A.6 Interatomic potentials

The interactions between the particles are based on the potential energy of the atomic arrangement, and the interatomic potential can be expressed in an analytical form. The approximate analytical form of the interatomic potential aims to reproduce essential macroscopic properties. Over the last century, several different formulations aimed at modelling a particular bonding environment and varying levels of accuracy have been developed. The earliest and most noteworthy potential developed was the Lennard-Jones (Jones 1924a; Jones 1924b) pair potential for ideal gases. The Lennard-Jones pair potential is the simplest model for describing interatomic behavior, where the potential energy is only a function of the interatomic distance.

$$E = \frac{1}{2}\sum_{j \neq i} \varphi_{ij}(r_{ij}) \tag{A6}$$

Where, $r_{ij}$ is the interatomic distance between atoms *i* and *j* and $\varphi_{ij}$ is the pair-wise interaction energy. In many pair potentials, the pair-wise interaction energy is decomposed into attractive and repulsive components (Jones 1924a; Buckingham 1938) to capture both the long and short range interactions and best describe noble gas behavior. However, due to the simple description this fails to capture the change in bond strength with varying atomic environment. This behavior is critical in metals as the quantum effect changes the bond properties in the vicinity of a surface.

This has led to the development of the many body potentials that incorporate the effect of the local environment on the bond strength. In the case of metals, the embedded atom method (EAM) (M. S. Daw and Baskes 1984; M. S. Daw et al. 1985) that is based on the density functional theory incorporating the approximated many-body interactions.

$$E = \sum_i F_i(\rho_i) + \frac{1}{2}\sum_{j \neq i} \varphi_{ij}\left(r_{ij}\right) \tag{A7}$$

Here, the summation of the electron density ($\varphi_{ij}$) at the atomic site $i$ from all the atoms $j$ gives the local electron density at atomic site $i$. The embedding energy $F_i$ is defined as the interaction energy between an atom and the surrounding electron cloud created by the neighboring atoms. The EAM potentials allow an accurate reproduction of the elastic properties. For instance, the pair-wise description of a solid would yield, $C_{12} = C_{44}$ also known as the Cauchy relationship. However, only noble gases are known to obey this relation while metals violate this relationship (Murray S. Daw, Foiles, and Baskes 1993). The use of the many-body EAM formulation accurately captures this phenomenon. Similarly, the defect formation energies in metallic systems are accurately captured with the many-body formulation. The modified EAM (Baskes 1992) and the angular dependent potential (ADP) (Mishin, Mehl, and Papaconstantopoulos 2005) were developed to include an angular description of bonding that had been lacking in the EAM. The angular description is essential for modeling of body-centered cubic transition metals and hexagonal close packed metals as they capture in a semi-empirical manner the covalent nature of the bonding. Further, these angular descriptions are critical to development of alloy interatomic potentials (Mishin, Mehl, and Papaconstantopoulos 2005; B.-J. Lee et al. 2010; Apostol and Mishin 2011).

The bond order potentials (BOPs) (Tersoff 1986; Tersoff 1988a; Tersoff 1988b) represent an intriguing class of the many-body potentials with a wide range of analytic formulations. The BOPs expression for energy of a system is a sum of the repulsive $\left(V^R(r_{ij})\right)$ and attractive $\left(V^A(r_{ij})\right)$ interactions for the valence electrons.

$$E = \frac{1}{2}\sum_i \sum_{j \neq i} \left[V^R(r_{ij}) - b_{ij} V^A(r_{ij})\right] \tag{A8}$$

where $b_{ij}$ is a function of the local environment of atoms *i* and *j* called "bond order". This helps in capturing the effect of the environment surrounding an atom and was introduced by Coulson (Coulson 1939). Tersoff (Tersoff 1986) was first to employ the BOP formulation successfully to silicon. Abell (Abell 1985) developed the tight binding (TB), where the bond order term was solved with the help a TB Hamiltonian operator $\left(\hat{H}\right)$.

$$b_{ij} = -\frac{2}{\pi} Im \int_0^{\varepsilon^F} G_{ij}(\varepsilon) d\varepsilon \tag{A9}$$

$$G_{ij}(\varepsilon) = \langle i \left| \left(\varepsilon - \hat{H}\right)^{-1} \right| j \rangle$$

Where, $G_{ij}$ is the Green's function matrix, $\varepsilon$ is the occupied orbital energy assumed to contain a small imaginary part and $\varepsilon^F$ is the Fermi energy. To derive analytical expressions for the bond order the concepts of moment and path-counting (Cyrot-Lackmann 1967) and Lanczos recursion chain (Lanczos 1950) were used. Since then, a great deal of research has been conducted on the development of BOP for various materials (Pettifor 1989; D. W. Brenner 1990; Girshick et al. 1998; D. W. Brenner et al. 2002; Pettifor and Oleinik 2002; Mrovec et al. 2004; Mrovec, Elsässer, and Gumbsch

2009). For details on the application of BOP on transition metals (Drautz and Pettifor 2006; Pettifor et al. 2002) and hydrocarbons (D. W. Brenner 1990; D. w. Brenner 2000).

The empirical description has been found to lack the ability to accurately capture complex bonding environments, such as interfaces between dissimilar materials and the transitions during a chemical reaction. The reactive empirical bond order (REBO) (D. W. Brenner 1990; D. W. Brenner et al. 2002), adaptive intermolecular reactive empirical bond order (AIREBO) (Stuart, Tutein, and Harrison 2000), reactive force field (ReaxFF) (van Duin et al. 2001) and charge optimized many body (COMB) (Shan et al. 2010; Noordhoek et al. 2013) are a few of the different formulations that can address this limitation. Here we review the COMB formulation that shares the fundamental concepts with ReaxFF. The formulation has concepts that aid in the transition in bonding character of the molecule, and can take into account the long range interactions (Coulomb and van der Waals). The total energy of a system in the COMB formulation is expressed in terms of the sum of several chemical interactions.

$$E = \sum_i \left[ E_i^{self}(q_i) + \sum_{j>i} \left[ E_{ij}^{short}\left(r_{ij}, q_i, q_j\right) + E_{ij}^{Coul}\left(r_{ij}, q_i, q_j\right) \right] + E^{vdW}\left(r_{ij}\right) + E^{polar}\left(r_{ij}, q_i\right) + E^{barr}(q_i) + E^{corr}\left(r_{ij}, \theta_{ijk}\right) \right] \tag{A10}$$

Here $q_i, q_j$ represents the partial charge around atoms and $E_i^{self}$ is the energy to form a charge on atom *i*, $E_{ij}^{short}$ is the bond-order potential between atoms *i* and *j*. The Coulomb interactions are given by $E_{ij}^{Coul}$, $E^{polar}$ is the polarization energy term, $E^{vdW}$ are the van-der Waals interactions, $E^{barr}$ is the charge barrier, $\theta_{ijk}$ is the angle between the three atoms *i*, *j* and *k* and $E^{corr}$ is the angular correction term. In this method, a self-consistent

approach has been employed for dynamic determination of charge according to the varying local environment. The thermodynamic requirement that electronegativity be equal at all atomic sites in chemical equilibrium is the basic principle behind the approach (Parr et al. 1978; Sanderson 1983). These reactive potentials have been applied with a great deal of success in the study of a) dissimilar material heterogeneous interfaces; b) surface chemistry; c) metals (with limited success) (D. w. Brenner 2000; T. Liang et al. 2013).

Despite these efforts, there is still a lack of a consistent approach capable of handling various bonding environments. The interatomic potentials at present are designed for use in specific applications and the functional form is mostly selected by the intuition of the designer. This has led to lack of reliability of atomistic findings (M. S. Daw et al. 1985; Murray S. Daw, Foiles, and Baskes 1993; Jonathan A. Zimmerman, Gao, and Abraham 2000; Gröger, Bailey, and Vitek 2008; Mrovec, Elsässer, and Gumbsch 2009; Foiles and Baskes 2012; Christopher R. Weinberger, Tucker, and Foiles 2013; Ventelon et al. 2013; Hale, Zimmerman, and Weinberger 2014). For instance, Zimmerman et al. (Jonathan A. Zimmerman, Gao, and Abraham 2000) found large variations in stacking fault energy curves for face-centered-cubic (FCC) metals because of the interatomic description. In the case of body-centered-cubic (BCC) metals, the presence of an unphysical metastable configuration during the screw dislocation glide was found due to the choice of interatomic description (Clouet, Ventelon, and Willaime 2009; Itakura, Kaburaki, and Yamaguchi 2012; Ventelon et al. 2013; Hale, Zimmerman, and Weinberger 2014; Christopher R. Weinberger, Tucker, and Foiles 2013). In order to serve as a robust and accurate interatomic potential, Brenner (D. w. Brenner 2000) discussed the importance

of: a) a potential function robust enough to accommodate a wide range of fitting data; b) a high level of fidelity in the reproduction of the parameter fitting database; c) the ability of the potential to predict accurate properties outside the fitting database; d) and lastly, the computational cost and scale-ability. These interdependent criterions create a tough balancing situation for the developers.

The design of atomistic studies necessitates great regards to the small length and time scales accessible. The time scale limitation seriously hinders the ability to observe phenomenon in laboratory experiments on much different time scales. The lack of quantum mechanics in the MD approach limits the reproducibility of several physical properties. This requires development of a new class of interatomic potentials that can describe the complex quantum effects. The electron force field (eFF) (Su and Goddard 2007; Kim, Su, and Goddard 2011) model attempts to address this issue by solving a simplified Schroedinger equation for practical non adiabatic electron dynamics simulations of materials. Despite these limitations, MD simulations have provided valuable insights into the mechanical behavior of metals at the nano-scale (Farkas, Van Swygenhoven, and Derlet 2002; Van Swygenhoven, Derlet, and FrA 2004; Warner, Curtin, and Qu 2007; Spearot et al. 2007; Tschopp et al. 2011; Tschopp et al. 2012b; Jonathan A. Zimmerman, Gao, and Abraham 2000; Lim et al. 2015; Christopher R. Weinberger, Tucker, and Foiles 2013; Olmsted, Foiles, and Holm 2009; Holm et al. 2011). In particular MD simulations have contributed greatly in the study of crystalline defects (vacancies, self-interstitials, dislocations, grain boundaries and cracks) (Smith, Vitek, and Pond 1977; Spearot et al. 2007; Jonathan A. Zimmerman, Gao, and Abraham

2000; Tschopp et al. 2011; Lim et al. 2015; Gröger, Bailey, and Vitek 2008; Olmsted, Foiles, and Holm 2009) as understanding defect behavior is critical for optimizing mechanical properties of crystalline materials.

A.7 Estimating stress in atomistic simulation

A critical issue in using MD simulations for mechanics is the accurate estimation of stress at the atomic scale. The virial theorem used to define the ensemble stress by Clausius (Clausius 1870) was initially developed to estimate the stress field applied to a surface of a fixed volume of particles.

$$\sigma_i = \frac{1}{\Omega_i}\left[\frac{1}{2}\sum\nolimits_i \sum_{i \neq j} \frac{U'}{r_{ij}} r_{ij}^{\alpha} r_{ij}^{\beta} - \sum_i m \boldsymbol{v}_i \boldsymbol{v}_i\right] \tag{A11}$$

where, $U$ is the potential energy, $U'$ is the spatial derivate of the potential energy, $r_{ij}$ is the vector between atom *i* and *j*, the superscript $\alpha$ and $\beta$ denote the direction components of the vector and $\Omega_i$ represents the approximate atomic volume.

The virial stress has been erroneously applied to estimate the local stress state as it offers an attractive diagnostic tool during material deformation. Irving and Kirkwood (Irving and Kirkwood 1950) attempted to address this by defining instantaneous mass, momentum and energy densities at a spatial point based on the statistical distribution of neighboring particles. The formulation was a noteworthy contribution, but it was found to be difficult to implement within a MD framework. Since then, several attempts have been made to address the shortcomings of the Irving and Kirkwood formulation (Tsai 1979;

Lutsko 1988; Cormier, Rickman, and Delph 2001). Zhou et al. (Zhou and McDowell 2002) developed a virial-like expression for stress defined over an arbitrary volume containing a single atom. Zimmerman et al. (J. A. Zimmerman et al. 2004) explored various scenarios of non-finite deformation and finite temperatures. It was found that the virial definition of stress had large fluctuations at finite temperature even for unstrained states of the crystal. However, time and spatial averaging was found to reduce the fluctuations. Further, Zimmerman et al. (J. A. Zimmerman et al. 2004) examined the applicability of the Hardy formulation for atomic stress and it was found to perform much better than the virial stress. Finally, Zimmerman et al. observed a lower limit to spatial and temporal resolution to make a connection between atomistic and continuum definitions of stress. These studies clearly show that the quantification of stress at the atomic scale while maintaining continuum equivalence is still an unresolved issue. Nonetheless, meaningful estimates of stress at atomic scale can be extracted by evaluating the virial part of Equation A11 (Zhou and McDowell 2002).

$$\sigma_i = \frac{1}{\Omega_i}\left[\frac{1}{2}\sum\nolimits_i \sum_{i \neq j} \frac{U'}{r_{ij}} r_{ij}^{\alpha} r_{ij}^{\beta}\right] \tag{A12}$$